



UNIVERSITAT DE
BARCELONA

Facultat de Matemàtiques
i Informàtica

GRAU DE MATEMÀTIQUES

Treball final de grau

Dynamical Analysis of Mushroom Bifurcations: Deterministic and Stochastic Approaches

Author: Mariona Fucho Rius

Director: Dr. Alejandro Haro Provinciale^{1,2}

Codirector: Dr. Josep Sardanyés Cayuela²

Realitzat a: 1. Departament de Matemàtiques i Informàtica

2. Centre de Recerca Matemàtica

Barcelona, 13 de juny de 2023

Abstract

Bifurcation theory has found contemporary applications in synthetic biology, particularly in the field of biosensors [43]. The aim of this thesis is to expand upon the framework presented in the referenced paper, which introduces a model depicting the behavior of mushroom bifurcations. The mushroom bifurcation diagram exhibits four saddle-node bifurcations and involves bistability. Our goal is to develop a comprehensive mathematical formalism that can effectively describe this behavior, both deterministically and stochastically. By doing so, we seek to uncover additional properties regarding the transients exhibited by these biosensors, specifically focusing on optimizing their timer-effect, memory properties, and signaling capabilities. We will introduce stochastic dynamics by considering intrinsic noise in the molecular processes, allowing us to investigate the slowing-down effects in the vicinity of the saddle-nodes and transcritical bifurcations. To conduct this study, we will use three fundamental mathematical tools, which can be regarded as the backbone of our analysis. These mathematical vertebrae include the Lemma of Morse, the Weierstrass Preparation Theorem and, most notably, the Implicit Function Theorem. Through this rigorous analysis, we aim to enhance our understanding of the underlying dynamics of these biosensors and facilitate their further improvement and utilization in various applications.

Resum

La teoria de bifurcacions ha trobat aplicacions contemporànies en la biologia sintètica, particularment en el camp dels biosensors [43]. L'objectiu d'aquesta tesi és ampliar el marc establert en l'article referenciat, el qual presenta un model que descriu el comportament de les bifurcacions bolet. El diagrama de bifurcació bolet presenta quatre bifurcacions sella-node i involucra bistabilitat. El nostre objectiu és desenvolupar un formalisme matemàtic exhaustiu que pugui descriure eficaçment aquest comportament, tant de manera determinística com estocàstica. D'aquesta forma, pretenem descobrir propietats addicionals relacionades amb els transitoris que presenten aquests biosensors, amb un enfocament específic en l'optimització de l'efecte *timer*, les propietats de memòria i les capacitats de senyalització. Introduïrem la dinàmica estocàstica considerant el soroll intrínsec en els processos moleculars, el que ens permetrà investigar els efectes de retard en la proximitat dels punts de sella i les bifurcacions transcrítiques. Per dur a terme aquest estudi, utilitzarem tres eines matemàtiques fonamentals, que es poden considerar el fonament del nostre anàlisi. Aquestes eines matemàtiques inclouen el Lema de Morse, el Teorema de Preparació de Weierstrass i, sobretot, el Teorema de la Funció Implícita. Amb aquest anàlisi rigorós, pretenem millorar la nostra comprensió de la dinàmica subjacent d'aquests biosensors i facilitar-ne la millora i ús en diverses aplicacions.

Acknowledgements

Primerament, gràcies als meus tutors: gràcies Àlex, per ensenyar-me i fer-me discutir amb les matemàtiques. Gràcies per ser-hi i per no perdre mai el toc d'enginy i humor per ensortir-nos-en. Gràcies, Josep, per proposar-me aquest model i mai perdre el somriure i la imaginació davant la pissarra. Per trobar el temps de xerrar d'on no l'hi havia.

Gràcies a tots els professors que m'han recolzat en la seva respectiva branca: Rubén Pérez, Tomás Alarcón, Ernest Fontich, Damià Torres i Àngel Jorba. Gràcies a la Beatriz Del Valle Pérez, per mostrar-me tanta proximitat i ajuda en els conceptes bioquímics; per trencar-se el cap amb mi.

Gràcies al Centre de Recerca Matemàtica per concedir-me la beca i així poder fer un tast d'una de les meves passions que he tingut des de petita com és la investigació.

Gràcies als meus pares i al meu germà. Gràcies a la meva mare, que tot i tenir la torre de Babel entre nosaltres cada vegada que li parlo de Matemàtiques, no deixa de preguntar: "i aquests bolets no són com els gargots que feies de petita? Què és tot això?".

Gràcies als meus amics, per confiar en tot moment en mi: Albert, Caterina, Laia, Mercè i Víctor, sou família en aquest camí.

Gràcies al Pau, per tots els sospirs. Gràcies per ser el petit tros de terra ferma en alta mar.

Finalment, gràcies a mi i gràcies a les Matemàtiques.

Contents

Introduction	iv
1 A Systematic Description of the Mushroom Bifurcation Model	1
1.1 Topology of the Mushroom Bifurcation: Biology Basics	2
1.1.1 Introduction to Biological Fundamentals	2
1.1.2 Definition of the Model: Biological Description	5
1.2 Bifurcation Analysis of the Model	7
1.2.1 Saddle-Node (S-N) Bifurcation	7
1.2.2 Transcritical Bifurcation: Lemma of Morse	11
1.3 Robustness of Bifurcations: Structural Stability	21
1.3.1 Codimension 1 Bifurcations	22
1.3.2 Codimension 2 Bifurcations	23
2 Deterministic Study of Delayed Transitions	25
2.1 Bottleneck effect	25
2.2 Weierstrass Preparation Theorem	26
2.3 Saddle-node Scaling Law	30
2.3.1 Normal Form of the S-N	30
2.3.2 General Non-Degenerate S-N Bifurcation	31
2.4 Transcritical Scaling Law	34
3 Stochastic Dynamics	36
3.1 Introduction	36
3.2 Theoretical Basis	37
3.2.1 Markov process	37
3.2.2 The Propensity Function	38
3.2.3 Consequences of the Propensity function: Master Equation	40
3.3 Gillespie Algorithm	41
3.4 Analyzing the Transition from Deterministic to Stochastic Systems and Its Implications	41
3.4.1 From deterministic to stochastic scenario: Law of large Numbers	41
3.4.2 Deriving the rates: Law of Mass Action	42

4 Results and Discussion	44
4.1 Bottleneck effect	44
4.1.1 Monostability and Bistability: Analysis of the Potential Function	44
4.1.2 S-N Scaling Law	44
4.1.3 Critical Slowing Down: the transcritical bifurcation	46
4.2 Stochastic study	48
4.2.1 Markovian stochastic system	48
4.2.2 Heat Maps and Time Lags	48
4.2.3 Coupling effect of SN bifurcations	50
 Conclusions	 53
 Bibliography	 55
 Appendix A	 61
.1 Additional insight	61
.1.1 Proof of Theorem 1.12 using Hamiltonian arguments	61
.1.2 Structure of the Gillespie Algorithm (SSA)	62
.1.3 Law of Mass Action and Michaelis-Menten-Hill equation	62
 Appendix B	 65
.1 Numerical Tools	65
.1.1 Newton-Raphson and Citardauq formula	65
.1.2 Gillespie Algorithm: Heat map Stochastic scenario	70
.1.3 Saddle-node Scaling Law	74
.1.4 Transcritical Scaling Law	76
 Appendix C	 78

Introduction

Synthetic biology is a scientific discipline that focuses on the modification of organisms to enhance their functionality by introducing novel abilities through genetic engineering [58]. In essence, scientists combine extensive stretches of DNA and integrate them into an organism's genetic material. These synthesized DNA segments may originate from genes found in different organisms or be entirely new constructs.

The primary objective of synthetic biology is to modify organisms so that they can generate substances such as medicines or fuels, or acquire novel abilities such as environmental sensing. Remarkable examples of accomplishments in synthetic biology include:

1. Microorganisms utilized for bioremediation to clean pollutants from our water, soil and air [26].
2. Rice modified to produce beta-carotene, a nutrient usually associated with carrots, that prevents vitamin A deficiency. Vitamin A deficiency causes blindness in 250,000 - 500,000 children every year and greatly increases a child's risk of death from infectious diseases [64].

Modern applications of synthetic biology demand the design of gene circuits to complex and versatile functionalities, such as division, cognition, and motility exhibited by engineered biological systems. These behaviors involve sophisticated interactions and responses orchestrated by gene circuits within cells [43]. However, the limited resources within a cell pose a challenge when combining multiple functional circuits within a single organism. Therefore, it becomes crucial to design regulatory networks that can exhibit distinct dynamical behaviors, enabling a cell to respond differently to various signals [43,63].

Bifurcation theory offers valuable tools to address these design challenges. It allows us to understand the relationship between the network's topology -represented by a set of parameterized differential equations- and its different dynamic behaviors under controllable inputs or signals. Each bifurcation in the system alters the number and nature of long-term dynamics, such as transitioning from a single stable state to multiple stable states or from a stable steady state to an oscillatory behavior.

This thesis focuses on investigating the robustness of the so-called mushroom bifurcations in gene circuits, exploring their ability to effectively respond to various signals even in the face of parameter perturbations and intrinsic noise. Mushroom bifurcations represent circuit topologies that exhibit resilience, maintaining functionality despite smooth and small changes in parameters. The study we present examines these bifurcations from both deterministic and stochastic perspectives. One significant contribution of this research is the exploration, to the best of our knowledge, of a previously unexplored area related to mushroom bifurcations. Specifically, we investigate the approximation and overlapping of two saddle nodes, their interaction, and the potential synergistic effect at the level of transients. The limited understanding in this area prompted our investigation, recognizing its substantial importance in comprehending these complex behaviors, which can have a relevant applied impact.

Chapter one presents a comprehensive overview of our theoretical model, followed by an investigation of the behavior of ghosts and transients near the bifurcations in Chapter two. In Chapter three, we undertake a stochastic study using the Gillespie algorithm, illustrating the robustness of mushroom bifurcations even in noisy intra-cellular environments. Chapter four presents our main results, detailing the interplay between two saddle nodes and its influence on transients and scaling laws.

Trickey and Virgin [61] were pioneers in exploring the concept of "ghosts", specifically in the context of electronic circuits. These authors provided the first experimental evidence of this phenomenon. Interestingly, Dai *et al.* built a saddle-node bifurcation diagram in their experiments involving yeast *Saccharomyces cerevisiae*; their work included the direct observation of critical slowing down before the population collapse [9]. The term "ghost" [6,11,18,51,55] refers to a region of the phase space where the dynamics of the system are extremely slow due to the lingering influence of two fixed points that have collided and been destroyed in a bifurcation event such as a saddle-node bifurcation. This phenomenon shows a form of system 'memory', which involves a delay in the time in which a trajectory spends in the vicinity of the destroyed attractor.

Remark 0.1. Although the terminology "destruction" of the attractor point is commonly used, a more accurate description involves the transition of the fixed points into the complex phase space. For further details, please refer to the research paper by Fontich and Sardanyés [11], as well as the work by Canela *et al.* [7].

A **time transient** [7] refers to the temporary behavior that a system exhibits before it settles down to its long-term behavior.

When the system resides in the proximity of a bifurcation point, the trajectories experience a notable deceleration in their evolution. This slowdown effect is considered a 'time delay' phenomenon associated with the ghost, as it represents a temporary but prolonged period during which the trajectories are delayed in their evolution before returning to their expected behavior over an extended period.

One remarkable property observed near critical points is the presence of universal scaling laws, which describe the characteristic slowing down of processes.

A **scaling law** refers to a mathematical relationship that quantifies the systematic variation of properties of the system, such as time scales, amplitudes, or frequencies, as characteristic dependencies on the control parameters, near critical transitions or bifurcation points.

In particular, when observing scaling laws associated with ghosts, one typically encounters a power law behavior, where the relevant quantities vary as a power of the distance from the critical point. These power law relationships provide insights into the underlying mechanisms governing the system's dynamics and can often reveal universal behavior across different systems and scales. Such a power-law behaviour was indeed found in the abovementioned experiments with the electronic circuit [61].

Specifically, in the context of the deterministic s - n bifurcation, the scaling behavior is represented by a power law relationship between the transient time (τ) and the difference ($|\epsilon - \epsilon_c|$) between the control parameter (ϵ) and its critical value (ϵ_c). This power law relationship is given by $\tau \sim |\epsilon - \epsilon_c|^{-1/2}$.

Notably, this scaling power law and the appearance of "ghosts" have been identified in mathematical models of phenomena such as electronic circuits [61], charge density waves [56] and metapopulations¹ without habitat destruction [11, 18]. These phenomena represent a universal property of saddle-node bifurcations [55].

Example 0.2. Let us describe an autocatalytic replicator model with intra-specific competition and density-independent degradation, as discussed in [18]. The state variable $x(t)$ represents the population of a replicator species that undergoes self-replication. The dynamical system describing this process can be written as:

$$\frac{dx}{dt}(t) = f(x) = kx^2(t) \left(1 - \frac{x(t)}{k}\right) - \epsilon x(t)$$

where k represents the replication rate, k is the carrying capacity of the environment, and ϵ denotes the degradation rate.

The dynamical system has three equilibrium points, denoted as $x^* \in \{x_0, x_{\pm}\}$, where $x_0 = 0$ and $x_{\pm} = \frac{1}{2} \left(1 \pm \sqrt{1 - \frac{4\epsilon}{k}}\right)$.

The ghost phenomenon becomes apparent following the saddle-node bifurcation (Figure 1).

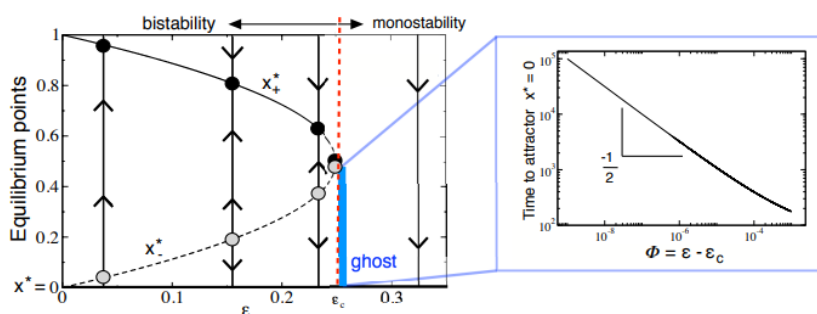


Figure 1: The bifurcation diagram illustrates the autocatalytic replicator system increasing the degradation rate (ϵ) while keeping $k = 1$ constant. It shows the stable (x_+) and unstable (x_-) equilibria denoted by solid and dashed lines, respectively. Arrows indicate the flow direction in the one-dimensional phase space, with x_+ marked by a black circle and x_- by a gray one. At $\epsilon = \epsilon_c$, a saddle-node bifurcation occurs, causing the equilibria to converge (vertical red line). Following the bifurcation, there is a transient phase with a delayed transition towards the remaining attracting fixed point $x^* = 0$, represented by a small blue rectangle. This delayed transition exhibits an inverse square-root law relative to the distance Φ from the bifurcation value ϵ_c (see the inset). Obtained from [18].

¹A metapopulation consists of a group of spatially separated populations of the same species which interact at some level.

To account for the stochastic nature of cellular systems [50], we introduce noise by implementing small fluctuations in molecule concentrations. This stochastic scenario enables us to explore the influence of intrinsic fluctuations on cellular dynamics, providing valuable insights into the behavior of gene circuits. To simulate these dynamics, we use the well-known Gillespie algorithm [14, 15], widely used in stochastic simulations in systems biology.

Intrinsic fluctuations arise from the inherent randomness observed in molecular processes within cells. Molecular events such as molecule binding and unbinding, enzymatic reactions, and transcription processes involve random interactions, resulting in stochastic dynamics within the system. Furthermore, small molecule numbers contribute to inherent stochasticity in cellular contexts [31,49]. By considering these intrinsic fluctuations, we gain a deeper understanding of how cells are influenced by the inherent stochasticity of their molecular processes, being our analyses more realistic from a biological point of view. This knowledge is crucial for comprehending the behavior of gene circuits in synthetic biology, as it analyzes the extremely important impact of variability on cellular dynamics.

Motivation and Goals

This thesis aims to apply the knowledge gained during my academic journey on this degree to contribute to the field of synthetic biology, with a specific focus on understanding the mushroom bifurcation and the implications of overlapping local bifurcations, such as the saddle-node and transcritical bifurcations, and their influence on transients. A core objective of this research is to explore the robustness of our model in the face of parameter variations and to elucidate its qualitative properties, both deterministic and stochastic.

Throughout this research, I aim to showcase the complexities involved in understanding mushroom bifurcations, shedding light on their broader implications for the design and optimization of gene circuits in synthetic biology. Ultimately, this study seeks to advance our understanding of the intersection between mathematics and biology, particularly in the field of bifurcation theory. Furthermore, this thesis aims to open up new possibilities for the application of synthetic biology in the development of novel treatments and solutions for various disease-related challenges.

“The difference between the poet and the mathematician is that the poet tries to get his head into the heavens while the mathematician tries to get the heavens into his head.”

- G.K. Chesterton

Chapter 1

A Systematic Description of the Mushroom Bifurcation Model

A multifunctional behaviour of special interest for synthetic biology applications is the mushroom bifurcation, named after its mushroom-shaped bifurcation diagram. It was initially observed in models for neural stem cell differentiation [52, 53]. The mushroom bifurcation diagram is formed by combining two toggle switches, resulting in four saddle node bifurcations and three disconnected stable steady states [43]. The presence of a mushroom-shaped locus of equilibria provides the system with unique hysteresis properties, where the state of the cell will be determined by the signal history. Furthermore, it supplies the system with bistability - the capacity for the system to inhabit one of two stable states under the same parameter conditions. This phenomenon bears profound significance in various fields such as synthetic biology, microbiology, and mammalian cellular biology [45].

Bistability serves a pivotal role in cellular differentiation [10, 46], a process whereby a homogeneous cell population differentiates into two distinct cell types based on the stable state they adopt. Furthermore, bistability is thought to be indispensable for embryonic development [40], where distinct cell types are needed in different regions. Maternal signals play a critical role in providing positional information, signals present within an organism that provide spatial guidance and determine the identity or fate of cells within specific positions or regions during development for further tissular differentiation.

Moreover, bistability plays an integral role in cellular decision-making processes [19], often regarded as a form of cellular memory. Under this mechanism, a cell retains information about its state and bestow this information to its progeny during cell division. This attribute can also confer a degree of robustness to the system against inherent stochasticity prevalent in gene expression, which can cause protein-level fluctuations. In the context of cancer cells [48], cellular decision-making processes play a crucial role in the fate and behavior of tumor cells, as well as into the path towards malignancy.

Mushroom bifurcations have been experimentally observed in hormone-related systems prone to generating conditions such as Post Traumatic Stress Disorder (PTSD)

or other stress-related disorders [54]. A detailed exploration near the mushroom bifurcation reveals the potential for isola bifurcation diagrams, which have not been experimentally confirmed yet.

1.1 Topology of the Mushroom Bifurcation: Biology Basics

A mushroom bifurcation (Figure 1.1) refers to a dynamic system with four saddle-node (SN) bifurcations that mark the boundaries of steady-state branches, giving rise to an intermediary steady state. The intermediary steady state, labeled as the "ON" state, exists within a specific range of signal values s (Figure 1.1 (C)). On the other hand, the remaining steady states, denoted as the "OFF" states, correspond to the extremities of the signal spectrum, high and low signal values.

An important aspect of mushroom bifurcations is that, while the signal varies, the expression levels along each locus also change correspondingly. Therefore, these changes do not alter the overall structure of the bifurcation diagram. A bifurcation diagram is a graphical representation which displays the possible long-term changes of the system behavior when the value of the control parameter is varied [1]. Typically, to depict the branches corresponding to the stable fixed points of the bifurcations, solid lines are used, while dashed lines represent the branches corresponding to unstable fixed points. This convention is exemplified in Figure 1.1.

A distinctive feature of the mushroom bifurcation is its multidimensionality, it is dependent on more than one parameter. This characteristic enables the classification of the mushroom bifurcation to remain independent of the specific genes employed in its representation. Thus, it can be applied in a range of contexts within biological systems.

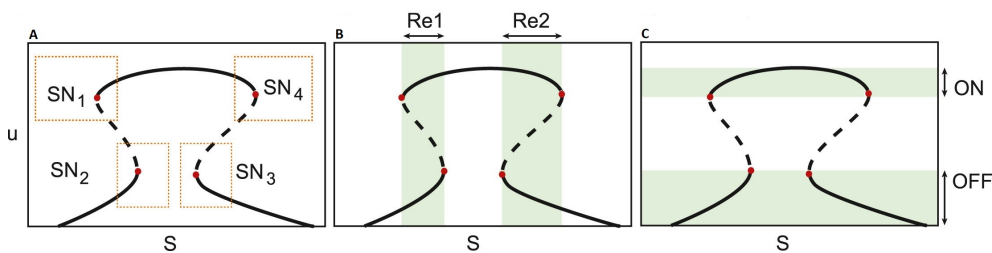


Figure 1.1: (A) Mushroom bifurcation diagram showcasing four saddle-nodes, accompanied by their corresponding stability branches stable in solid lines and unstable in dashed ones. (B) Both bistability regions are highlighted as Re1 and Re2. (C) "ON" and "OFF" states represented. Images from [43].

1.1.1 Introduction to Biological Fundamentals

In the field of biology, **autocatalysis** is the ability of systems, such as molecules, to promote copies of themselves. Systems where autocatalysis is accompanied by information transfer, the transmission of the genetic instructions or molecular information necessary for replication, and heredity, referring to the replication of the

genetic material with a high degree of fidelity, are said to be **self-replicating** [38]. DNA and RNA exemplify self-replicating molecules.

A self-replicating molecule can operate both as a **catalyst** and a **template**, as ribozymes (catalytic RNAs). A catalyst is a substance that accelerates the rate of a chemical reaction, defined as the change in concentration of a substance divided by the time interval during which this change is observed, without itself undergoing any permanent chemical change. The template is the strand of DNA or RNA that guides the creation of a complementary strand during the replication process.

To provide an example of a catalyzed reaction, let us talk about **enzyme-catalyzed reactions**. Enzyme catalysis is the process by which enzymes accelerate or facilitate chemical reactions. Enzymes are specialized proteins that act as biological catalysts, meaning they increase the rate of a chemical reaction without being consumed or permanently altered in the process.

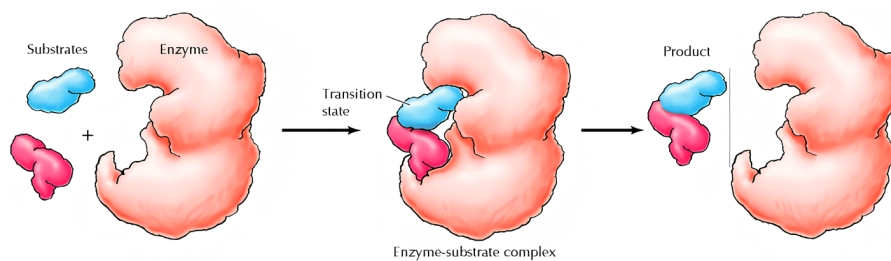


Figure 1.2: Enzymatic catalysis of a reaction between two substrates. The enzyme provides a template upon which the two substrates are brought together in the proper position and orientation to react with each other. Figure from [8].

In order to define our model, it is important to introduce the concept of hypercycles (refer to Figure 1.3), a set of self-replicating entities, such as molecules or genes, that mutually depend on each other for replication, forming a cyclic network [51, 57].

Definition 1.1. (Hypercycle) An hypercycle refers to an abstract model that describes the organization of self-replicating molecules interconnected in a cyclic and autocatalytic manner.

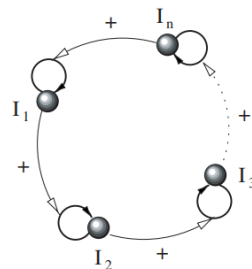


Figure 1.3: General catalytic hypercycle of n species. Self-replication is represented with thick closed arrows and catalytic aid with thin arrows [51].

To present the mushroom bifurcation model comprehensively, it is necessary to introduce several additional definitions, including the concept of a gene circuit. A **gene circuit** is defined as an assembly of biological parts encoding RNA or protein that enables individual cells to respond and interact with each other to perform some logical functions, such as boolean logic operations, using gene regulatory elements and their interactions to process input signals and generate specific cellular responses [29].

In the context of gene circuits, the property of **signaling** is essential for understanding how different components influence one another. Signaling refers to the mechanism by which cells and organisms communicate to coordinate various physiological and behavioral responses. It covers the exchange of molecular signals to transmit information and trigger appropriate reactions within the system. One important aspect related to signaling is the concept of **affinity** between molecules. Affinity reflects the strength of the interaction between molecules, and it influences the system's response to signals. For instance, high affinity implies that even with low signal levels, the system exhibits a robust and pronounced response. This affinity-driven response is crucial for understanding how molecular components within the gene circuit coordinate and modulate their behaviors based on the incoming signals.

The process of **transcription** holds significant importance when examining genes and proteins. It involves the synthesis of an RNA from a gene's DNA sequence, akin to translating a book from one language to another [59]. Please see Figure 13 in Appendix C.

Furthermore, when considering a cellular model, it is essential to recognize and provide a definition for the concept of **housekeeping genes**. Housekeeping genes are constitutive genes, which means that they are always transcribed and **translated** -the process by which a cell makes proteins using the genetic information carried in messenger RNA. They play a vital role in maintaining fundamental cellular functions, irrespective of their specific functions in a tissue or organism. As a result, these genes are typically expressed in all cell types within an organism [25].

To complete the necessary definitions, the final concept to expose is as follows:

Definition 1.2. (Hill-Langmuir function) *A Hill-Langmuir function is a mathematical representation commonly used to describe the binding behavior between a ligand, the binding molecule, and a receptor protein, a protein that has binding sites and can interact with specific ligands. It is characterized by the equation:*

$$\theta = \frac{[L]^n}{K_d + [L]^n}, \quad n \in \mathbb{N}.$$

Here, $[L]$ represents the total concentration of the ligand, n represents the Hill coefficient, which determines the cooperative interaction strength between the ligand, the binding molecule, and the receptor, and K_d is the apparent dissociation constant, which describes binding affinity of an enzyme for its substrate.

Remark 1.3. In the context of the mushroom bifurcation, we will focus our analysis

on the case $n=2$. By considering this restriction, we can still capture the essential properties of the system, both from a biological perspective, where it implies that two molecules are required for protein transcription, and from a mathematical standpoint, as it simplifies the study of parameters.

1.1.2 Definition of the Model: Biological Description

Pérez-Carrasco et al. [43] employed a mixed-integer programming (MIP) framework to develop a model for the mushroom bifurcation based on the gene circuit depicted in Figure 1.4. MIP is a powerful approach that addresses problems where some of the decision variables are constrained to be integer values at the optimal solution [12]. The dynamics of gene regulation within this model involve the interaction between the gene circuit and the signaling of the substrate S , subsequently influencing the gene U . These dynamics are represented by a one-dimensional deterministic autonomous ordinary differential equation.

Definition 1.4. (Mushroom bifurcation model) We define the mushroom bifurcation model as:

$$\dot{u} = f(u, r, s) = r + a(s) \frac{u^2}{1 + u^2} - u, \quad r \in \left(0, \frac{1}{3\sqrt{3}}\right). \quad (1.1)$$

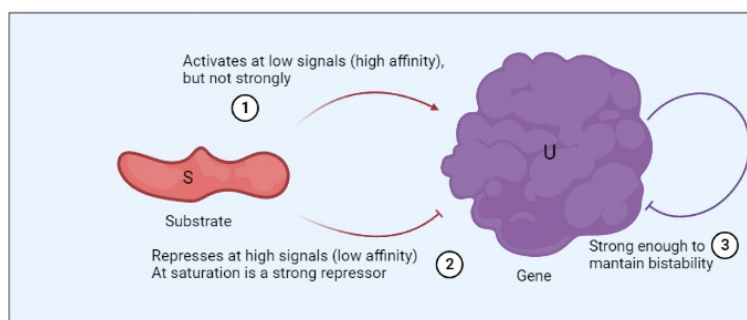


Figure 1.4: Schematic diagram of the system modeled by Eq. (1.1) exhibiting mushroom bifurcation behavior, linked to the signaling of substrate S and its effect on gene U . 1) Represents the substrate S 's capacity to activate the expression of gene U , translating the gene's information into a functional protein. 2) Gene translation inhibition. 3) As U reaches saturation due to high levels of concentration, self-inhibition occurs, leading to a decrease of its activity.

Notation	Meaning
u	State variable: concentration of the protein expressed by gene U
r	Parameter: concentration of constitutive housekeeping gene
s	Parameter: concentration of biochemical signal inducer S
$H(s, u) = a(s) \frac{u^2}{1+u^2}$	Hill function that indicates the concentration of activating transcription factor, the protein that increases transcription of the gene, regulated by s

Given $q \in \mathbb{R}_+$,

$$a(s) = sq - s^2, \quad s \in [0, q] \quad (1.2)$$

encodes the incoherent signalling. Due to $a(s)$ parabola-shape (see Figure 1.5), given $a(s)$ defines the transcription factor, at low signals -small values of s -, S activates the transcription of U ; oppositely, at high signals, when having a low affinity, the transcription process is repressed (refer to Figure 1.4). Moreover, the Hill-Langmuir form of $H(s, u)$ captures the phenomenon of autosaturation, which occurs in the presence of high concentrations of u .

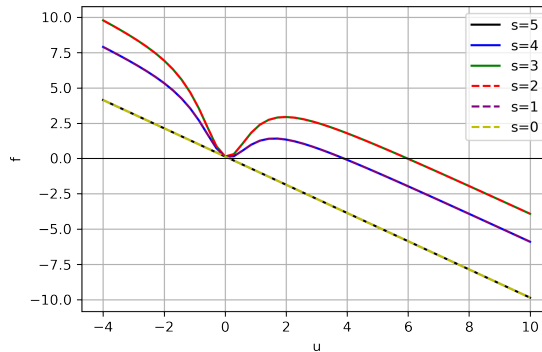


Figure 1.5: Function $f(u, r, s)$ with $r = 0.14$ and varying values of s . A distinctive observation from the graph is the parabolic pattern exhibited, particularly evident when comparing the effects of $s = 1$ and $s = 4$.

Remark 1.5. While the concepts of protein and gene may overlap in certain contexts within this study, it is important to clarify that a protein is the product of a gene, and they are distinct entities. In our specific case, the gene U is responsible for producing proteins u , which subsequently exerts an influence on it.

Understanding the stability of branches in the mushroom bifurcation (Figure 1.6), specifically the neck region, is important in biology. The neck acts as a unique biosensor [43] by enabling precise activation levels of a target signal within a limited range, given the "ON state" is only available for a reduced range of signals. Moreover, the size of the mushroom head provides memory, preserving the activation state for a broader range of signals than necessary. By regulating parameters like the gene degradation rate, it becomes possible to control the size of the neck in the mushroom bifurcation. This control enables the manipulation of both the range and the required duration of target signals. This way the mushroom not only serves as an accurate signal detector but also as a timer. Additionally, the isola in the bifurcation diagram, a closed curve in the bifurcation diagram, serves as a sensor of extreme values with infinite memory, capable of detecting past high or low signal levels.

Remark 1.6. The chosen domain for the parameter r , specifically $r \in \left(0, \frac{1}{3\sqrt{3}}\right)$, is non-trivial. It is important to note that for values of r greater than $\frac{1}{3\sqrt{3}}$, there are no

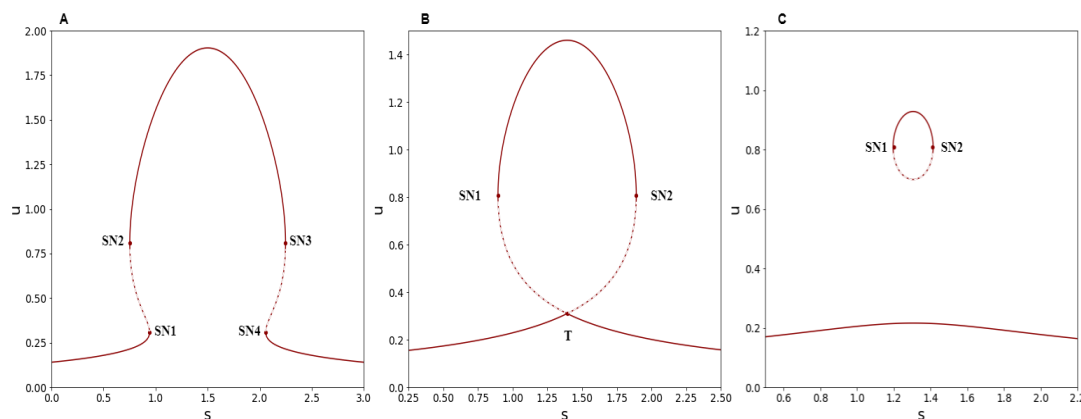


Figure 1.6: (A) Mushroom bifurcation represented with $0 \leq s \leq 3$ for $r = 0.14$ and $q = 3$. Solid and dashed lines respectively indicate stable and unstable branches. (B) Mushroom bifurcation for $r = 0.14$ and $q =$. (B) The emergence of an isola is observed, exhibiting a transcritical (T) bifurcation alongside two saddle-node (SN) bifurcations, for a value of q equal to 2.7849536194134643. (C) Isola formed with the absence of a transcritical bifurcation, with q set to 2.61.

positive roots. Consequently, in the real space, no bifurcation would occur in this range, rendering it unsuitable for further analysis.

1.2 Bifurcation Analysis of the Model

In the context of continuous dynamical systems described by the differential equation $\dot{x} = f(x)$, fixed points are solutions to the equation $f(x) = 0$. These fixed points represent constant solutions or steady states of the system.

Definition 1.7. (Continuable fixed point) A continuable fixed point, denoted by a point where $f(x_0, \lambda_0) = 0$ and $\frac{\partial f}{\partial x}(x_0, \lambda_0) \neq 0$, is locally continuable in the sense that a path of zeroes extends from it through a neighborhood of (x_0, λ_0) .

Consequently, the Implicit Function Theorem can be applied, enabling the description of the graph of a function locally within the set of zeros of its derivative.

1.2.1 Saddle-Node (S-N) Bifurcation

Let $f : I \times \Lambda \rightarrow \mathbb{R}$ be a continuously differentiable function, where $I, \Lambda \subset \mathbb{R}$ are open intervals, giving rise to a family of continuous dynamical systems $\dot{x} = f_\lambda(x)$, where $f_\lambda : I \rightarrow \mathbb{R}$ is given by $f_\lambda(x) = f(x, \lambda)$ for each $\lambda \in \Lambda$. Let $(x_0, \lambda_0) \in I \times \Lambda$ be a point in the bifurcation diagram, i.e., a point where $f(x_0, \lambda_0) = 0$.

Theorem 1.8. (Saddle-Node Bifurcation) Assume

$$\frac{\partial f}{\partial x}(x_0, \lambda_0) = 0, \quad A := \frac{\partial f}{\partial \lambda}(x_0, \lambda_0) \neq 0, \quad B := \frac{\partial^2 f}{\partial x^2}(x_0, \lambda_0) \neq 0.$$

Then, there exists $\lambda_* : (x_0 - \eta, x_0 + \eta) \rightarrow \mathbb{R}, C^\infty$, such that

$$\begin{aligned} (1) \quad \lambda_*(x_0) &= \lambda_0, & (3) \quad \lambda'_*(x_0) &= 0, \\ (2) \quad f(x, \lambda_*(x)) &= 0, & (4) \quad \lambda''_* &= -\frac{B}{A} \neq 0. \end{aligned}$$

Proof. To prove the existence of λ_* , it is necessary and sufficient to verify that the conditions required for the application of the Implicit Function Theorem around the point (x_0, λ_0) are satisfied. Under the given assumptions that (x_0, λ_0) is a continuable fixed point, there exists a C^∞ function $\lambda_*(x)$ such that $\lambda_*(x_0) = \lambda_0$ and $f(x, \lambda_*(x)) = 0$ for all x in a small enough interval around x_0 , namely, $(x_0 - \eta, x_0 + \eta)$, for a certain η . This follows from the Implicit Function Theorem, which states that if the conditions for a local inversion are satisfied, then there exists a unique function $\lambda_*(x)$ that locally solves the equation $f(x, \lambda_*(x)) = 0$ and satisfies the initial condition $\lambda_*(x_0) = \lambda_0$. Therefore, the existence of λ_* is established; furthermore, (1) and (2) are a direct consequence of the definition of the implicit function λ_* .

$$(3) \quad \lambda'_*(x_0) = 0.$$

We have

$$f(x, \lambda_*(x)) = 0$$

Let us compute the derivative of this equation with respect to the variable x :

$$0 = \frac{df}{dx}(x, \lambda_*(x)) = \frac{\partial f}{\partial x}(x, \lambda_*(x)) \frac{dx}{dx} + \frac{\partial f}{\partial \lambda_*}(x, \lambda_*(x)) \frac{d\lambda_*}{dx}(x). \quad (1.3)$$

Evaluating this equation at $(x, \lambda_*(x)) = (x_0, \lambda_*(x_0))$ and noticing that $\frac{dx}{dx} = 1$, we obtain

$$\left. \frac{d\lambda_*}{dx}(x) \right|_{x=x_0} = -\frac{\frac{df}{dx}(x_0, \lambda_*(x_0))}{\frac{\partial f}{\partial \lambda_*}(x_0, \lambda_*(x_0))} = 0$$

$$(4) \quad \lambda''_*(x_0) \neq 0.$$

Differentiating (1.1) with respect to x once more, we obtain:

$$\frac{d^2\lambda_*}{dx^2}(x, \lambda_*(x)) = \frac{-\frac{\partial^2 f}{\partial x^2}(x, \lambda_*(x)) \frac{\partial f}{\partial \lambda_*}(x, \lambda_*(x)) + \frac{\partial^2 f}{\partial \lambda_*^2}(x, \lambda_*(x)) \frac{\partial f}{\partial x}(x, \lambda_*(x))}{\left(\frac{\partial f}{\partial \lambda_*}(x, \lambda_*(x))\right)^2}. \quad (1.4)$$

Hence, evaluating (1.2) at $(x, \lambda_*(x)) = (x_0, \lambda_*(x_0))$, we obtain $\lambda''_*(x_0) = -\frac{B}{A} \neq 0$, provided.

The stability of the branches emerging from the bifurcation point (x_0, λ_0) can be determined by examining the sign of the second partial derivative of the function f with respect to x , denoted as $\partial_{xx}f$ [22]. To simplify notation, let $\partial_{xx}f$ be denoted as f_{xx} .

1. If $f_{xx}(x_0, \lambda_0) < 0$, the upper branch (for $x > x_0$) consists of stable fixed points. In this case, any perturbation from the bifurcation point will lead the system to converge back to the upper branch. Conversely, the lower branch (for $x < x_0$) is composed of unstable fixed points.
2. If $f_{xx}(x_0, \lambda_0) > 0$, the upper branch becomes unstable. Any perturbation from the bifurcation point will cause the system to diverge from the upper branch. Meanwhile, the lower branch remains stable

□

Remark 1.9. When considering and defining the model, it is crucial to examine its differentiability. For instance, in the case of $n = 1.8$, the function f would be continuously differentiable (C^1) but not twice continuously differentiable (C^2) at $u = 0$. However, outside of $u = 0$, the function f is infinitely differentiable (C^∞).

Application to Equation 1.1

The mushroom bifurcation model describes a dynamical system in which the rate of change of a quantity u is governed by a function $f(u, r, s)$. Let us investigate the system for conditions under which a saddle-node bifurcation occurs, and to further analyze the bifurcation.

Let us describe equation 1.1 as:

$$\dot{u} = f(u, s, r) = r + a(s)g(u) - u, \quad (1.5)$$

Here, $a(s) > 0$. The function $g(u)$ is defined as $g(u) = \frac{u^n}{1+u^n}$, which has a derivative $g'(u) = \frac{nu^{n-1}}{(1+u^n)^2}$. It can be observed that $g(0) = 0$, $g(u)$ is increasing, and $\lim_{u \rightarrow \infty} g(u) = 1$. It can be seen $g'(u) > 0$ and there exists a unique point u_* where $g''(u) = 0$.

The saddle-node bifurcation occurs when the following system is satisfied:

$$\begin{cases} 0 = f(u, s) = r + a(s)g(u) - u, \\ 0 = \frac{\partial f}{\partial u} = a(s)g'(u) - 1, \\ 0 \neq \frac{\partial f}{\partial s}(u, s), \\ 0 \neq \frac{\partial^2 f}{\partial x^2}(u, s). \end{cases} \quad (1.6)$$

To investigate the saddle-node bifurcation, we will need to find the value of s , for q, r fixed, for which the above system has a single solution, and evaluate the stability of that solution.

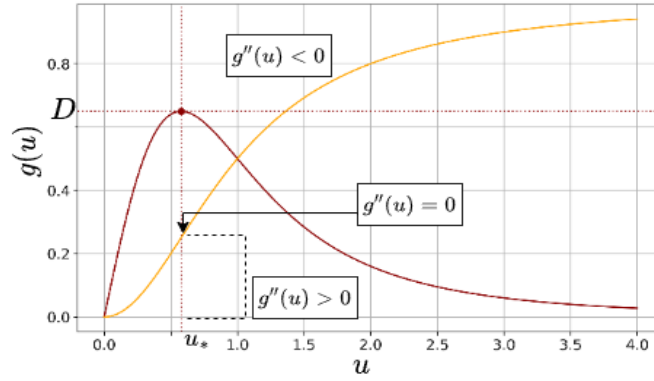


Figure 1.7: Function g represented by the orange curve, along with its first derivative g' displayed in dark red. Prior to the dotted line, the function displays a convex shape, indicating that the second derivative $g''(u)$ is greater than zero. At the inflection point denoted as u_* , marked by the dotted line, the curvature of g undergoes a transition, characterized by a switch from a positive to a negative sign of $g''(u)$, leading to a concave shape in the subsequent region.

In the case of $g(u) = \frac{u^n}{1+u^n}$, the derivative $g'(u) = \frac{nu^{n-1}}{(1+u^n)^2}$, and we have $\frac{df}{du} = a(s)g'(u) - 1$. Substituting this back into our system of equations, we find the equilibrium points and the associated values of s .

In order to evaluate the stability of the equilibrium points, we need to compute the second derivative of f with respect to u , $\frac{\partial^2 f}{\partial u^2} = a(s)g''(u)$. If the second derivative is negative, the equilibrium point is stable, while if it is positive, the point is unstable.

As $a(s)$ is parabola-shaped, there exists $a'(s_0) = 0$ such that $a(s_0)$ is maximized. Consider u_* the inflection point, and let $g'(u_*) = D$. Based on the constraint $g'(u) > 0$, we have three cases:

1. If $\frac{1}{a(s_0)} > D$, there are no solutions to system 1.6 .
2. If $\frac{1}{a(s_0)} = D$, then $u = u_*$, the inflection point. We find $a(s_0) = -\frac{r-u_*}{g'(u_*)}$. Therefore, the Jacobian matrix of f at (s_0, u_*) in this case is singular, given $f_s(s_0, u_*) = a'(s_0)g(u_*) = 0$ and $f_{uu}(s_0, u_*) = a(s_0)g''(u_*) = 0$. Due to the non-degeneracy conditions of system 1.6, there are no solutions to the system.
3. If $\frac{1}{a(s_0)} < D$, there exists at least one solution to the system.

Remark 1.10. Given the mushroom-shaped form, it is possible that depending on the value of q and r , we will have two or four saddle-nodes.

Remark 1.11. It is worth mentioning that in the case where $\frac{1}{a(s_0)} = D$, the described situation serves as the foundation to characterize the collision of two degenerate saddle-node bifurcations, which results in a transcritical bifurcation.

As $a(s)$ reaches a maximum at D for some s_0 , we will have a situation where the stability of the equilibrium point changes as s varies.

Numerically, the objective is to identify Saddle-Node bifurcations in the nonlinear function described by Equation 1.1. The system will be solved by employing the Newton-Raphson numerical method, where q and r are fixed while treating s as the parameter. The implementation specifics of this method can be found in Appendix B.1.

$$\begin{cases} f(u_0, s_0) = r + s(q - s)\frac{u^2}{1+u^2} - u = 0, \\ \frac{\partial}{\partial u}f(u_0, s_0) = \frac{2qs_0u_0 - 2s_0^2u_0 - (u_0^2+1)^2}{(u_0^2+1)^2} = 0. \end{cases} \quad (1.7)$$

The expression $s(q - s)$ can be considered as $a(s, q)$ for convenience. Solving system 1.7, we obtain $a(s, q) = \frac{(1+u^2)^2}{2u}$. Substituting this expression into f , it gives:

$$\tilde{f}(u) = u^3 - u + 2r. \quad (1.8)$$

Once Equation 1.8 has been solved for $r = 0.14$, the subsequent step involves solving the following equation for $q = 3$ and the specific positive values of u , considering it must be biologically meaningful, as there can only be positive concentrations of proteins:

$$-s^2 + sq = \frac{(1 + u^2)^2}{2u}. \quad (1.9)$$

Hence:

u_{0_i}	$s_{0_{1_i}}$	$s_{0_{2_i}}$
0.309706449507606	0.942318787810669	2.057681212189331
0.808506228591647	0.752459879654676	2.247540120345324

Table 1.1: Values of u_{0_i} and s_{0_i} for $i \in \{1, 2\}$.

1.2.2 Transcritical Bifurcation: Lemma of Morse

Describing f as in the beginning of the previous section:

Theorem 1.12. (Transcritical Bifurcation [23]) Assume

$$\frac{\partial f}{\partial x}(x_0, \lambda_0) = 0, \quad \frac{\partial f}{\partial \lambda}(x_0, \lambda_0) = 0, \quad A_{11}A_{22} - A_{12}^2 < 0, \quad A_{11} \neq 0,$$

where

$$A_{11} := \frac{\partial^2 f}{\partial x^2}(x_0, \lambda_0), \quad A_{12} := \frac{\partial^2 f}{\partial \lambda \partial x}(x_0, \lambda_0), \quad A_{22} := \frac{\partial^2 f}{\partial \lambda^2}(x_0, \lambda_0)$$

Then, there exist two curves of fixed points given by $x_{\pm} : (\lambda_0 - \eta, \lambda_0 + \eta) \rightarrow \mathbb{R}, C^{\infty}$, such that

- (1) $x_{\pm}(\lambda_0) = x_0,$
- (2) $f(x_{\pm}(\lambda), \lambda) = 0.$
- (3) $x'_{\pm}(\lambda_0) = (-A_{12} \pm \sqrt{A_{12}^2 - A_{11}A_{22}}) / A_{11},$

In order to prove Theorem 1.12, let us define the concept of the index of a non-degenerate critical point, *i.e.*, a point where the Hessian is non-singular.

Definition 1.13. (Index) *The index of a non-degenerate critical point is the number of negative eigenvalues of the Hessian matrix.*

The Morse lemma [21] allows for the local characterization of non-degenerate critical points of a function based on their index. In order to prove this theorem, we will employ the method of deformation or homotopy [13] in conjunction with Differential Equations.

Definition 1.14. (Homotopy) *Let X and Y be topological spaces, and let $f_0, f_1 : X \rightarrow Y$ be continuous maps. We say that f_0 and f_1 are homotopic if there exists a continuous map $F : X \times [0, 1] \rightarrow Y$ such that $F(x, 0) = f_0(x)$ and $F(x, 1) = f_1(x)$. In this case, we write $f_0 \sim F \sim f_1$ and we say that the map F is a homotopy between f_0 and f_1 .*

Theorem 1.15. (Lemma of Morse) *Let $f : U \rightarrow \mathbb{R}$ be a C^3 function defined on the open set $U \subset \mathbb{R}^n$. Suppose $x_0 \in U$ is a non-degenerate critical point of f with index s . Then, there exists a C^1 diffeomorphic immersion $G : V \rightarrow U$, where $V \subset \mathbb{R}^n$ is an open set, such that $g = f \circ G : V \rightarrow \mathbb{R}$ is of the form*

$$g(x) = f(x_0) - x_1^2 - \dots - x_s^2 + x_{s+1}^2 + \dots + x_n^2.$$

Before proceeding with the proof of the theorem, we will introduce the Lemma of Hadamard [41], which will be used in the proof. Firstly, let us define the concept of convexity of subsets:

Definition 1.16. (Convex subset) *A subset S of a vector space X over K is convex if, whenever S contains two points x and y , S also contains the segment of the straight line joining them, *i.e.*,*

$$\forall x, y \in S, \forall \alpha, \beta \in \mathbb{R} \text{ such that } \alpha, \beta \geq 0 \text{ and } \alpha + \beta = 1, \text{ we have } \alpha x + \beta y \in S.$$

Lemma 1.17. (Lemma of Hadamard [41]) *Let f be a C^∞ function in a convex neighborhood V of 0 in \mathbb{R}^n , with $f(0) = 0$. Then*

$$f(x_1, \dots, x_n) = \sum_{i=1}^n x_i g_i(x_1, \dots, x_n)$$

for some suitable C^∞ functions g_i defined in V , with $g_i(0) = \frac{\partial f}{\partial x_i}(0)$.

Proof. We have

$$f(x_1, \dots, x_n) = \int_0^1 \frac{d}{dt} f(tx_1, \dots, tx_n) dt = \int_0^1 \sum_{i=1}^n \frac{\partial}{\partial x_i} f(tx_1, \dots, tx_n) x_i dt.$$

In the first equality, we have used the Fundamental Theorem of Calculus, which states that if $F(t)$ is an antiderivative of $f(t)$, then $\int_a^b f(t) dt = F(b) - F(a)$. In this case $F(t) = f(tx_1, \dots, tx_n)$, we have

$$f(x_1, \dots, x_n) = f(x_1, \dots, x_n) - f(0, \dots, 0).$$

For the second equality, by using the chain rule, we express the derivative as a sum of partial derivatives.

Therefore, we can define functions $g_i(x_1, \dots, x_n)$ as follows:

$$g_i(x_1, \dots, x_n) = \int_0^1 \frac{\partial}{\partial x_i} f(tx_1, \dots, tx_n) dt.$$

□

At this stage, the proof of Theorem 1.15 can be presented:

Proof of Theorem 1.15. Assume that $x_0 = 0$ and $f(x_0) = 0$ by making appropriate translations. Similarly, the open ball U centered at $x_0 = 0$ can also be assumed. By applying the Hadamard lemma (1.17), the following expression can be obtained:

$$f(x) = \sum_{i=1}^n x_i F_i(x), \quad F_i(x) = \int_0^1 \frac{\partial}{\partial x_i} f(tx_1, \dots, tx_n) dt.$$

For easier notation, let us consider writing $tx = (tx_1, \dots, tx_n)$. Since $F_i(0) = 0$ for $i = 1, \dots, n$, applying the Hadamard lemma again on F_i , we have:

$$F_i(x) = \frac{1}{2} \sum_{j=1}^n x_j H_{ij}(x), \quad H_{ij}(x) = 2 \int_0^1 \frac{\partial^2 f}{\partial x_i \partial x_j}(\mu x) d\mu = 2 \int_0^1 \int_0^1 \frac{\partial^2 f}{\partial x_i \partial x_j}(\mu tx) \mu d\mu dt.$$

Defining the vector function $F(x) = (F_i(x))_i$ and the symmetric matrix function $H(x) = (H_{ij}(x))_{ij}$, we easily obtain the following identities:

$$f(x) = F(x)^T x = \frac{1}{2} x^T H(x) x, \quad F(x) = \frac{1}{2} H(x) x.$$

The differential matrix of $G(x)$ is denoted as $DG(x)$. Using the differentiation rule for transposed matrices, we find that the differential of the transposed function, $D(F(x)^T)$, is equivalent to the transpose of the differential matrix, $(DF(x))^T$. Employing the property that for any matrix F and vector x , the product $x^T F$ equals Fx and applying the product rule for differentiation:

$$Df(x) = (DF(x))^T x + F(x) = x^T DF(x) + F(x).$$

Next, we express $DF(x)$ in terms of $H(x)$.

$$DF(x) = \frac{1}{2} DH(x) x + \frac{1}{2} H(x).$$

Substituting $DF(x)$ into the expression for $Df(x)$, we get

$$Df(x) = x^T \left(\frac{1}{2}DH(x)x + \frac{1}{2}H(x) \right) + F(x) = x^T(DF(x) + \frac{1}{2}H(x)).$$

Note that due to regularity properties, since f is C^3 , then F is C^2 and H is C^1 . Furthermore, $H(0) = D^2f(0) = Hf(0)$ is the Hessian matrix at the critical point, and $DF(0) = \frac{1}{2}H(0)$.

In order to find the function F , we will define immediately a homotopy represented by Φ_t . This homotopy enables us to gradually deform the function f while preserving its critical properties. Through this deformation process, we aim to simplify f and determine the appropriate function F .

Let us define the homotopy $\Phi_t = \Phi_t(t; 0, \cdot)$, induced by a non-autonomous vector field $X_t = X(t, \cdot)$, such that

$$f_t(x) = (1-t)\frac{1}{2}x^T H(0)x + t\frac{1}{2}x^T H(x)x,$$

satisfies $f_t \circ \Phi_t = f_0$ for all $t \in [0, 1]$ in a neighborhood of 0. Therefore, for $F = \Phi_1$, we have $f \circ F = f_0$, which is a quadratic function. The result will follow from the theorem of diagonalization of quadratic forms [4] and Sylvester's inertia law [2].

Theorem 1.18. (Sylvester's Law of Inertia) *Given a real quadratic form $Q : \mathbb{R}^n \rightarrow \mathbb{R}$, which can be represented in the form:*

$$Q(\mathbf{x}) = \sum_{i=1}^n a_i x_i^2$$

for some coefficients $a_i \in \{0, 1, -1\}$, and for a suitable non-singular linear transformation, the quadratic form Q can be transformed to a diagonal form.

The law of inertia then states that the number of positive, negative, and zero coefficients a_i are invariants of Q . This means, regardless of the choice of diagonalizing basis, the count of positive, negative, and zero coefficients remains the same. In mathematical notation, the number of $a_i > 0$, $a_i = 0$, and $a_i < 0$ are conserved under any suitable basis transformation.

The rate of change of f_t along the flow lines of X_t can be represented by $\frac{\partial}{\partial t}(f_t \circ \Phi_t)$. If we focus on a critical point of f_t , by definition, the rate of change of f_t at this point along any direction, including along the flow lines of X_t , should be zero.

Thus, $\Phi_t = \Phi(t; 0, \cdot)$, where Φ is the evolutionary process of an ordinary differential equation $\dot{x} = X_t(x)$, must satisfy the equation:

$$0 = \frac{\partial}{\partial t}(f_t \circ \Phi_t) = \frac{\partial f_t}{\partial t}(\Phi_t(x)) + Df_t(\Phi_t(x))\frac{\partial \Phi_t}{\partial t} = \frac{\partial f_t}{\partial t}(\Phi_t(x)) + Df_t(\Phi_t(x))X_t(\Phi_t(x)).$$

Here, $\frac{\partial f_t}{\partial t}(x)$ represents the partial derivative of f_t with respect to t , and $Df_t(x)$ denotes the derivative of f_t with respect to x . Since Φ_t is a diffeomorphic immersion, the derivative of Φ_t with respect to t can be expressed as $X_t(\Phi_t(x))$. Therefore, the equation simplifies to:

$$\frac{\partial f_t}{\partial t}(x) + Df_t(x)X_t(x) = 0 \quad (1.10)$$

We obtain an equation for the non-autonomous vector field X_t . Since

$$\frac{\partial f_t}{\partial t}(x) + Df_t(x)X_t(x) = x^T \left(\frac{1}{2}(H(x) - H(0))x + \left(H(0) + t \left(\frac{1}{2}DH(x) + H(x) - H(0) \right) \right) X_t(x) \right).$$

we have

$$\frac{\partial f_t}{\partial t}(x) + Df_t(x)X_t(x) = x^T \left(\frac{1}{2}(H(x) - H(0))x + \left(H(0) + t \left(DF(x) + \frac{1}{2}H(x) - H(0) \right) \right) X_t(x) \right).$$

Let us define $H(0) + t(DF(x) + \frac{1}{2}H(x) - H(0)) = H_t(x)$. To make 1.10 vanish, we take

$$X_t(x) = \frac{1}{2}H_t(x)^{-1}(H(x) - H(0))x,$$

where $H_t(0)$ is non-degenerate for all $t \in \mathbb{R}$, then there exists a neighborhood $U_1 \subset U$ of 0 such that $H_t(x)$ is non-degenerate for $t \in (-\frac{1}{2}, \frac{3}{2})$. Thus, as $H_t(x)$ remains invertible in U_1 , $X_t(x)$ is defined in the open set $\Omega = (-\frac{1}{2}, \frac{3}{2}) \times U_1$.

Since X_t is C^1 , the associated evolutionary process Φ is C^1 in an open set $D \subset (-\frac{1}{2}, \frac{3}{2}) \times \Omega$. Furthermore, $X_t(0) = 0$ for all $t \in (-\frac{1}{2}, \frac{3}{2})$, and thus $\Phi(t; t_0, 0) = 0$ for all $t, t_0 \in (-\frac{1}{2}, \frac{3}{2})$. In particular, there exists a neighborhood $V \subset U_1$ of 0 such that $(t; 0, x) \in D$ for all $t \in (-\frac{1}{4}, \frac{5}{4})$ and $x \in V$.

Therefore, $G = \Phi_1 : V \rightarrow U$ satisfies $f \circ G = f_0$. \square

We have seen that the Morse lemma is a fundamental theorem in Differential Topology that relates the geometry of a smooth function close to a critical point. Now we are ready to prove Theorem 1.12:

Proof of 1.12. Let us consider the Hessian matrix of f :

$$H = \begin{bmatrix} A_{11} & A_{12} \\ A_{21} & A_{22} \end{bmatrix}.$$

The determinant of H , denoted as $\text{Det}(H)$, is defined as $\text{Det}(H) = A_{11}A_{22} - A_{12}A_{21}$. By hypothesis, it is negative, which implies that H is non-degenerate, as it is not zero.

By applying the Morse Lemma, we can assert that there exists a local diffeomorphism

$$h : (0, 0) \in J_1 \times J_2 \longrightarrow I_0 \times \Lambda_0 \ni (x_0, \lambda_0) \\ (j_1, j_2) \mapsto (x, \lambda)$$

such that $h(0, 0) = (x_0, \lambda_0)$ and $f \circ h(j_1, j_2) = j_1 j_2$.

Taking $h^{-1} = (j_1, j_2)$, there exists $j_1, j_2 : I_0 \times \Lambda_0 \longrightarrow \mathbb{R}$ that are C^∞ such that for every $(x, \lambda) \in I_0 \times \Lambda_0$:

- $f(x, \lambda) = j_1(x, \lambda)j_2(x, \lambda)$,

- $\begin{vmatrix} \partial_x j_1 & \partial_\lambda j_1 \\ \partial_x j_2 & \partial_\lambda j_2 \end{vmatrix} \neq 0$, as at least $\partial_x j_1$ or $\partial_x j_2 \neq 0$ at (x_0, λ_0) ,
- $j_1(x_0, \lambda_0) = j_2(x_0, \lambda_0) = 0$.

From the hypothesis conditions, we note that $j_1(x_0, \lambda_0) = j_2(x_0, \lambda_0) = 0$.

We then translate the conditions over j_1, j_2 on conditions over f :

$$\begin{aligned} \frac{\partial f}{\partial x} &= \frac{\partial j_1}{\partial x} j_2 + j_1 \frac{\partial j_2}{\partial x}, \\ \frac{\partial f}{\partial \lambda} &= \frac{\partial j_1}{\partial \lambda} j_2 + j_1 \frac{\partial j_2}{\partial \lambda}, \\ \frac{\partial^2 f}{\partial x^2} &= \frac{\partial^2 j_1}{\partial x^2} j_2 + 2 \frac{\partial j_1}{\partial x} \frac{\partial j_2}{\partial x} + j_1 \frac{\partial^2 j_2}{\partial x^2}, \\ \frac{\partial^2 f}{\partial \lambda^2} &= \frac{\partial^2 j_1}{\partial \lambda^2} j_2 + 2 \frac{\partial j_1}{\partial \lambda} \frac{\partial j_2}{\partial \lambda} + j_1 \frac{\partial^2 j_2}{\partial \lambda^2}, \\ \frac{\partial^2 f}{\partial x \partial \lambda} &= \frac{\partial^2 j_1}{\partial x \partial \lambda} j_2 + \frac{\partial j_1}{\partial x} \frac{\partial j_2}{\partial \lambda} + j_1 \frac{\partial^2 j_2}{\partial \lambda^2} + \frac{\partial j_1}{\partial \lambda} \frac{\partial j_2}{\partial x}. \end{aligned}$$

The determinant of the Hessian of f evaluated at (x_0, λ_0) is then given by:

$$\begin{vmatrix} 2\partial_x j_1 \partial_x j_2 & \partial_x j_1 \partial_\lambda j_2 + \partial_\lambda j_1 \partial_x j_2 \\ \partial_x j_1 \partial_\lambda j_2 + \partial_\lambda j_1 \partial_x j_2 & 2\partial_\lambda j_1 \partial_\lambda j_2 \end{vmatrix} = -(\partial_x j_1 \partial_\lambda j_2 - \partial_\lambda j_1 \partial_x j_2)^2 < 0,$$

which is not equal to zero since

$$\begin{vmatrix} \partial_x j_1 & \partial_\lambda j_1 \\ \partial_x j_2 & \partial_\lambda j_2 \end{vmatrix} \neq 0.$$

From the transcritical bifurcation, we find that $f_{xx}(x_0, \lambda_0) \neq 0$, which implies $\partial_x j_1(x_0, \lambda_0) \partial_x j_2(x_0, \lambda_0) \neq 0$.

Let us analyze this locally. Given $f_{xx}(x_0, \lambda_0) \neq 0$, then there exist $\bar{x}_1, \bar{x}_2 : \Lambda_0 \rightarrow I_0$ that are C^∞ such that

$$\{(x, \lambda) \in I_0 \times \Lambda_0 : g(x, \lambda) = 0\} = \{(\bar{x}_-(\lambda), \lambda) | \lambda \in \Lambda_0\} \cup \{(\bar{x}_+(\lambda), \lambda) | \lambda \in \Lambda_0\}.$$

Now we can prove (1) and (2) by rewriting noting that:

1. $0 = f(x_\pm(\lambda), \lambda)$, meaning that $x_\pm(\lambda)$ is a root of the function f for each λ ,
2. $0 = \partial_x f(x_\pm(\lambda), \lambda) x'_\pm(\lambda) + \partial_\lambda f(x_\pm(\lambda), \lambda)$.

By taking the derivative again, we get

$$0 = \partial_{xx} f(x_\pm(\lambda), \lambda) (x'_\pm(\lambda))^2 + 2\partial_{x\lambda} f(x_\pm(\lambda), \lambda) x'_\pm(\lambda) + \partial_x f(x_\pm(\lambda), \lambda) x''_\pm(\lambda) + \partial_{\lambda\lambda} f(x_\pm(\lambda), \lambda).$$

Evaluating at $\lambda = \lambda_0$ and $x_\pm(\lambda) = x_0$, we get

$$x'_{\pm}(\lambda_0) = \frac{-\partial_{x\lambda}g(x_0, \lambda_0) \pm \sqrt{(\partial_{x\lambda}g(x_0, \lambda_0))^2 - \partial_{xx}g(x_0, \lambda_0)\partial_{\lambda\lambda}g(x_0, \lambda_0)}}{\partial_{\lambda\lambda}g(x_0, \lambda_0)},$$

which proves (3).

In conclusion, the transcritical bifurcation conditions are satisfied, and the proof is complete.

We aim to study the stability of the two curves. For simplicity, we denote \pm as \pm and similarly for x_0 and λ_0 .

The derivative of f at \pm and λ can be expanded as:

$$\frac{\partial f}{\partial x}(x_{\pm}, \lambda) = \frac{\partial f}{\partial x}(x_0, \lambda_0) + \frac{\partial^2 f}{\partial x^2}(x_{\pm}, \lambda_0)x'_{\pm}(\lambda_0) + \frac{\partial^2 f}{\partial x \partial \lambda}(x_{\pm}, \lambda_0)(\lambda - \lambda_0) + O((\lambda - \lambda_0)^2).$$

We have $0 = f(x_{\pm}, \lambda)$, and thus $\frac{\partial f}{\partial x}(x_{\pm}, \lambda)$ can be rewritten as:

$$\frac{\partial f}{\partial x}(x_{\pm}, \lambda) = 0 \pm \sqrt{-\det(\text{Hessian}(f(x_0, \lambda_0)))} + O(\lambda - \lambda_0)^2.$$

The stability of the curves $x_{\pm}(\lambda)$ is then determined by the sign of the right-hand side. The \pm sign implies that the stability of $x_{\pm}(\lambda)$ changes at the bifurcation value $\lambda = \lambda_0$. When the square root term is positive, $x_{\pm}(\lambda)$ is stable, and when it is negative, $x_{\pm}(\lambda)$ is unstable. The term $O((\lambda - \lambda_0)^2)$ indicates the error when approximating near $\lambda = \lambda_0$, and it tends to 0 as λ approaches λ_0 . \square

Theorem 1.12 can also be proven based on interpreting it from a Hamiltonian point of view. This approach involves the introduction of a lemma by Liu *et al.* [39] which addresses the existence of two intersecting curves. let us first introduce the (Un)Stable Manifold Theorem [44].

Theorem 1.19. (The Stable Manifold Theorem) *Let E be an open subset of \mathbb{R}^n containing the origin, let $f \in C^1(E)$, and let ϕ_t be the flow of the nonlinear system $\dot{x} = f(x)$. Suppose that $f(0) = 0$ and that $Df(0)$ has k eigenvalues with negative real part and $n - k$ eigenvalues with positive real part. Then there exists a k -dimensional differentiable manifold S tangent to the stable subspace E^s of the linear system $\dot{x} = Df(x_0)x$ at 0 such that for all $t \geq 0$, $\phi_t(S) \subseteq S$ and for all $x_0 \in S$,*

$$\lim_{t \rightarrow \infty} \phi_t(x_0) = 0.$$

Similarly, there exists an $(n - k)$ -dimensional differentiable manifold U tangent to the unstable subspace E^u of $\dot{x} = Df(x_0)x$ at 0 such that for all $t \leq 0$, $\phi_t(U) \subseteq U$ and for all $x_0 \in U$,

$$\lim_{t \rightarrow -\infty} \phi_t(x_0) = 0.$$

Lemma 1.20. *Suppose that $(x_0, y_0) \in \mathbb{R}^2$ and U is a neighborhood of (x_0, y_0) . Assume that $f : U \rightarrow \mathbb{R}$ is a C^p function for $p \geq 2$, $f(x_0, y_0) = 0$, $\nabla f(x_0, y_0) = 0$, and the Hessian $H = H(x_0, y_0)$ is non-degenerate. If H is indefinite, then there exist two C^{p-1} curves $(x_i(s), y_i(s))$, $i = 1, 2$, $s \in (-\delta, \delta)$, such that the solution set of $f(x, y) = 0$ consists of exactly the two curves near (x_0, y_0) , $(x_i(0), y_i(0)) = (x_0, y_0)$. Moreover, t can be rescaled and indices can be rearranged so that $(x'_1(0), y'_1(0))$ and $(x'_2(0), y'_2(0))$ are the two linear independent solutions of*

$$f_{xx}(x_0, y_0)\eta^2 + 2f_{xy}(x_0, y_0)\eta\tau + f_{yy}(x_0, y_0)\tau^2 = 0. \quad (1.11)$$

Proof. Consider the differential equation described by the following Hamiltonian system:

$$\dot{x} = \frac{\partial f(x, y)}{\partial y}, \quad \dot{y} = -\frac{\partial f(x, y)}{\partial x}, \quad (x(0), y(0)) \in U. \quad (1.12)$$

Here, $f(x, y)$ represents the potential function, and (x_0, y_0) is the only equilibrium point within the region U . The Jacobian of this Hamiltonian at (x_0, y_0) is given by:

$$J = \begin{bmatrix} f_{xy}(x_0, y_0) & f_{yy}(x_0, y_0) \\ -f_{xx}(x_0, y_0) & -f_{xy}(x_0, y_0) \end{bmatrix} \quad (1.13)$$

Since the trace of J is zero, and the determinant of J is negative, it follows that (x_0, y_0) is a saddle-type equilibrium of the system described in Eq. (1.12). The eigenvalues of J are $\pm k$ for some positive k .

Based on the theory of invariant manifolds in differential equations, there exist two unique curves, namely the stable manifold Γ_s and the unstable manifold Γ_u , both lying within the region U . These curves are invariant under the dynamics of the system, and for initial conditions $(x(0), y(0)) \in \Gamma_s$ or Γ_u , the trajectory $(x(s), y(s)) \rightarrow (x_0, y_0)$ as t approaches infinity or negative infinity, respectively. According to the stable and unstable manifold theorem, both Γ_s and Γ_u are C^{p-1} one-dimensional manifolds.

On $\Gamma_s \cup \Gamma_u \cup \{(x_0, y_0)\}$, the Hamiltonian function $f(x, y)$ equals zero since it represents the potential function of the system. Conversely, for any point (x, y) not lying on $\Gamma_s \cup \Gamma_u \cup \{(x_0, y_0)\}$, the function $f(x, y)$ does not equal zero. This property is a consequence of the Morse lemma, indicating that the C^{p-1} curves must coincide with $\Gamma_s \cup \Gamma_u$.

Lastly, let us consider the tangential direction of Γ_s and Γ_u . Denoting the curves as $(x_i(s), y_i(s))$ for $i = 1, 2$, we have:

$$f(x_i(t), y_i(s)) = 0. \quad (1.14)$$

Differentiating equation (1.14) twice with respect to t :

$$\begin{aligned} f_{xx}(x(s), y(s))(x'(s))^2 + 2f_{xy}(x(s), y(s))x'(s)y'(s) + f_{yy}(x(s), y(s))y'(s)^2 \\ + f_x(x(s), y(s))x''(s) + f_y(x(s), y(s))y''(s) = 0 \end{aligned}$$

and evaluating at $s = 0$ with $\nabla f(x_0, y_0) = 0$, we obtain equation (1.11). \square

Remark 1.21. If we prove theorem 1.12 using the Lemma of Morse, we deduce the curves belong to the class C^{p-2} since this Lemma is applicable for functions C^p for $p \geq 3$. Alternatively, if we apply Hamiltonian arguments, the regularity condition is $p \geq 1$, therefore we conclude that the curves are C^{p-1} . See Appendix A.1.1 to see a proof of Theorem 1.12 using Hamiltonian arguments.

Corollary 1.22. *If the determinant of the Hessian matrix of a smooth function $f(x, \lambda)$ at a non-degenerate critical point is positive, then the function exhibits isolas in a small neighborhood around the critical point.*

Proof. By hypothesis, the Hessian matrix H of f is positive, therefore, H is non-degenerate, as it is not zero. By applying the Morse Lemma, we can assert that there exists a local diffeomorphism

$$h : (0, 0) \in J_1 \times J_2 \longrightarrow I_0 \times \Lambda_0 \ni (x_0, \lambda_0) \\ (j_1, j_2) \mapsto (x, \lambda)$$

such that $h(0, 0) = (x_0, \lambda_0)$ and $(f \circ h)(j_1, j_2) = j_1^2 + j_2^2$, where we assume without loss of generality that $\partial_{xx}f > 0$, in case it was negative, we define $f \circ h(j_1, j_2) = -j_1^2 - j_2^2$. Distinctly as in the case of the transcritical bifurcation, here the level of function $f(x, \lambda) = 0$ is just a point. The set of points satisfying the equation $f \circ h(j_1, j_2) = 0$ forms a set of isolas in the j_1 - j_2 plane. Since the transformation h is a local diffeomorphism, these isolas map to a set of isolas in the x - λ plane.

The equation $(f \circ h)(j_1, j_2) = 0$ implies $j_1^2 + j_2^2 = 0$, which corresponds to the point $(0, 0)$. Now, if we look at a small neighborhood around $(0, 0)$, the equation $(f \circ h)(j_1, j_2) = c$ for small $c > 0$ describes a set of points forming a circle with radius \sqrt{c} around the origin. This is due to the fact that for small $c > 0$, $j_1^2 + j_2^2 = c$ corresponds to a circle with radius \sqrt{c} in the j_1 - j_2 plane.

When these circles are transformed by h into the x - λ plane, they form isolas in a small neighborhood around the critical point (x_0, λ_0) . This is possible because the transformation h preserves the topology of the small neighborhood around the origin, and thus the isolas in the j_1 - j_2 plane become isolas in the x - λ plane.

Therefore, if the determinant of the Hessian matrix of a smooth function $f(x, \lambda)$ at a non-degenerate critical point is positive, then the function exhibits isolas in a small neighborhood around the critical point. This argument relies on the local structure of the function around the critical point, captured by the Morse Lemma, and the positive determinant of the Hessian matrix ensuring a non-degenerate critical point. \square

Application to Equation 1.1

The transcritical bifurcation with respect to s , for a fixed r occurs when the following system is satisfied:

$$\begin{cases} 0 = f(u, s, q) = r + a(s, q)g(u) - u, \\ 0 = \frac{\partial f}{\partial u} = a(s, q)g'(u) - 1, \\ 0 = \frac{\partial f}{\partial s} = a'(s, q)g(u), \\ 0 = \frac{\partial^2 f}{\partial u^2} \frac{\partial^2 f}{\partial s^2} - \frac{\partial^2 f}{\partial s \partial u}^2, \\ 0 = \frac{\partial^2 f}{\partial u^2} = a(s, q)g''(u). \end{cases} \quad (1.15)$$

As $a(s, q)$ is parabola-shaped, there exists $a'(s_0, q_0)$ such that $a(s_0, q_0)$ is maximized. Consider u_* the inflection point, and let $g'(u_*) = D$. Based on the constraint $g'(u) > 0$, we have three cases:

1. If $\frac{1}{a(s_0, q_0)} > D$, there are no solutions to system 1.6 .
2. If $\frac{1}{a(s_0, q_0)} = D$, then $u = u_*$, the inflection point. We find $a(s_0, q_0) = -\frac{r-u_*}{g(u_*)}$. The Hessian matrix of f at (u_0, s_0, q_0) in this case is singular. Due to the non-degeneracy conditions of system 1.6, there are still no solutions to the system.
3. If $\frac{1}{a(s_0, q_0)} < D$, there exist $u_- < u_* < u_+$ such that $g'(u_{\pm}) = \frac{1}{a(s_0)}$. We have $a(s_0, q_0) = -\frac{r-u_{\pm}}{g(u_{\pm})}$. Consider u_+ :

$$a(s_0)g''(u_+)a''(s_0)g(u_+) > 0$$

Therefore, the isola condition is met, given $g''(u_+) < 0$.

Consider u_- :

$$a(s_0)g''(u_-)a''(s_0)g(u_+) < 0$$

Therefore, there is a transcritical bifurcation, given $g''(u_+) > 0$.

The stability of the two branches involved in the bifurcation is determined by the sign of the second derivative of f with respect to u , which is $\frac{\partial^2 f}{\partial u^2}(s_0, \pm u_{\pm})$, given the second derivative provides information about the local curvature of f at these fixed points. If the second derivative of f with respect to u is negative at a particular fixed point, it indicates that the function f is locally concave at this point, indicating stability. Conversely, if the second derivative of f with respect to u is positive at a particular fixed point, f is locally convex at this point, indicating instability. The negative branch (u_-) becomes unstable as the system parameter r increases, while the positive branch (u_+) becomes stable.

Finally, if we define $a(s(q), q)$ as $s(q - s)$, the condition $s(q) = \frac{q}{2}$ is satisfied. Thus, $a(s(q), q) = \frac{q^2}{4}$.

In this section, we aim to solve the system 1.7 with the inclusion of a third equation. The system is represented as follows, considering s, q as parameters and r fixed:

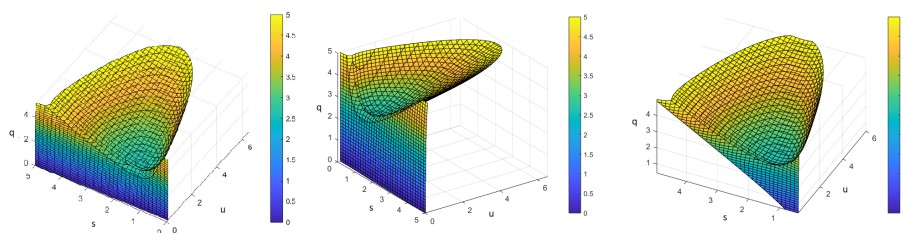


Figure 1.8: 3D representations of the mushroom bifurcation, with the values of q ranging from 0 to 5 and r fixed at 0.14. The progression from continuous trajectories to transcritical and saddle-node bifurcations can be observed.

$$\begin{cases} f(u_0, s_0) = r + s(q - s) \frac{u^2}{1 + u^2} - u = 0 \\ \frac{\partial f(u_0, s_0)}{\partial u} = \frac{2qs_0u_0 - 2s_0^2u_0 - (u_0^2 + 1)^2}{(u_0^2 + 1)^2} = 0 \\ \frac{\partial f(u_0, s_0)}{\partial s} = \frac{(q - 2s)u^2}{(1 + u_0^2)} = 0 \end{cases} \quad (1.16)$$

By analyzing these equations, we derive the relationship $a(s, q) = \frac{(1+u^2)^2}{2u}$ from equation (2), and subsequently substitute it into equation (1) to determine the corresponding value of u_0 . Equation (3) provides us with the constraint $q = 2s$. To explore the critical behavior of the system, we consider the function $f(u, s, q)$ and focus on identifying the value of q_c at which a transcritical bifurcation occurs. For our analysis, we fix the value of $r = 0.14$. Our calculations reveal a unique critical value, denoted as q_{critical} , where the transcritical bifurcation manifests.

q_{critical}	u_{critical}	s_{critical}
2.7849536194134648	0.309706449507606	1.3924768097067324

Using Corollary 1.22, it can be seen that the emergence of an isola is observed at a critical value denoted as $q_{\text{isola}} = 2.6009104317327796$. At this point, two saddle-nodes are formed within the isola, representing crucial bifurcation points. In contrast, the other branch of solutions does not exhibit any distinct behavior. Beyond the critical value q_c , the system no longer undergoes transcritical bifurcations. This finding implies that the transcritical bifurcation phenomenon ceases to occur beyond a certain threshold.

Summing up, the table below displays the properties of the system under study:

1.3 Robustness of Bifurcations: Structural Stability

A phase portrait is said to be **structurally stable** if its topology cannot be changed by an arbitrarily small perturbation to the vector field [55].

Value of q	Value of s	Bifurcation
$0 < q < q_{\text{isola}}$	$s \in [0, q]$	None
$q \in (q_{\text{isola}}, q_{\text{trans}})$	$s \in [s_{\text{critic}_1}, s_{\text{critic}_2}]$ for a certain $u > 0$	One isola and two Saddle-Node bifurcations with a symmetry axis $s = q/2$
$q = q_{\text{trans}}$	$s \in [s_{\text{critic}_1}, s_{\text{critic}_2}]$ for a certain $u > 0$ such that: $\max\{r + \frac{(1+u^2)u}{2} - u = 0\}$	A Transcritical bifurcation at $s = q/2$ with 2 Saddle-Node bifurcations having a symmetry axis $s = q/2$
$q > q_{\text{critical}}$	$s \in [s_{\text{critic}_1}, s_{\text{critic}_4}]$ for certain $u_1, u_2, u_i > 0$ such that: $r + (1 + u^2)u/2 - u = 0$	Four Saddle-Node bifurcations with a symmetry axis $s = q/2$

1.3.1 Codimension 1 Bifurcations

In dynamical systems, **codimension** refers to the number of dynamic variables that are necessary to fully describe the behavior of a system in relation to the number of fixed parameters.

Given a parameter value of $r = 0.14$ and considering our dynamical system with a codimension of 1, we can establish the robustness of the saddle-node bifurcation. This implies that the saddle-node bifurcation persists and maintains its qualitative behavior in the system under small perturbations or variations of the parameter values.

Theorem 1.23. *Let $f = f(x, s, q)$ be a smooth function. If, for a fixed value q_0 , the function f undergoes a saddle-node bifurcation at the point (x_0, s_0) , then for any q within the interval $(q - \epsilon, q + \epsilon)$, where $\epsilon > 0$, the function $f(x, s, q)$ exhibits a saddle-node bifurcation at the point $(x(q), s(q))$. As a consequence, the function $f(x, s, q)$ is structurally stable.*

Proof. By adjusting q within a neighborhood of q_c , we produce a smooth disturbance in the dynamical system. For the system represented by $f(x, s, q)$, we have the associated Jacobian matrix as follows:

$$J = \begin{bmatrix} \frac{\partial f}{\partial x}(x_c, s_c, q_c) & \frac{\partial f}{\partial s}(x_c, s_c, q_c) \\ \frac{\partial^2 f}{\partial x^2}(x_c, s_c, q_c) & \frac{\partial^2 f}{\partial x \partial s}(x_c, s_c, q_c) \end{bmatrix}$$

Under the given hypothesis, the Jacobian matrix J is nonsingular. Thus, by applying the Implicit Function Theorem, we can infer the existence of a unique smooth curve of solutions to the system given by

$$\begin{cases} x = x(q), \\ s = s(q) \end{cases}$$

with $x(q_c) = x_c$ and $s(q_c) = s_c$. Consequently, for q in a neighborhood of q_c , it holds that $f(x, s, q)$ exhibits a saddle-node bifurcation at the point $(x(q), s(q))$. \square

Remark 1.24. The Jacobian matrix has dimensions of 2x2 in this context because the variable q is treated as a parameter rather than a variable. Specifically, the Jacobian

matrix characterizes the relationship between changes in the variables x and s and their corresponding effects on the values of f and f_x , while keeping the parameter q constant.

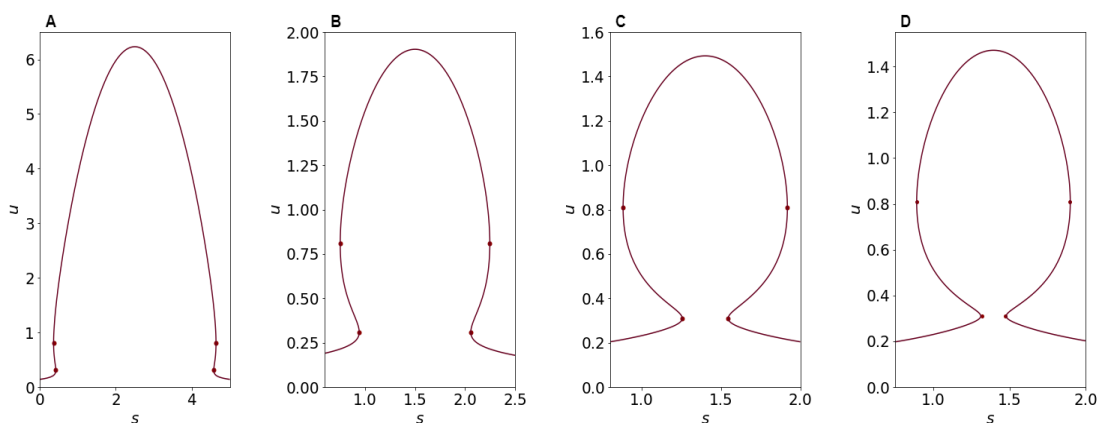


Figure 1.9: Structural stability of the four saddle-nodes for different values of q and their corresponding bifurcation parameter (s) values : (a) $q=5$, (b) $q=3$, (c) $q=2.8$, (d) $q=2.79$.

However, it is important to note that the transcritical bifurcation is not robust in this context. This is evident as it occurs only for one isolated value of the parameter q , indicating that slight changes or perturbations in the parameter value can cause the transcritical bifurcation to disappear or transition into a different type of bifurcation.

1.3.2 Codimension 2 Bifurcations

Due to the inherent robustness of the codimension 1 saddle-node bifurcation, we can assert that if the system exhibits this bifurcation for a specific parameter, it will continue to exhibit similar qualitative behavior when subjected to perturbations in a new parameter, therefore the structural stability holds for the codimension 2 scenario as well.

If we introduce a parameter, denoted as r , that perturbs our system, we can investigate the robustness of the transcritical bifurcation:

Theorem 1.25. *Let $f = f(x, s, q, r)$ be a smooth function. If, for a fixed value r_0 , the function f undergoes a transcritical bifurcation at the point (x_0, s_0, q_0) , then for any r in a sufficiently small neighbourhood $(r - \delta, r + \delta)$, where $\delta > 0$, the function $f(x, s, q, r)$ exhibits a transcritical bifurcation at the point $(x(r), s(r), q(r))$. As a consequence, the function $f(x, s, q, r)$ is structurally stable.*

Proof. By adjusting r within a neighborhood of r_c , we produce a smooth disturbance in the dynamical system. For the system represented by $f(x, s, q, r)$, consider the associated Jacobian matrix as follows:

$$J = \begin{bmatrix} \frac{\partial f}{\partial x} & \frac{\partial f}{\partial s} & \frac{\partial f}{\partial q} \\ \frac{\partial^2 f}{\partial x^2} & \frac{\partial^2 f}{\partial x \partial s} & \frac{\partial^2 f}{\partial x \partial q} \\ \frac{\partial^2 f}{\partial s \partial x} & \frac{\partial^2 f}{\partial s^2} & \frac{\partial^2 f}{\partial s \partial q} \end{bmatrix}_{(x_c, s_c, q_c, r_c)}$$

Let us analyze the determinant of the Jacobian matrix, denoted as $Det(J)$, which is computed as follows:

$$Det(J) = f_x f_{xs} f_{sq} + f_{xx} f_{ss} f_q + f_{sx} f_s f_{xq} - f_q f_{xs} f_{sx} - f_{xx} f_s f_{sq} - f_x f_{ss} f_{xq}.$$

This determinant is evaluated at the point (x_c, s_c, q_c, r_c) . Given the conditions that $f_x = 0$ and $f_s = 0$, the determinant simplifies to:

$$Det(J) = f_q (f_{xx} f_{ss} - f_{xs}^2)$$

According to the Transcritical Bifurcation theorem 1.12, for the system to exhibit a transcritical bifurcation, it is necessary that the expression $f_{xx} f_{ss} - f_{xs}^2$ is negative. Additionally, to ensure the form of a transcritical bifurcation, the coefficient f_q must not equal zero. As a consequence, the determinant of the Jacobian matrix, denoted as $Det(J)$, is non-zero. Hence, we can apply the implicit function theorem once again. This theorem guarantees the existence of a unique smooth curve of solutions to the system represented by:

$$\begin{cases} x = x(r), \\ s = s(r), \\ q = q(r) \end{cases}$$

with $x(r_c) = x_c, s(r_c) = s_c$. Consequently, for r in a neighborhood of r_c , it holds that $f(x, s, q, r)$ exhibits a transcritical bifurcation at the point $(x(r), s(r), q(r))$. \square

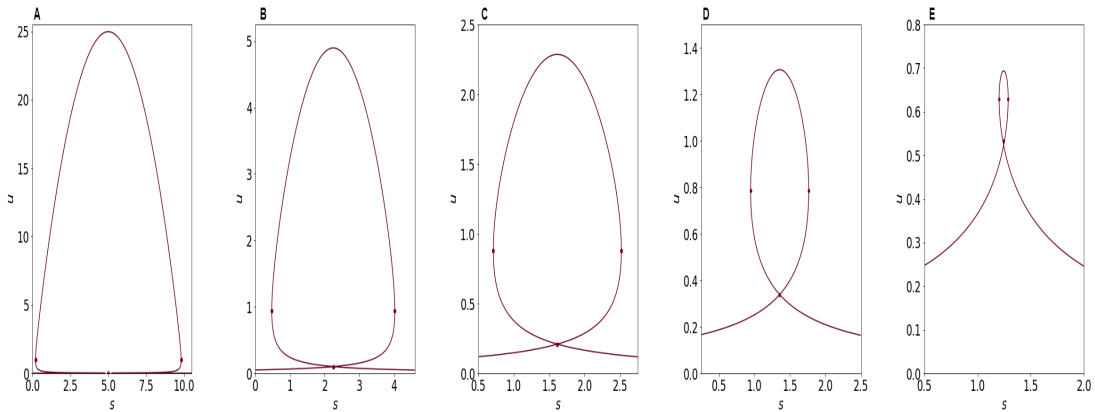


Figure 1.10: Structural stability of the transcritical bifurcation - and the two saddle-nodes - for different values of r and their corresponding bifurcation parameter (s, q) values : (A) $r=0.01$, (B) $r=0.05$, (C) $r=0.1$, (D) $r=0.15$, (E) $r=0.19$.

Chapter 2

Deterministic Study of Delayed Transitions

2.1 Bottleneck effect

The dynamics of complex systems involve intricate interactions and transitions influenced by multiple factors. To comprehensively understand these dynamics and transitions, it is crucial to examine the underlying system structure, behavior, and their response to perturbations. This section focuses on a specific phenomenon in system dynamics known as the bottleneck effect.

In the field of dynamical systems, the bottleneck effect [6,11,18,51], occurs when the system's evolution undergoes a significant slowdown due to a "bottleneck" in its phase space. This effect becomes apparent when the system encounters regions that force it to spend an extended period of time within them, resulting in a perceived delay in the overall system evolution. One particular manifestation of this phenomenon is known as a "delayed transition" or "ghost", which arises right after a saddle-node bifurcation:

Definition 2.1. (Ghost) *A delayed transition or ghost is defined as a region G in the phase space Ω where the system's dynamics exhibit prolonged temporal behavior characterized by reduced rates of evolution. This phenomenon arises due to the persistent influence of an attractor A , which was destroyed via a saddle-node bifurcation. The ghost region G can be described as $G = \{x \in \Omega : \phi(t, x) \approx R \text{ for } t \geq T\}$, where $\phi(t, x)$ represents the system's trajectory at time t starting from the initial condition x , R denotes the remnants of the destroyed attractor, and T is a threshold time indicating the duration for trajectories to spend near the remnants.*

In the context of bifurcation theory, the understanding of such ghost regions can lead to the derivation of scaling laws to the saddle-node. Moreover, post-bifurcation delays are also found in other bifurcations, such as the transcritical. The investigation, verification, and formalization of these delayed transitions following both types of bifurcations will be addressed in sections 2.3 and 2.4. Prior to that, we will introduce several theoretical fundamentals in the following section.

2.2 Weierstrass Preparation Theorem

In complex analysis, one of the central objects of study are holomorphic functions [33]. These are complex functions that exhibit relevant properties connected to the smoothness and differentiability of real functions.

Definition 2.2. (Holomorphic) Let $U \subset \mathbb{C}^n$ be open. A function $f : U \rightarrow \mathbb{C}$ is holomorphic if it is locally bounded and holomorphic in each variable separately. That is, f is holomorphic if it is locally bounded and complex-differentiable in each variable separately:

$$\lim_{\zeta \in \mathbb{C} \rightarrow 0} \frac{f(z_1, \dots, z_k + \zeta, \dots, z_n) - f(z)}{\zeta}$$

exists for all $z \in U$ and all $k = 1, 2, \dots, n$

The ring of holomorphic functions ties together algebra and complex analysis, by endowing the set of all holomorphic functions with the structure of a ring. Therefore, making it an algebraic object and providing a natural context for studying the properties and behavior of holomorphic functions.

Definition 2.3. (Ring of holomorphic functions) Let $U \subset \mathbb{C}^n$ be an open set. Define $\mathcal{H}(U)$ to be the ring of holomorphic functions.

The notion of a germ of a function is fundamental for comprehending the local behavior of functions. It arises from the recognition that in mathematics, our interest extends beyond the global behavior of a function to the examination of its characteristics within infinitesimally small neighborhoods of specific points.

Definition 2.4. (Germ of a function) Let p be a point in a topological space X . Let Y be a set and $U, V \subset X$ be open neighborhoods of p . We say that two functions $f : U \rightarrow Y$ and $g : V \rightarrow Y$ are equivalent if there exists a neighborhood W of p such that $f|_W = g|_W$.

An equivalence class of functions defined in a neighborhood of p is called a germ of a function.

The notation $n\mathcal{H}_p = \mathcal{H}_p$ represents the ring of germs at p of holomorphic functions.

The order of vanishing of a function at a point provides valuable insight into the behavior of the function in the vicinity of its zeros. It quantifies the number of times the function is required to pass through the origin when its argument approaches a specific value.

Suppose f is (a germ of) a holomorphic function at a point $p \in \mathbb{C}^n$. Write

$$f(z) = \sum_{k=0}^{\infty} f_k(z - p),$$

where f_k is a homogeneous polynomial of degree k , i.e., $f_k(tz) = t^k f_k(z)$.

Definition 2.5. (Order of vanishing) Let $p \in \mathbb{C}^n$ and f be a holomorphic function in a neighborhood of p . If f is not identically zero, define

$$\text{ord}_p f = \min\{k \in \mathbb{N}_0 : f_{(k)} \neq 0\}$$

If $f \equiv 0$, then define $\text{ord}_p f = \infty$. The number $\text{ord}_p f$ is called the order of vanishing of f at p .

The Weierstrass polynomial is a significant intermediary tool connecting holomorphic functions and polynomial functions. These polynomials possess a specific structure that enables them to emulate the behavior of arbitrary holomorphic functions in a particular manner.

Definition 2.6. (Weierstrass polynomial) Let $U \subset \mathbb{C}^{n-1}$ be open, and let $z' \in \mathbb{C}^{n-1}$ denote the coordinates $z' = (z'_1, \dots, z'_{n-1})$. Suppose a polynomial $P \in \mathcal{H}(U)[z_n]$, the ring of holomorphic functions defined on the open set $U \subset \mathbb{C}^{n-1}$, extended by the variable z_n , is monic of degree $k \geq 0$, that is,

$$P(z', z_n) = z_n^k + \sum_{j=0}^{k-1} c_j(z') z_n^j,$$

where c_j are holomorphic functions defined on U , such that $c_j(0) = 0$ for all j . Then, P is called a Weierstrass polynomial of degree k . If the c_j are germs in $\mathcal{H}_0 = {}_{n-1}\mathcal{H}_0$, then $P \in \mathcal{H}_0[z_n]$ and P is a germ of a Weierstrass polynomial.

The Weierstrass Preparation Theorem is a crucial result in complex analysis that establishes a relationship between holomorphic functions and Weierstrass polynomials. It serves as a powerful tool for dissecting the structure of a holomorphic function and uncovering its fundamental properties.

The objective of this section is to demonstrate that every holomorphic function within the ring \mathcal{H}_0 can be expressed, up to a unit and a possible small rotation, as a Weierstrass polynomial. This polynomial effectively represents the zeros of the original function. Consequently, the algebraic and geometric properties of \mathcal{H}_0 can be comprehended through the analysis of the algebraic and geometric properties of ${}_{n-1}\mathcal{H}_0[z_n]$.

It should be noted that definition 2.2 and theorem 2.8 remain applicable even when considering the case where $n = 1$. In such instances, the only Weierstrass polynomial of degree k is simply z^k . Additionally, when $k = 0$, the polynomial P becomes the constant function 1.

Definition 2.7. (Polydisc) For $\rho = (\rho_1, \dots, \rho_n)$, where $\rho_j > 0$ and $a \in \mathbb{C}^n$, we define the polydisc of center a and polyradius or simply radius ρ as:

$$\Delta_\rho(a) = \{z \in \mathbb{C}^n : |z_j - a_j| < \rho_j \text{ for } j = 1, 2, \dots, n\}$$

Theorem 2.8. (Weierstrass Preparation Theorem [33]) Suppose $f \in \mathcal{O}(U)$ for an open $U \subset \mathbb{C}^{n-1} \times \mathbb{C}$, where $0 \in U$ and $f(0) = 0$. Suppose $z_n \mapsto f(0, z_n)$ is not identically zero near the origin, and its order of vanishing at the origin is $k \geq 1$.

Then, there exists an open polydisc $V = V' \times D \subset \mathbb{C}^{n-1} \times \mathbb{C}$ with $0 \in V \subset U$, a unique $u \in \mathcal{O}(V)$ such that $u(z) \neq 0$ for all $z \in V$, and a unique Weierstrass polynomial P of degree k with coefficients holomorphic in V' such that

$$f(z', z_n) = u(z', z_n)P(z', z_n)$$

and such that all k zeros (counting multiplicity) of $z_n \mapsto P(z', z_n)$ lie in D for all $z' \in V'$.

Before introducing the proof, we need some one-variable previous results [33,62].

Definition 2.9. (Piecewise- C^1) A function $P \in C[a, b]$ is Piecewise- C^1 (denoted $P \in C^1[a, b]$) provided that there is a finite (irreducible) partition $a = C_0 < C_1 < \dots < C_{N+1} = b$ such that P may be regarded as a function in $C^1[C_k, C_{k+1}]$ for each $k = 0, 1, 2, \dots, N$. When present, the interior points C_k for $k = 1, 2, \dots, N$ are called corner points of P .

Theorem 2.10. (Argument Principle) Suppose $U \subset \mathbb{C}$ is an open set, and γ is a piecewise- C^1 simple closed path in U such that the interior of γ is in U . Suppose that $f : U \rightarrow \mathbb{P}^1$ is a meromorphic function, a function that can locally be written as a quotient of holomorphic functions, with no zeros or poles on γ . Then:

$$\frac{1}{2\pi i} \int_{\gamma} \frac{f'(z)}{f(z)} dz = N - P,$$

where N is the number of zeros of f inside γ and P is the number of poles inside γ , both counted with multiplicity.

Furthermore, suppose $h : U \rightarrow \mathbb{C}$ is holomorphic. Let z_1, \dots, z_N be the zeros of f inside γ and w_1, \dots, w_P be the poles of f inside γ . Then:

$$\frac{1}{2\pi i} \int_{\gamma} h(z) \frac{f'(z)}{f(z)} dz = \sum_{j=1}^N h(z_j) - \sum_{j=1}^P h(w_j) \quad (7.2.27)$$

Proof of Theorem 2.8. Consider a small disk D centered at the origin. This disk is chosen such that it lies within U and $f(0, z_n) \neq 0$ for $z_n \in \bar{D} \setminus \{0\}$

By continuity of f , we know that f remains non-zero on a neighborhood of any point where it is initially non-zero. Therefore, if we fix z' in a neighborhood of the origin, the function $z_n \mapsto f(z', z_n)$ will not be zero when z_n is on the boundary of the disk D . This holds true for a suitable choice of the neighborhood V' of z' , and therefore, for a suitable polydisk $V = V' \times D$.

We then apply the argument principle to find out the number of zeros of the function $z_n \mapsto f(z', z_n)$ within D . The argument principle is expressed as a contour integral over the boundary of D :

$$\frac{1}{2\pi i} \int_{\partial D} \frac{\frac{\partial f}{\partial z_n}(z', \zeta)}{f(z', \zeta)} d\zeta$$

The integral is a continuous integer-valued function of z' , which means it doesn't jump abruptly for small changes in z' . Since we know that $f(z', z_n)$ has a zero of multiplicity k at $z_n = 0$ when z' is close to 0, the value of this integral is k when $z' = 0$. Therefore, due to its continuity, the integral remains constant and equals k for all z' in the neighborhood V' .

Next, we associate each zero of the function $z_n \mapsto f(z', z_n)$ within D with a function $\alpha_j(z')$, and these zeros are ordered arbitrarily. We then construct the Weierstrass polynomial P which is a product of linear factors corresponding to these zeros. By design, the polynomial P has the same zeros as f within D :

$$P(z', z_n) = \prod_{j=1}^k (z_n - \alpha_j(z')) = z^{kn} + c_{k-1}(z')z^{(k-1)n} + \dots + c_0(z'),$$

The coefficients of P , c_j are defined in terms of symmetric functions of the zeros of f . We will prove that the functions c_j are holomorphic. The Fundamental Theorem of Symmetric Polynomials demonstrates that the elementary symmetric functions can be expressed as polynomials in the power sum functions involving the α_j values.

$$s_m(z') = \sum_{j=1}^k \alpha_j(z')^m, \quad m = 1, \dots, k.$$

Therefore, if we establish that the power sums s_m are holomorphic functions, it follows that the functions c_ℓ are also holomorphic.

A more refined version of the argument principle states the following: If h and g are holomorphic functions on a disc D , continuous on \bar{D} , where g has no zeros on ∂D , and $\alpha_1, \dots, \alpha_k$ are the zeros of g in D , then

$$\frac{1}{2\pi i} \int_{\partial D} h(\zeta) \frac{g'(\zeta)}{g(\zeta)} d\zeta = \sum_{j=1}^k h(\alpha_j).$$

The formula above, with $h(\zeta) = \zeta^m$ and $g(\zeta) = f(z', \zeta)$, says that

$$s_m(z') = \sum_{j=1}^k \alpha_j(z')^m = \frac{1}{2\pi i} \int_{\partial D} \zeta^m \frac{\frac{\partial f}{\partial z_n}(z', \zeta)}{f(z', \zeta)} d\zeta$$

The function s_m is evidently continuous, and by differentiating under the integral with respect to $\frac{\partial}{\partial z_\ell}$ for $\ell = 1, \dots, n-1$. Hence, it follows that s_m is holomorphic.

Our goal is to demonstrate that P divides f as claimed. To do so, we consider each fixed value of z' . According to the one-variable theory, the function $z_n \mapsto f(z', z_n)P(z', z_n)$ only has removable singularities, and the zeros of $f(z', z_n)$ coincide with the zeros of $P(z', z_n)$. This implies that the singularities can be "cancelled out" by multiplying $f(z', z_n)$ with $P(z', z_n)$.

Furthermore, we have defined the Weierstrass polynomial P to have the same zeros as $f(z', z_n)$ within the disc D . Therefore, when we multiply $f(z', z_n)$ by $P(z', z_n)$, the zeros of f are cancelled out by the zeros of P . Consequently, the function $f(z', z_n)P(z', z_n)$ has no zeros within D .

By applying the Cauchy formula to $\frac{f}{p}$, we can conclude that the function

$$u(z', z_n) = \frac{1}{2\pi i} \int_{\partial D} f(z', \zeta) P(z', \zeta) (\zeta - z_n) d\zeta$$

The function u is equal to $f(z', z_n) P(z', z_n)$. Moreover, u is clearly continuous and holomorphic in z_n for each fixed z' . By differentiating under the integral, we find that it is also holomorphic in z' .

Therefore, the Weierstrass polynomial P and the function u have been constructed such that they satisfy all the conditions of the Weierstrass Preparation Theorem, thereby completing the proof. \square

2.3 Saddle-node Scaling Law

From now on, we shall consider one-dimensional flows only, such as:

$$\dot{x} = f(r, x) \quad \text{for } x \in \mathbb{R} \quad \text{and} \quad r \in \mathbb{R}$$

2.3.1 Normal Form of the S-N

Saddle-node bifurcations have been extensively studied in dynamical systems. The normal form in the context of ordinary differential equations is given by

$$\dot{x} = r + x^2 \quad \text{for } x \in \mathbb{R} \quad \text{and} \quad r \in \mathbb{R} \quad (2.1)$$

where $x \in \mathbb{R}$ is the state variable and $r \in \mathbb{R}$ is the bifurcation parameter.

To determine the fixed points of the system, we solve the equation $r + x^2 = 0$. This equation has two solutions: $x_{\pm} = \pm\sqrt{-r}$.

For $r > 0$, there are no real solutions to the equation $r + x^2 = 0$, indicating that there are no fixed points in this parameter range. At the bifurcation parameter value $r = 0$, the equation $r + x^2 = 0$ yields a single solution, namely $x_{\pm} = 0$. However, this fixed point is non-hyperbolic since the linearization of the system at $x = 0$ results in a zero eigenvalue. For $r < 0$, the equation $r + x^2 = 0$ has two distinct real solutions: an attracting fixed point x_- and a repelling fixed point x_+ . This configuration of fixed points indicates the presence of a saddle-node bifurcation at $r = 0$.

Suppose we consider the initial condition $x(0) = x_0$. In order to investigate the scaling law provided by the ghost, our focus lies in determining the perturbations on the time it takes trajectories for each value of r after the saddle-node bifurcation, gradually approaching the bifurcation parameter until $r = r_c + \epsilon$.

To determine the time evolution, we can solve equation (2.1) by employing the method of separation of variables.

$$\int_{x_0}^{x(t)} \frac{1}{r + s^2} ds = \int_0^t dt \quad \text{as } r \rightarrow 0$$

By applying trigonometric substitution, we obtain:

$$\arctan\left(\frac{x(t)}{\sqrt{r}}\right) - \arctan\left(\frac{x_0}{\sqrt{r}}\right) = t\sqrt{r}$$

Consequently, using the oddness of the \tan^{-1} function, the duration of time that a trajectory spends within the interval $I = [-1, 1]$ can be calculated as:

$$\frac{2 \arctan\left(\frac{1}{\sqrt{r}}\right)}{\sqrt{r}} = t$$

In the limit as r approaches zero, we have:

$$t \sim \frac{\pi}{\sqrt{r}}$$

Remark 2.11. The scaling law states that $\tau \sim (r - r_c)^{-1/2}$, which remains unchanged regardless of the longitude of the interval I . The only requirement is that the value x_c lies within the interval I .

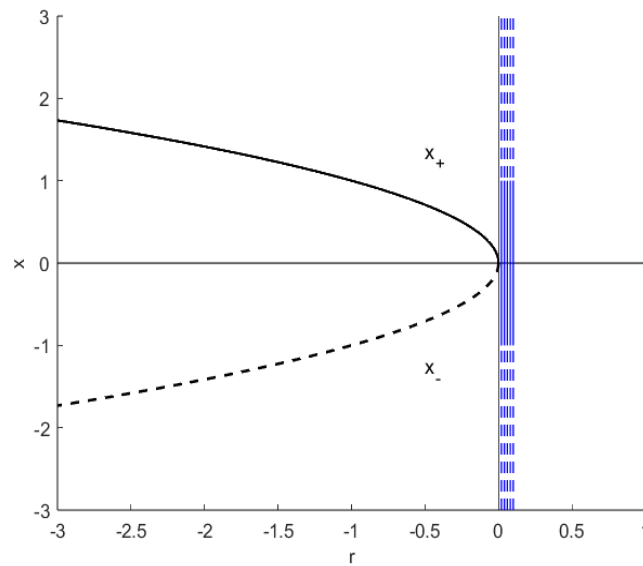


Figure 2.1: The unstable branch is denoted as x_- (represented by dashed lines). The stable branch is denoted as x_+ (solid lines). Within this plot, there are several trajectories depicted in blue color. These trajectories correspond to the values of x that will be evaluated. The solid lines represent the exact x -values that are being evaluated.

2.3.2 General Non-Degenerate S-N Bifurcation

Definition 2.12. The genericity and transversality conditions in this case are:

$$\frac{\partial^2 f}{\partial x^2}(0, 0) \neq 0 \quad (2.2)$$

$$\frac{\partial f}{\partial r}(0,0) \neq 0 \quad (2.3)$$

If the necessary conditions and (2.2)-(2.3) are satisfied, we call a saddle-node *non-degenerate*.

To prove the scaling law in non-degenerate saddle-nodes, we can utilize a special case of Theorem 2.8, as presented in [28], but considering the complex phase space as [11], to take advantage of the information of the features of the dynamics in \mathbb{C} .

Corollary 2.13. *Suppose $f(r, x)$ is an analytic function with respect to $x \in \mathbb{C}$ in a neighbourhood of $x=0$ such that it exhibits a saddle-node bifurcation at the origin. Then, there exists a smooth function $c(r, x)$ which is nonzero in a neighborhood near the origin $N = [-\epsilon, \epsilon]^2$, such that f can be locally given by:*

$$f(x, r) = c(r, x)(r + a(x))$$

where $a(x)$ satisfies $a(0) = a'(0) = 0$ and $a''(0) \neq 0$.

Proof. Given the assumptions, we can consider the function $f(x, r)$ as an analytic function on the complex plane \mathbb{C}^2 , with variables r and x . By assumption, $f(0,0) = 0$ and the function isn't identically zero near the origin. Additionally, the order of vanishing at the origin is 2 with respect to the variable x , which can be seen from the requirement of the saddle node bifurcation that the second derivative of f with respect to x is nonzero at the origin. The Weierstrass Preparation Theorem implies that there exists an analytic function $u : \mathbb{C}^2 \rightarrow \mathbb{C}$ and a Weierstrass polynomial $P : \mathbb{C}^2 \rightarrow \mathbb{C}$ of degree 1 respect r such that

$$f(r, x) = u(r, x)P(r, x)$$

in a neighbourhood of the origin, identifying $z' = x$ and $z_n = r$.

The given conditions state that the function $a(x)$ has no dependence on r and only depends on x . It is known that $f(0,0) = 0$ and $u(0,0) \neq 0$, which implies $a(0) = 0$. For a saddle-node bifurcation, it is required that $\partial_x f(0,0) = 0$. By expanding this expression, we find $\partial_x f(0,0) = u(0,0)a'(0)$. Hence, $a'(0) = 0$ to satisfy the condition. Additionally, a saddle-node bifurcation occurs when the sign of the real part of $\partial_{xx} f(0,0)$ changes. This condition implies that $a''(0) \neq 0$.

Then there exists a function $c : \mathbb{C}^2 \rightarrow \mathbb{C}$, which is analytic in a neighbourhood of the origin, such that $f(x, r) = c(r, x)(r + a(x))$, where $c(r, x) = u(r, x)$.

Furthermore, the derivative of f with respect to r is given by

$$\frac{df}{dr} = \frac{dc}{dr}(r + a(x)) + c(r, x).$$

Upon evaluation at the origin and taking into account that $a(0) = 0$, we get

$$\left. \frac{df}{dr} \right|_{(0,0)} = \left. \frac{dc}{dr} \right|_{(0,0)} \cdot 0 + c(0,0) \cdot 1 = c(0,0).$$

Therefore, at the origin, the derivative of f with respect to r equals the value of the function $c(r, x)$ at the same point, which aids in justifying this transformation, by

showing that the system's dynamics in the r direction at the origin are governed by the factor $c(r, x)$, as expected in this normal form.

In conclusion, in a neighbourhood of the origin, $f(r, x) = c(r, x)(r + a(x))$, where $c(r, x)$ is the analytic function guaranteed by the Weierstrass Preparation Theorem, and $a(x)$ is an holomorphic function of degree 2 satisfying $a(0) = a'(0) = 0$ and $a''(0) \neq 0$. This confirms that the function $f(r, x)$ is of the form typically associated with a saddle-node bifurcation. \square

The sign of $(0, 0)$ determines the stability of the fixed point at the origin along the \mathbf{r} -direction. If $c(0, 0) > 0$, the fixed point is stable; if $c(0, 0) < 0$, it is unstable. This comes directly from the derivative of f with respect to \mathbf{r} at the origin being equal to $c(0, 0)$.

The sign of $a''(0)$, on the other hand, is tied to the behavior of the system along the x -direction near the bifurcation. More specifically, the sign of $a''(0)$ dictates the directional unfolding of the bifurcation. If $a''(0) > 0$, the saddle-node bifurcation opens towards the positive x -axis. On the other hand, if $a''(0) < 0$, the bifurcation opens towards the negative x -axis.

Assume, for the sake of concreteness, that both $c(0, 0)$ and $a''(0)$ are positive. The other scenarios can be readily obtained by switching $x \rightarrow -x$ and/or $r \rightarrow -r$. Thus, we'll present the reasoning for one of the four potential cases.

The conditions imposed on the function $a(x)$ can be formally encapsulated by writing $a(x) = \hat{a}(x)x^2$, where $\hat{a}(x) \neq 0$. With $r > 0$ and $\hat{a}(0) > 0$, we stipulate that $\hat{a}(x)$ is bounded as $a_2 \geq \hat{a}(x) \geq a_1 > 0$, and that $c(0, 0) > 0$, with $c(x, r)$ similarly bounded as $c_2 \geq c(x, r) \geq c_1 > 0$. Given these conditions, the scaling behavior near a generic non-degenerate saddle-node bifurcation can be characterized through the following inequality:

$$\int_{-\epsilon}^{\epsilon} \frac{1}{c_2(r, x)(r + a_2x^2)} dx \leq \int_{-\epsilon}^{\epsilon} \frac{1}{c(r, x)(r + \hat{a}(x)x^2)} dx \leq \int_{-\epsilon}^{\epsilon} \frac{1}{c_1(r, x)(r + a_1x^2)} dx$$

Suppose that $c(r, x)$ is a bounded and nonzero function on the interval $[-\epsilon, \epsilon]$. We then obtain:

$$\int_{-\epsilon}^{\epsilon} \frac{1}{c(r + ax^2)} dx = \frac{1}{cr} \int_{-\epsilon}^{\epsilon} \frac{1}{1 + (\sqrt{\frac{a}{r}}x)^2} dx = \frac{1}{cr} \frac{\arctan(\sqrt{\frac{a}{r}}x)}{\sqrt{\frac{a}{r}}} \Big|_{-\epsilon}^{\epsilon}$$

This simplifies to:

$$\frac{1}{c\sqrt{a}} \frac{1}{\sqrt{r}} 2 \arctan(\sqrt{\frac{a}{r}}\epsilon)$$

Finally, as $r \rightarrow 0^+$, the asymptotic behavior of the integral is given by $\tau \sim \frac{\pi}{\sqrt{r}}$. This approximation validates that the integral demonstrates a consistent scaling behavior as $r \rightarrow 0^+$, which is independent of the precise form of the function $c(r, x)$. Hence, this scaling law, characterized by an inverse square root dependency, reaffirms our argument.

Remark 2.14. This method of study can also be applied to analyze general degenerate saddle nodes, including systems of the form $\dot{x} = -r - x^2$.

2.4 Transcritical Scaling Law

In order to examine the transcritical slowing down effect, it is necessary to define the specific normal form under study:

Consider the system described by the differential equation

$$\dot{x} = x^2 - r^2 + c,$$

where c represents a positive real parameter and r represents a real parameter.

For $c < 0$, no bifurcation occurs. When $c = 0$, a transcritical bifurcation takes place, and for $c > 0$, two saddle-nodes approach each other, leading to a transcritical bifurcation (refer to Figure 2.2).

Let us consider a fixed value of c . We examine the scaling law by introducing $r = A\sqrt{c}$, where A ranges from -1 to 1 . We study the following integral for $r \rightarrow \pm\sqrt{c}$:

$$\begin{aligned} \int_{-\epsilon}^{\epsilon} \frac{1}{c - r^2 + x^2} dx &= \int_{-\epsilon}^{\epsilon} \frac{1}{c - A^2c + x^2} dx = \\ &= -2 \frac{1}{\sqrt{c(1 - A^2)}} \arctan \left(\frac{\epsilon}{\sqrt{c(1 - A^2)}} \right) = \frac{1}{\sqrt{c(1 - A^2)}} \pi \end{aligned}$$

As we consider the limit of r approaching $\pm\sqrt{c}$ (corresponding to moving towards the right or left saddle-node bifurcation, see Figure 2.2), we find that the scaling law is given by the factor $\tau \sim \frac{1}{\sqrt{1 - A^2}\sqrt{c}}$, following the inverse square root dependency found on the previous section, but now incorporating a factor depending on c as $\frac{1}{\sqrt{c}}$ that tends to infinity as c approaches 0.

If we consider c as the control parameter and examine the slowing down effect resulting from the transcritical bifurcation, we can observe a paradigm shift. To analyze the impact of the coupling between the two saddle-nodes on the observation, we keep the time trajectory constant at the symmetry axis, $r = 0$, and bring the functions closer to our perspective, as shown in Figure 2.2.

The integral representing the time scale $\tau(c, r)$ is given by:

$$\tau(c, r) = \int_{-\epsilon}^{\epsilon} \frac{1}{c - r^2 + x^2} dx = 2 \frac{1}{\sqrt{c - r^2}} \arctan \left(\frac{\epsilon}{\sqrt{c - r^2}} \right)$$

From this expression, we can deduce the following relationship:

$$\tau(c, r) \stackrel{c \rightarrow 0}{\sim} \frac{\pi}{\sqrt{(\sqrt{c} - r)(\sqrt{c} + r)}} \sim \frac{\pi}{(r - r_{\text{crt}})}$$

Hence, we can conclude that there exists an inverse dependency between τ and $(r - r_{\text{crt}})$, which follows a scaling law of the form $\tau \sim (r - r_{\text{crt}})^{-1}$.

It should be noted that due to the divergence factor mentioned earlier, this inverse dependency is only valid within a certain range of c .

Remark 2.15. Due to the divergence factor found before, this inverse dependency is only available for a certain range of c .

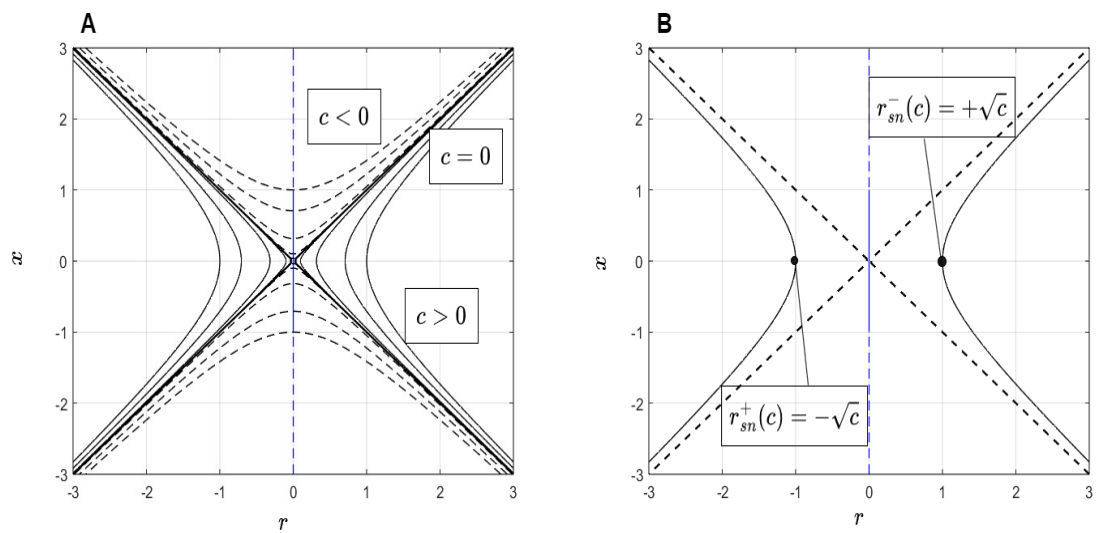


Figure 2.2: (A) Families of saddle-nodes with a fixed parameter c , as c approaches zero and its impact on time trajectories. The time trajectory of interest is depicted by a solid blue line, at $r=0$. For $c>0$, two saddle nodes converge, whereas no bifurcations occur when $c < 0$. In the case of $c=0$, the plot represents the transcritical bifurcation scenario with a bolder line. (B) The graph shows the significance of the parameter c , where the distances to the saddle nodes are given by \sqrt{c} .

Chapter 3

Stochastic Dynamics

In the study of chemical reaction systems, it is crucial to have a thorough comprehension of the temporal processes at play. This entails a careful consideration of why we opt for deterministic or stochastic approaches and the boundaries for treating the system as a -possibly- continuous or discrete process.

From a deterministic perspective, the progression of time can be viewed as a continuous process. However, the variation in molecular populations occurs in discrete integer increments. Additionally, the temporal evolution is not strictly deterministic, even when classical mechanics is considered without accounting for quantum effects. Predicting future molecular population levels with absolute precision is fundamentally unattainable. Such a prediction would require exhaustive knowledge of the exact positions and velocities of all the molecules involved, which is practically impossible [15].

Consequently, while the temporal behavior of a chemically reacting system may seem deterministic when considering the overall position-momentum phase space, this determinism fails to extend to the specific N-subspace representing the population numbers of individual species. This limitation hampers the effectiveness of deterministic equations, known as "reaction-rate equations", as they often struggle to capture fluctuations in molecular population levels. In certain cases, these limitations can have significant implications, emphasizing the need for a stochastic approach to studying these systems.

3.1 Introduction

In this work, the first two chapters have primarily focused on the deterministic approach for studying the temporal behavior of spatially homogeneous chemical systems, a system in which the concentration or distribution of chemical species is uniform throughout the entire system (*i.e.*, the limit of infinite diffusion). This deterministic perspective considers time progression as a continuous process, completely predictable in nature. It relies on an autonomous ordinary differential equation, commonly known as the reaction-rate equation.

Remark 3.1. In such systems, the properties and behavior of the chemical species

are assumed to be independent of their spatial position or location.

The field of chemical kinetics, particularly in the context of stochastic dynamics, has been profoundly influenced by the groundbreaking contributions of Daniel T. Gillespie (1938-2017) [14 - 16]. In 1976 he derived the stochastic simulation algorithm (SSA), broadly known as the Gillespie algorithm (see Section 3.3). It is important to recognize that earlier researchers, such as A. Rényi, A. Bartholomay and D. McQuarrie [36], have made significant preliminary contributions to the stochastic approach in chemical kinetics. One of the first attempts to apply stochastic concepts to chemical kinetics can be attributed to Kramers [27], who aimed to describe macroscopic rate processes using molecular parameters and treated chemical reactions as Brownian motions¹ of particles.

In contrast, this chapter explores the theoretical basis of the stochastic approach, which views temporal progression as a type of random-walk process.

In probability theory, a random walk process refers to a stochastic process used to determine the probable location of a point undergoing random movements. The process involves considering the probabilities, which remain constant at each step, of moving a certain distance in a specific direction.

Remark 3.2. Random walks [5] serve as illustrations of Markov processes, where the future behavior is independent of the past history, as will be explained in the following section.

This stochastic process is governed by a unique differential-difference equation, an equation in an unknown function and certain of its derivatives, evaluated at arguments which differ by any of a fixed number of values [3]. This equation is referred to as the "master equation." Therefore, the deterministic and stochastic approaches provide complementary perspectives to comprehend the dynamics of chemical reactions.

3.2 Theoretical Basis

In order to establish a theoretical foundation for incorporating intrinsic noise into chemical reaction processes, it is necessary to lay a basis of definitions. A Markov process [34], named after Andre Markov (1856-1922), is a random process that is indexed by time and possesses the property that the future is independent of the past, given the present.

3.2.1 Markov process

Definition 3.3. (*First-order Markov process*) A random process $\{X(t), t \in T\}$ is called a first-order Markov process if, for any $t_0 < t_1 < \dots < t_n$, the conditional cumulative distribution function (CDF) of $X(t_n)$, given the values of $X(t_0), X(t_1), \dots, X(t_{n-1})$, depends

¹The erratic random movement of microscopic particles in a fluid, caused by constant collisions with the molecules of the surrounding medium.

only on $X(t_{n-1})$. Mathematically, this can be expressed as:

$$\begin{aligned} \Pr(X(t_n) \leq x_n \mid X(t_{n-1}) \leq x_{n-1}, X(t_{n-2}) \leq x_{n-2}, \dots, X(t_0) \leq x_0) \\ = \Pr(X(t_n) \leq x_n \mid X(t_{n-1}) \leq x_{n-1}) \end{aligned}$$

This means that, in a first-order Markov process, given the present state of the process, the future state is independent of the past. This property is commonly referred to as the *Markov property*.

Remark 3.4. A Markov process may have various orders, with a first-order Markov process being the specific case where the future state depends only on the present state.

A Markov chain is a specific type of Markov process that involves a discrete-time, discrete-state sequence of random variables. In the case of a finite Markov chain, the set of possible states is finite, and the chain can only be in one of these states at any given time [37].

Definition 3.5. (Finite Markov chain) A finite Markov chain is a Markov chain in which there exists only a finite number, k , of possible states denoted by s_1, \dots, s_k . At any given time, the chain can be in one of these k states.

Definition 3.6. (Transition probability) The transition probability is the conditional probability that the next state, X_{n+1} , is equal to a particular state, s_j , given that the current state, X_n , is equal to another state, s_i . It can be expressed as:

$$P(X_{n+1} = s_j \mid X_n = s_i)$$

Therefore, the transition probability captures the dynamics of the Markov chain by quantifying the likelihood of moving from one state to another. It represents the conditional probability of observing a particular state in the next time step, given the current state.

3.2.2 The Propensity Function

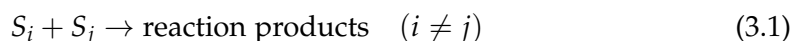
The general problem we address in this study can be formulated as follows: Consider a volume V containing molecules of N chemically active species S_i ($i = 1, \dots, N$), along with molecules of several inert species. Chemically active species are those involved in the reaction mechanism but not present as either reactants or final products. Inert species, also known as spectator species, remain unchanged throughout the reaction and are neither consumed nor produced.

It is further assumed that these N chemical species S_i , well-stirred and at a constant temperature, can participate in M chemical reactions R_μ ($\mu = 1, \dots, M$), each characterized by a numerical reaction parameter c_μ , which will be defined shortly. We specify the dynamical state of this system by $X(t) = (X_1(t), \dots, X_N(t))$, where $X_i(t)$ represents the number of S_i molecules in the system at time t , with $i = 1, \dots, N$.

The fundamental hypothesis of the stochastic formulation of chemical kinetics (and the sole assumption for the Gillespie method) is that the reaction parameter c_μ [14], which describe the reaction R_μ , can be defined as follows, which characterize reaction R_μ (R_i), can be defined as follows [14]:

Definition 3.7. (Average probability) *The quantity $c_\mu \delta t$ is the average probability, to first order, in δt , that a particular combination of R_μ reactant molecules will react accordingly in the next time interval δt .*

Example 3.8. Consider a reaction R_μ of the form:



The probability that a specific pair of molecules S_i and S_j will undergo a reaction of the type (3.1) within the next time interval δt , averaged over all possible S_i - S_j pairs, can be expressed as $c_\mu \delta t + o(\delta t)$. Here, $o(\delta t)$ represents unspecified terms that satisfy $\frac{o(\delta t)}{\delta t} \rightarrow 0$ as $\delta t \rightarrow 0$.

Remark 3.9. Note that every reaction R_μ is *unidirectional*, so any reversible reaction must be considered as two separate unidirectional reactions.

The molecular populations, denoted as $X_i(t)$, are inherently random variables since we do not track the precise positions and velocities of all the molecules in the system. Instead, we rely on numerous nonreactive molecular collisions to constantly 'stir' the system, promoting interactions between molecules. In this context, it can be demonstrated that each reaction channel, represented by R_j , possesses a distinct and well-defined function known as the propensity function, denoted as a_j [15].

Definition 3.10. (Propensity function) *The propensity function for R_j , denoted as $a_j(x)$, represents the probability, given $X(t) = x$, that one reaction R_j will occur somewhere inside V in the next infinitesimal time interval $[t, t + dt]$, where $j = 1, \dots, M$.*

The function $a_j(x)$ can be expressed mathematically as:

$$a_j(x) = c_j h_j(x) \quad (3.2)$$

Here, c_j is the reaction parameter or specific probability rate constant for channel, a possible pathway or route that a reaction can take, R_j . The function $h_j(x)$ in (3.2) is defined as the number of distinct combinations of R_j reactant molecules available in the state x . It can be determined by inspecting the left-hand side of reaction R_j .

Example 3.11. Let R_1 be the reaction $X_1 + X_2 \rightarrow 2X_1$, we would have $a_1(x) = c_1 x_1 x_2$. Now, suppose R_2 was the inverse of that reaction, we would have $a_2(x) = c_2 x_1 \left(\frac{x_1 - 1}{2} \right)$.

The propensity function a_j and the state-change vector v_j together completely specify the reaction channel R_j . The i th component of the state-change vector v_j is defined as follows:

v_{ji} (the change in the number of S_i molecules produced by one R_j reaction),

where $j = 1, \dots, M$ and $i = 1, \dots, N$.

Remark 3.12. Understanding the distinction between the reaction parameter and the propensity function can be challenging. The reaction parameter primarily characterizes the intrinsic rate of a reaction, whereas the propensity function incorporates both the reaction rate and the current state of the system. The propensity function is a mathematical entity that allows for the application of probability theory in the analysis of reaction kinetics.

3.2.3 Consequences of the Propensity function: Master Equation

The propensity function (3.10), seen as an evolution law, implies that the state vector $X(t)$ follows a jump-like or discrete Markov process on a non-negative N -dimensional integer lattice. To analyze such a process, the focus is often on its singly conditioned probability function $P(x, t|x_0, t_0)$, which represents the probability of $X(t)$ being in state x at time t , given that $X(t_0) = x_0$. We use an upper case letter to denote a random variable, and the corresponding lower case letter to denote a possible value of that random variable

To obtain a time evolution equation for the singly conditioned probability function, we consider a small time interval dt . During this interval, the probability of multiple reactions happening simultaneously is very small compared to the probability of a single reaction occurring. Therefore, we can focus on the probability of zero or one reaction taking place within dt .

Remark 3.13. The assumption of negligible probability for multiple reactions in a small time increment dt is not based on the total number of molecules, but rather on the average number of reactant molecules participating in a particular reaction.

Using (3.10) and the laws of addition and multiplication in probability theory, the probability of the system being in state x at time $t + dt$ [15], given the initial state x_0 at time t_0 , can be expressed as the sum of probabilities of mutually exclusive events involving zero or one reaction in $[t, t + dt)$:

$$P(x, t + dt|x_0, t_0) = P(x, t|x_0, t_0)x[1 - \sum_{j=1}^M a_j(x)dt] + \sum_{j=1}^M P(x - v_j, t|x_0, t_0)a(x - v_j)dt \quad (3.3)$$

Some algebraic rearrangements and taking the limit as $dt \rightarrow 0$ leads to the chemical master equation:

Definition 3.14. (Chemical master equation) *The chemical master equation is defined as follows:*

$$\frac{\partial}{\partial t}P(x, t|x_0, t_0) = \sum_{j=1}^M [a_j(x - v_j)P(x - v_j, t|x_0, t_0) - a_j(x)P(x, t|x_0, t_0)] \quad (3.4)$$

If it can be solved for P , then we can, in principle, determine all the information about the process $X(t)$. However, in practice, obtaining exact solutions of Equation (3.14) is rarely feasible.

3.3 Gillespie Algorithm

Another consequence of Equation (3.10) is the existence and form of the *next-reaction density function* $p(\tau, j|x, t)$, defined as the probability that, given $X(t) = x$, the next reaction in the volume V will occur in the infinitesimal time interval $[t + \tau, t + \tau + d\tau)$, and will be an R_j reaction.

Since $a_j(x)dt$ represents the probability of a reaction happening within the next small time interval dt , we can use basic probability reasoning to conclude that $\exp\left(-\sum_j a_j(x)t\right)$ corresponds to the probability that no reaction occurs during a time period t . By multiplying this probability with the probability stated in Equation (3.10), we obtain the probability described by the next-reaction density function. As a result, the function \mathbb{P} can be expressed as follows:

$$\mathbb{P}(\tau, j|x, t) = a_j(x) \exp\left(-\sum_{k=1}^M a_k(x)\tau\right) \quad \text{for } (0 < \tau < \infty; j = 1, \dots, M) \quad (3.5)$$

The formula mentioned above forms the fundamental framework for the stochastic simulation algorithm (SSA). SSA entails a straightforward digital computer algorithm that utilizes a Monte Carlo procedure to generate random pairs (τ, j) based on the joint density function (3.5). to simulate the temporal evolution of the given chemical system. Similar to the master equation, this *stochastic simulation algorithm* accurately considers the inherent fluctuations and correlations that the deterministic formulation overlooks. These random pairs are then used to construct "unbiased realizations" of the process $X(t)$. It is worth noting that these realizations are consistent to the chemical master equation (3.14), as they are derived from it. For a description of the SSA algorithm, please see the Appendix A.1.2.

Remark 3.15. Note that the stochastic simulation algorithm is not a method used to numerically solve the chemical master equation. Numerically solving the chemical master equation is typically a considerably more difficult undertaking.

3.4 Analyzing the Transition from Deterministic to Stochastic Systems and Its Implications

In reference to [31], we will introduce a change in notation for clarity. Instead of using the notation $a_j(x)$ for the transition rates and v_j for the propensity rates, we will adopt the notation $W_i(X)$ and r_i , respectively. Additionally, we will replace the symbol V with Ω to represent the system's size.

3.4.1 From deterministic to stochastic scenario: Law of large Numbers

Consider a system governed by certain dynamics or processes, where random fluctuations or noise are inherent. Let $X(t)$ represent the state of the system at time

t , and let $\mathcal{P}(X(t))$ denote the probability distribution function associated with the system's state.

As the system size Ω increases, due to the *law of large numbers*, the probability distribution function $\mathcal{P}(X(t))$ tends to converge towards a more concentrated distribution around a specific value or set of values, denoted as X_0 .

According to this law, as the number of independent random variables increases, the average behavior of these variables becomes more predictable and deterministic. Consequently, the system's overall behavior exhibits reduced randomness and tends to follow deterministic patterns.

The convergence can be expressed as:

$$\lim_{\Omega \rightarrow \infty} \mathcal{P}(X(t)) = \delta(X(t) - X_0)$$

where $\delta(X(t) - X_0)$ represents the Dirac delta function centered at X_0 .

This implies that as the system size grows, the probability of observing states other than X_0 diminishes significantly.

In order to proceed further with our analysis, we assume that the transition rates, upon rescaling, satisfy the following scaling relation [31]:

$$W_i(X) = \Omega w_i(x) + \mathcal{O}(\Omega^0) \quad (3.6)$$

where Ω is the system's size and $x = \frac{X}{\Omega}$ is the rescaled state variable.

Therefore, $x = \frac{X}{\Omega}$ is indeed a deterministic variable, often called the "macrostate" of the system. Here, X can be viewed as a "microstate" - a specific configuration of the system that might change stochastically over time due to random interactions, while Ω is the system's size or volume.

In equation (3.6) $W_i(X)$ is the stochastic rate of change (which can vary randomly), and $\Omega w_i(x)$ is the deterministic rate of change (which doesn't vary randomly). The $\mathcal{O}(\Omega^0)$ term represents the order of the approximation, essentially saying that any randomness becomes less important as the system size Ω increases.

Therefore, the relationship between the deterministic and stochastic scenarios can be understood as a system transition from stochastic behavior at small scales, characterized by randomness and uncertainty, to deterministic behavior at larger scales, where the system's behavior becomes more predictable and follows regular patterns.

Remark 3.16. The concept of transitioning from a deterministic to a stochastic approach (or vice versa) is rooted in the scales at which we study these systems.

3.4.2 Deriving the rates: Law of Mass Action

In chemistry, the law of mass action [32], formulated by Cato M. Guldberg and Peter Waage during 1864–1879, is a fundamental principle that describes the relationship between the rate of a chemical reaction and the concentrations of the reacting substances. It provides a mathematical framework for understanding how the concentrations of reactants influence the rate at which a reaction proceeds.

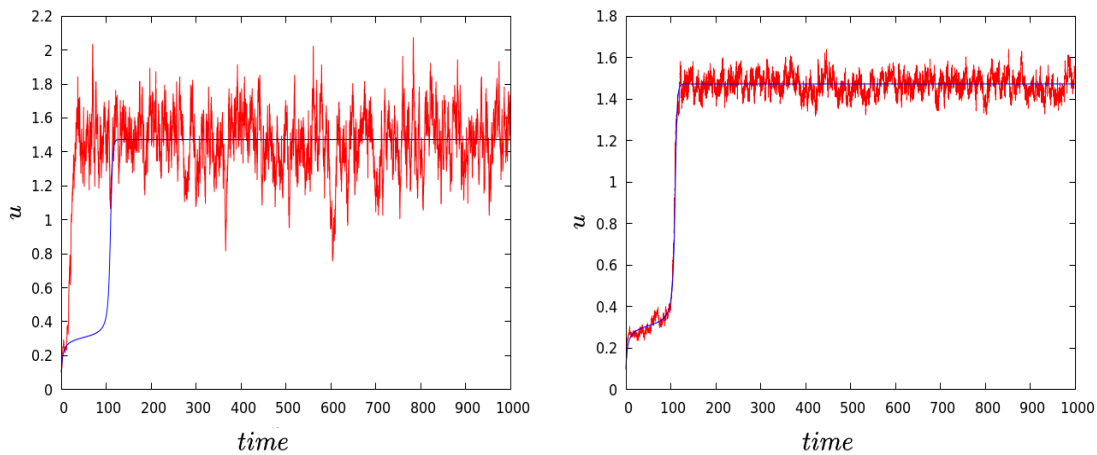


Figure 3.1: Application of the Gillespie Algorithm to the Mushroom Model, characterized by initial conditions $x(0) = 0.1\Omega$, parameters $q = 3$ and $s = 0.95$. The stochastic graph is rendered in red, while the deterministic counterpart is represented in blue. Two panels are presented with a system size of $\Omega = 200$ (left) and $\Omega = 2000$ (right). Notably, the panels demonstrate the convergence of the stochastic graph towards the deterministic graph, highlighting the approximation behavior.

An important application of the law of mass action is in the formulation of the Michaelis-Menten-Hill (MMH) kinetics, which describe enzyme-catalyzed reactions. The Michaelis-Menten-Hill equation demonstrates the relationship between the substrate concentration and the reaction rate. At low substrate concentrations, the reaction rate is directly proportional to the substrate concentration, approaching first-order kinetics. As the substrate concentration increases, the reaction rate approaches saturation, and further increases in substrate concentration have less impact on the reaction rate.

Corollary 3.17. Rates derived from the Law of Mass Action or Michaelis-Menten-Hill kinetics satisfy condition 3.6.

Please see Appendix A.1.3 for a detailed description of the Law of Mass Action, MMH kinetics and Corollary 3.17.

Chapter 4

Results and Discussion

In this section, the specific results obtained from our investigation will be discussed. These results are built upon the theoretical foundations established in Chapters 2 and 3.

4.1 Bottleneck effect

Let us calculate the potential function $U(u, a(s)) = \int -f(u, a(s))du$ of Eq. 1.1:

$$U(u, a(s)) = \frac{1}{2}u^2 - (r + a(s))u + a(s) \arctan(u) \quad (4.1)$$

4.1.1 Monostability and Bistability: Analysis of the Potential Function

In Figure 4.7, on the upper-left panel, a representation of the potential function is displayed based on the parameter value of s . At $s = 0.34$, the potential function demonstrates a single well. This well signifies a stable fixed point within the system. This fixed point is analogous to a ball at rest at the bottom of a well or valley, where the potential remains unchanged [49]. As we increase the parameter s , the potential function undergoes a transformation, evolving into a broad plateau. This change in landscape signifies a period of slow relaxation, exhibiting the delayed transition phenomenon, as showcased in the middle panels of Figure 4.7. When the parameter s surpasses a certain critical threshold, the plateau feature within the potential function dissipates.

More examples on the ghost phenomenon can be found in Appendix C.

4.1.2 S-N Scaling Law

The saddle-node scaling law, given by $\tau = (s_{crt} - s)^{-\frac{1}{2}}$, is investigated, approximating the two lower SN's in Figure 4.2. The phenomenon observed when reducing the distance ϕ between the two SN reveals that while the scaling law is preserved, there is a significant increase in the transients time to complete the trajectory, starting from an initial value of $u(0) = 0.28$ and reaching $u(\text{fin}) = 0.33$:

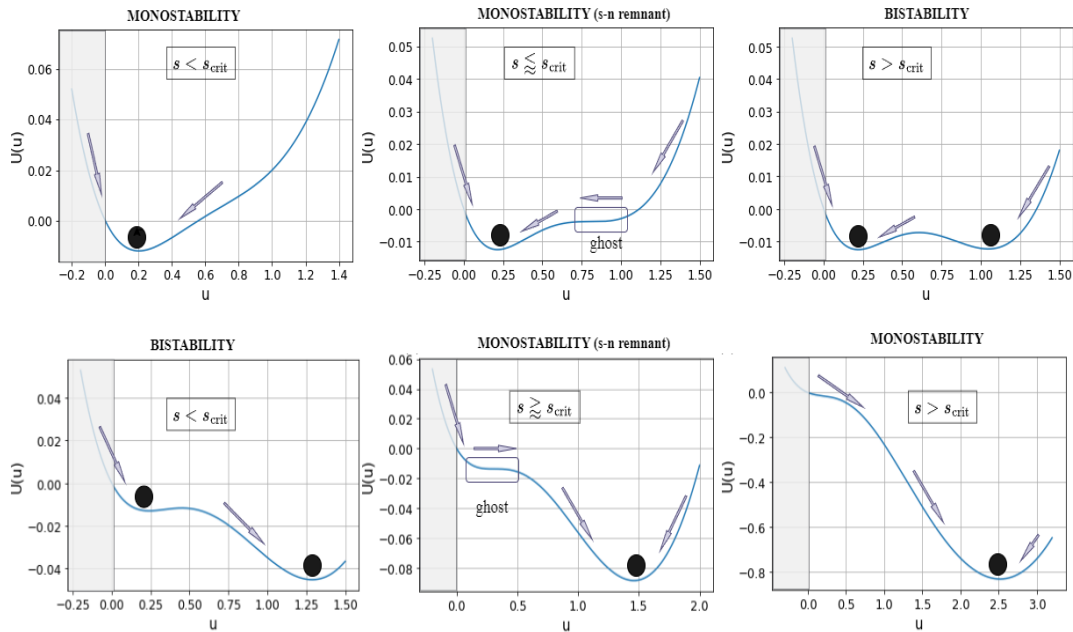


Figure 4.1: Potential function $U(x)$, computed using equation 4.1, with $r=0.14$ and $q=5$. The parameter values s are varied from left to right and top to bottom, taking values of 0.34, 0.364860, 0.375, 0.4, 0.423701, and 0.63. The gray region represents biologically meaningless population values ($u < 0$). Notably, there is an inverse relationship between the stabilities, resulting from the symmetry of the SN bifurcations. Similarly, the stabilities of SN3 and SN4 are symmetric to SN1 and SN2, respectively.

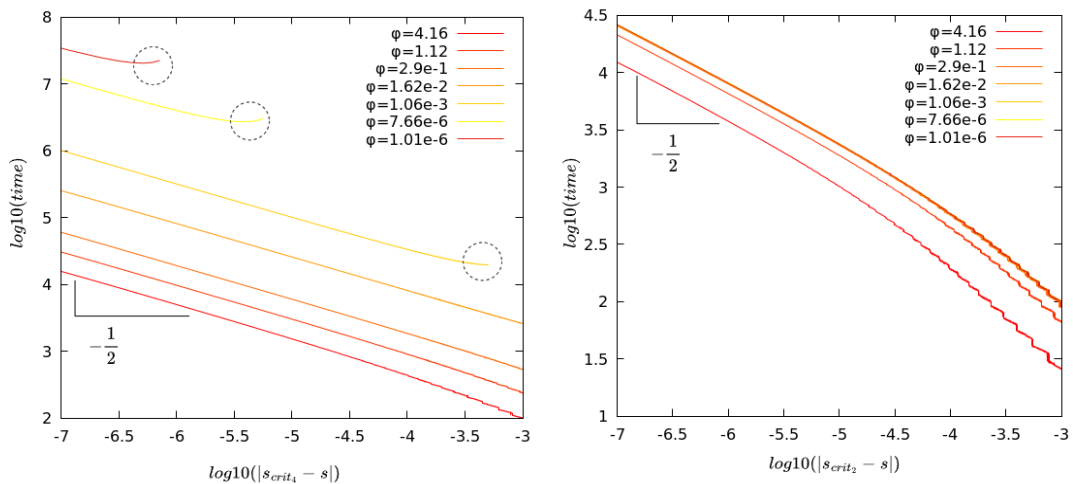


Figure 4.2: The left panel represents the scaling law on SN4, while the right panel shows the scaling law on SN2. By decreasing the value of q , the distance ϕ between SN1 and SN4 is reduced. This adjustment allows SN2 and SN3 to maintain a sufficient distance from each other, preventing mutual interference during the analysis of transients. Dotted circles are used to illustrate the impact of the proximity between SN1 and SN4.

If we study the relationship of the regression lines for the functions depicted on the left panel of Figure 4.2, we find that they follow approximately a function of the form $y = \frac{1}{\sqrt{x}}$, like the diverging coefficient we found in Section 2.4:

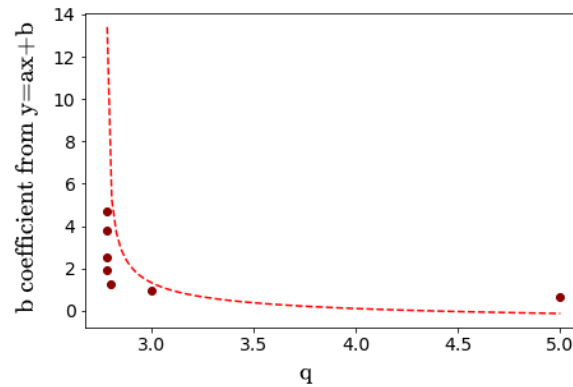


Figure 4.3: Function in dotted lines is $y = \frac{1}{\sqrt{x-2.78}} - 0.8$, the dots represent the b coefficient from the regression line applied to each function in Figure 4.2. We observe the inverse squared relationship.

4.1.3 Critical Slowing Down: the transcritical bifurcation

The transcritical scaling law, represented by $\tau = (s_{trans}(q_{trans}) - s)^{-1}$, is illustrated in Figure 4.4. The observed "divergence" phenomenon depicted within the dotted circle will be discussed continuously.

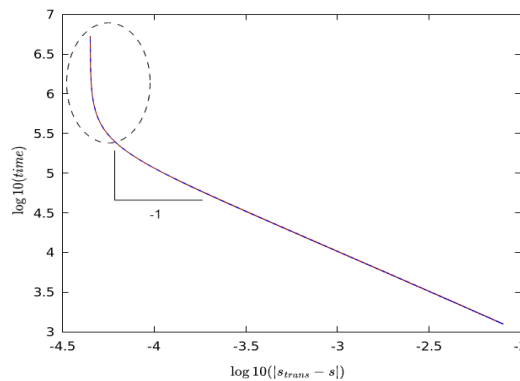


Figure 4.4: Transcritical slowing down law for the Mushroom Model. The red solid line represents the original form, while the overlapped dotted blue line represents a translated version to the origin, that retains the symmetry axis at $s=0$ and the same relationship.

Upon thorough examination, it becomes evident that there is an absence of perfect symmetry between SN1 and SN4. This observation is supported by the fact that the minimum values for the transients do not always align with the symmetry axis at $s=q/2$.

For instance, when $q = 2.8$, the anticipated minimum value is expected to occur at $s = 1.4$. The recorded values fluctuate around this point:

Transient Value	s Value
44.53813356283553	1.39999908088089
44.53813361380771	1.40000095088088
44.53813370361276	1.39999928088089
44.53813372096411	1.39999737088090

For $q = 2.785$, the minimum value should be at $s = 1.3925$:

Transient Value	s Value
1249.032288758	1.392203054
1249.033250866	1.392202893
1249.034038978	1.392202756
1253.830297479	1.392619724

For $q = 2.784953619413649$, the minimum value should be at $s = 1.3924768097068245$:

Transient Value	s Value
20416457.58951539173722	1.39247682092831
20416457.58951539173722	1.39247680699806863913

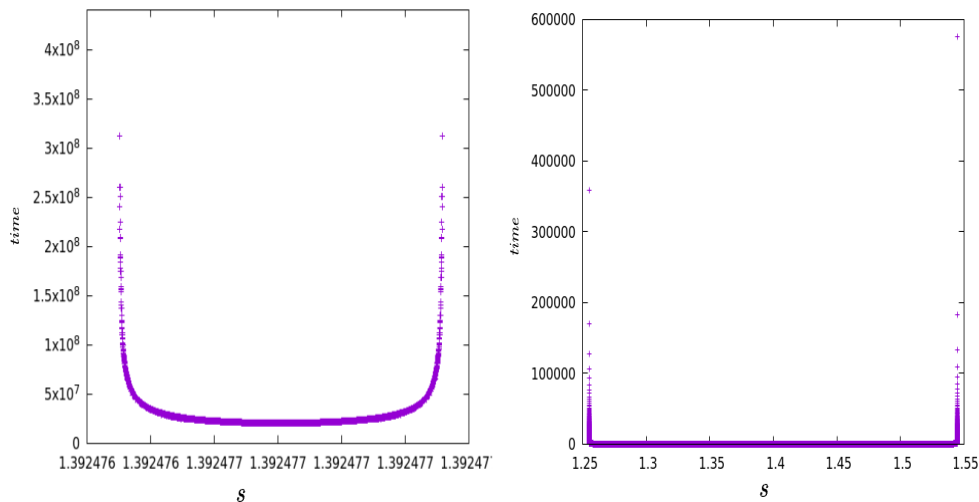


Figure 4.5: In the study of the transition from SN4 to SN1, we observe two distinct panels. In the left panel, the parameter q is measured to be approximately 2.784953619413649, while in the right panel, q is recorded as 2.8. A parabola-shaped function appears to be a plausible fit based on visual inspection. However, upon closer examination of the data, fluctuations can be observed, indicating a more complex behavior.

4.2 Stochastic study

4.2.1 Markovian stochastic system

Given the mushroom model defined by Eq. 1.1, let us consider the Markovian stochastic system whose mean-field limit undergoes our deterministic model f:

Transition rates	Stoichiometry coefficient	Description
$W_1 = \Omega r$	$r_1 = +1$	Constant housekeeping genes transcription
$W_2 = X$	$r_2 = -1$	Linear degradation
$W_3 = \Omega s q \frac{X^2}{\Omega^2 + X^2}$	$r_3 = +1$	Quadratic autocatalysis
$W_4 = \Omega s^2 \frac{X^2}{\Omega^2 + X^2}$	$r_4 = -1$	Quadratic inhibition

Table 4.1: Transition rates for the Mushroom Bifurcation Model, including constant transcription, saturation under a Hill function dynamic and linear degradation.

Defined by the following elementary processes:

Elementary process	Stoichiometry coefficient	Description
$\emptyset \xrightarrow{W_1} A$	$r_1 = +1$	Constant housekeeping genes transcription
$A \xrightarrow{W_2} \emptyset$	$r_2 = -1$	Linear degradation
$A + A \xrightarrow{W_3} A + A + A$	$r_3 = +1$	Quadratic autocatalysis
$A + A \xrightarrow{W_4} A$	$r_4 = -1$	Quadratic inhibition

Table 4.2: Elementary processes and their descriptions.

Taking $x = X/\Omega$ it follows that

$$\omega_1 = \frac{W_1(x\Omega)}{\Omega} = \frac{\Omega r}{\Omega} = r, \quad \text{as} \quad W_1(X) = \Omega r \quad \forall X \in \mathbb{N}, \quad \omega_2 = \frac{W_2(x\Omega)}{\Omega} = \frac{\Omega x}{\Omega} = x,$$

$$\omega_3 = \frac{W_3(\Omega s q \frac{x^2}{\Omega^2 + x^2} \Omega)}{\Omega} = s q \frac{x^2}{1+x^2}, \quad \omega_4 = \frac{W_4(\Omega s^2 \frac{x^2}{\Omega^2 + x^2} \Omega)}{\Omega} = s^2 \frac{x^2}{1+x^2}$$

4.2.2 Heat Maps and Time Lags

The presence of noise can cause transitions between stable states, even when both states are inherently stable. This phenomenon can be observed in the presence of bistability, where the system can switch between two stable branches. Including the graph presented in Figure 4.8, it becomes evident how noise-induced fluctuations can lead to a jump from one stable branch to another.

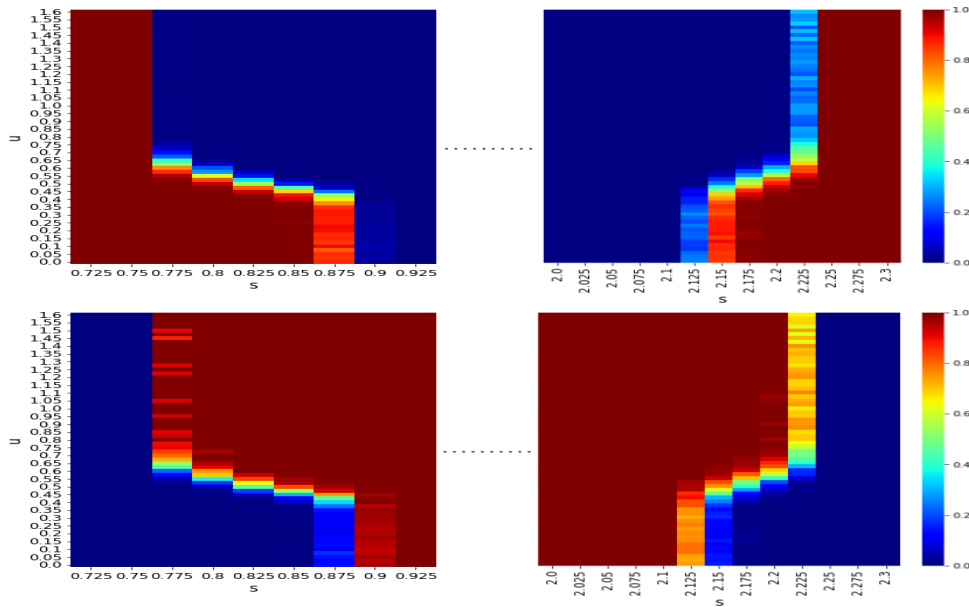


Figure 4.6: Averaged transition probabilities to the lower stable branch (upper panel) and the upper stable branch (lower panel) over 200 runs of the Gillespie algorithm, with a system size of $\Omega = 3000$ and a target concentration of $u = 1.6$. The analysis focuses on specific regions of interest in a mushroom, excluding the portion indicated by a dotted line, considered irrelevant for the analysis. Notably, an asymmetry in behavior between the left and right areas can be observed.

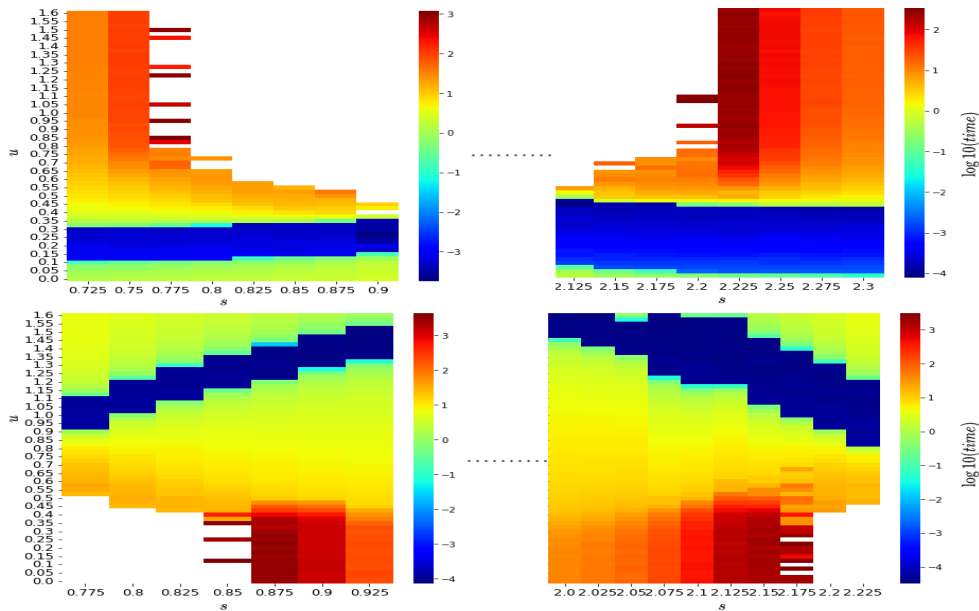


Figure 4.7: The heatmap presents the logarithmic-scale representation of the transient time required for transitions to the lower (upper panel) or upper (lower panel) stable branch. Blank spaces in the heatmap indicate regions where the probability of transitioning to a specific stable branch is zero. The presence of the ghost effect can be observed in the red darker areas.

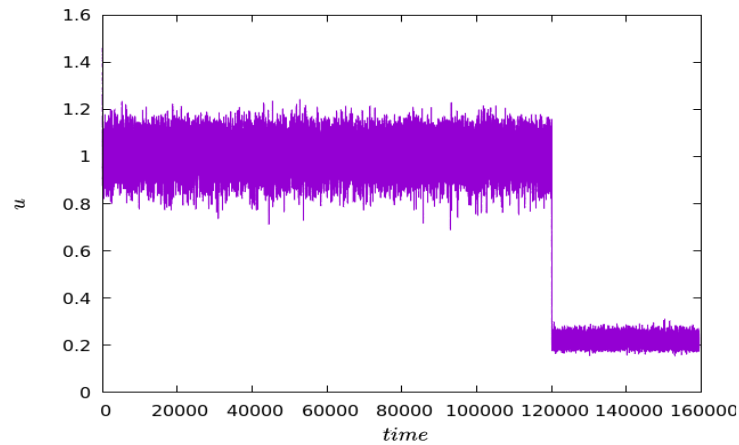


Figure 4.8: For a system's size of $\Omega = 3000$ and initial concentration $u(0) = 1.45\Omega$, the analysis is conducted over 10^9 iterations. In the deterministic scenario, the system should remain in the stable branch with $u=1.015$. However, due to the presence of noise induced by the system's size, over a sufficiently long period of time, the system undergoes a "jump" and transitions to the lower branch with $u=0.21873$.

In the stochastic field, an intriguing property is observed where the bifurcation value is influenced by the system size Ω [49]. The stochastic dynamics exhibit a more pronounced deviation from the deterministic behavior as the system size decreases, as in Figure 4.9.

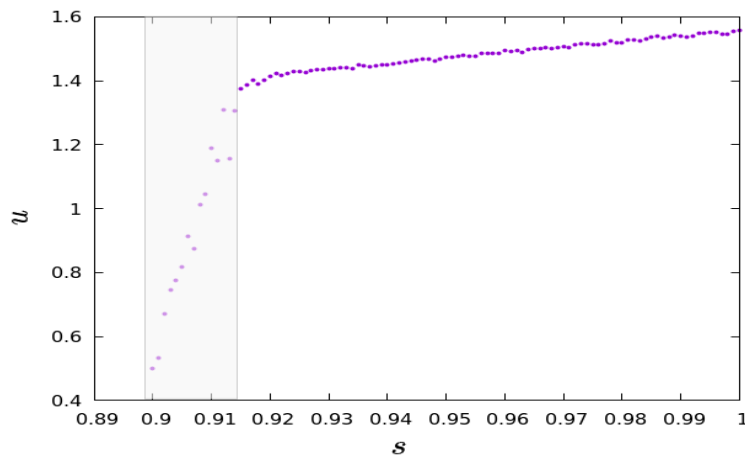


Figure 4.9: The gray area signifies the region where the bifurcation value is likely to occur. The study involves a system with a size of $\Omega = 500$ with the mean value of u calculated over 100 runs of the Gillespie algorithm at 10^7 number of inner iterations of the algorithm.

4.2.3 Coupling effect of SN bifurcations

To investigate the impact of noise induction on the transient times during the approximation of SN1 and SN4, let us consider the following graphics.

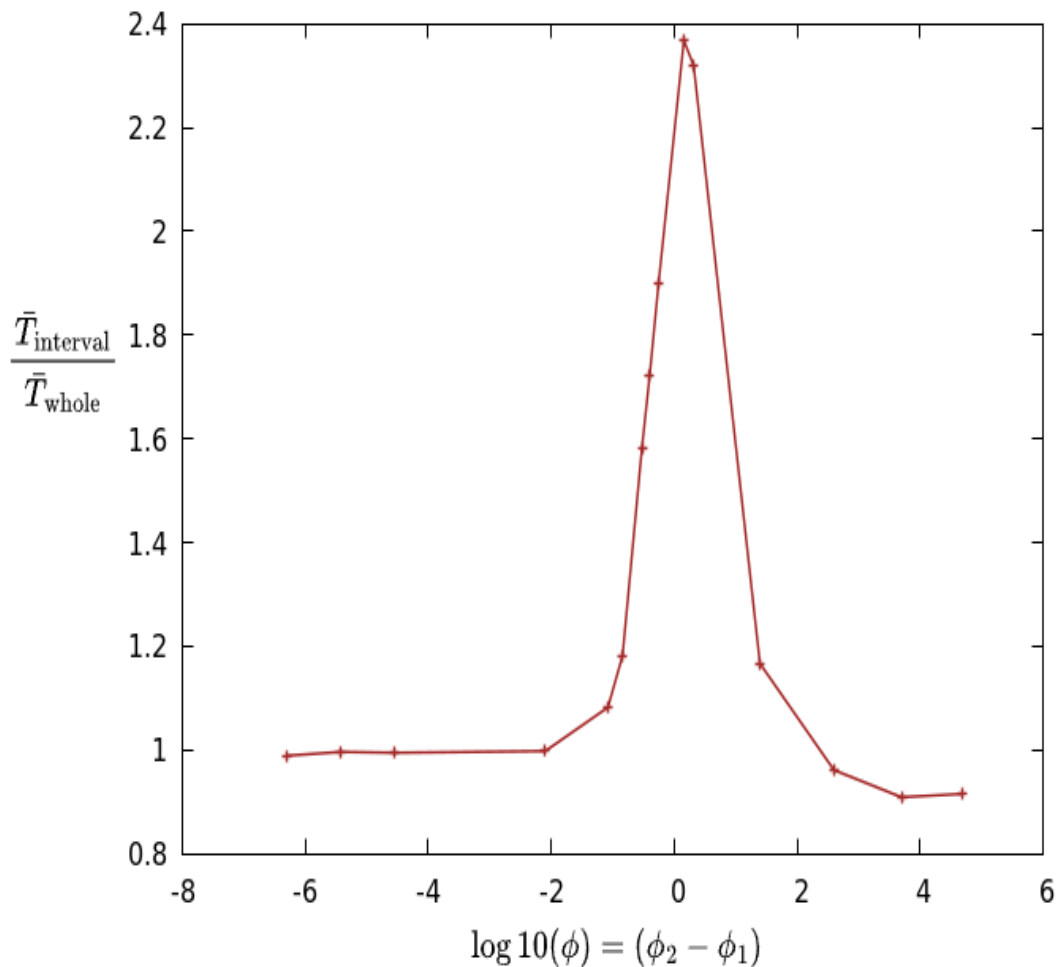


Figure 4.10: Taking a gap of $1/8$ from the initial SN (ϕ_1), we conducted a study on the mean time it takes to reach $u = 1.4$. The study was based on 50 Gillespie runs, with $CC = 3000$, starting from $u = 0.2$. The y-axis represents the relative increase obtained by studying the mean time ($\bar{T}_{\text{interval}}$) compared to the mean time it took when considering the entire interval between the two SN. We observed that when the two SN values are very close, their effects overlap and show minimal differences. Similarly, for larger distances (on the order of 10^2 and above), the interval under study of the two SN does not significantly influence the results.

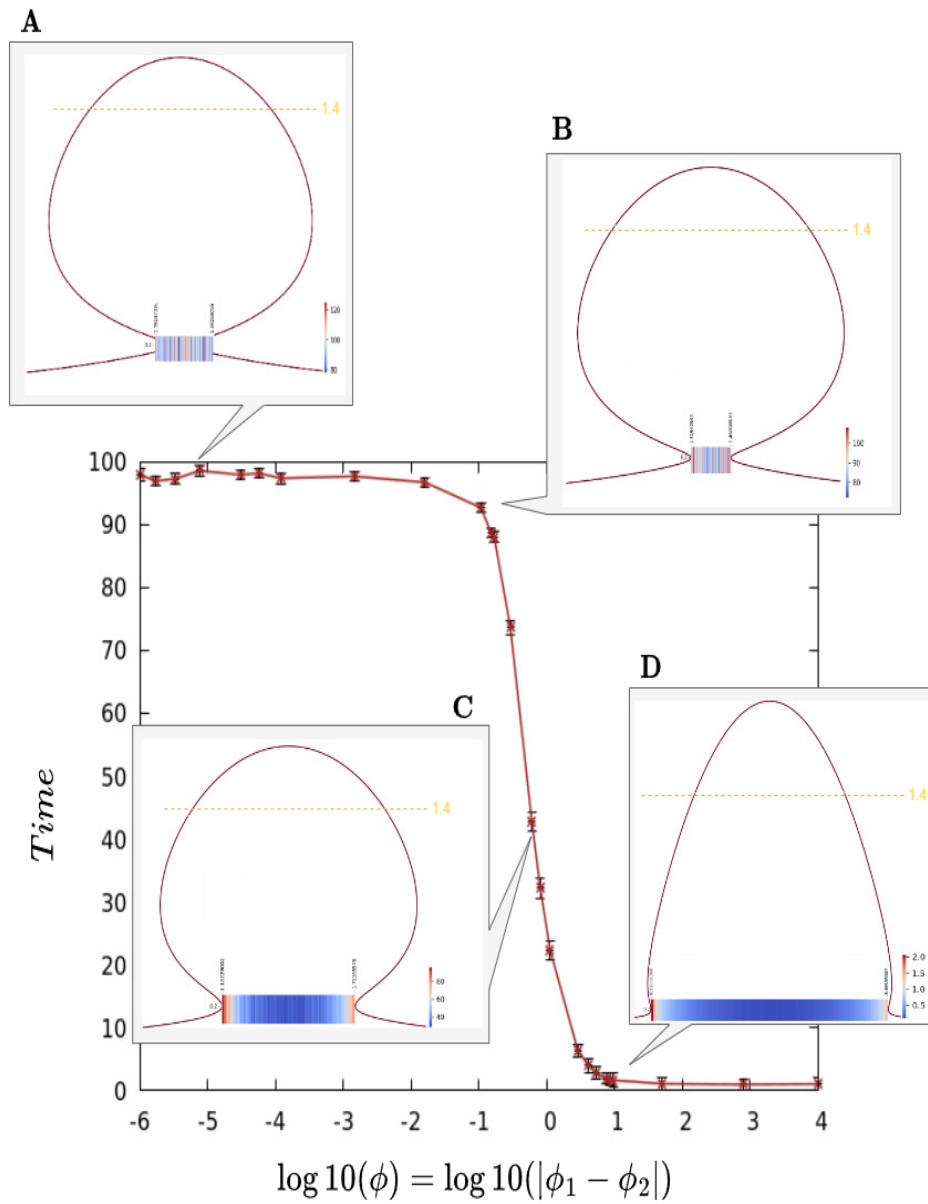


Figure 4.11: The colored band in each image represents a heatmap of the times required to reach $u=1.4$ using the Gillespie method (dashed line colored mustard). The wider figure applies a logarithmic rescaling (base 10) to accommodate the data distribution, which predominantly ranges from 0 to 1 but includes some higher values, approximately of the order of 10^2 . The analysis comprises 50 Gillespie runs with a system size $\Omega = 3000$ and 100 interval divisions. The images correspond to different parameter configurations: (A) $q=2.784953619424$, (B) $q=2.789$, (C) $q=2.85$, (D) $q=9$. The larger plot presents standard normalized deviation calculations and mean averages across 100 initial conditions, each involving 50 runs of the algorithm.

Conclusions

This work presents a thorough deterministic and stochastic mathematical analysis of the mushroom bifurcation, given the model developed in [43].

The first chapter laid the foundation of the mathematical and biological framework to describe the model. That allowed me to understand its implications on biology, particularly in the context of biosensors. Consequently, it inspired me to investigate further into mathematics, recognizing that a deeper understanding of them would enable me to contribute more effectively to the field of biology, fostering a synergy.

In the second chapter, we shifted our focus to the *ghost* effect and the numerical techniques required to accurately capture this phenomenon. We studied the specific numerical methods that were necessary to effectively simulate and represent the ghost effect in our models. The characterization of the slowing down effect on the convergence of two saddle nodes into a transcritical bifurcation moved our research further –an event that, to our knowledge, had not been previously identified.

In the third section, we discussed the fundamentals of stochastic dynamics, providing a solid foundation for conducting a noise-induced study on our model, which we explored further in the fourth chapter. This section enabled us to examine the interdisciplinary nature of our research: from understanding the biochemistry behind reaction definitions, to the analogies found on physics, when reading about the relationship of Hamiltonians and stochasticity on cells, as outlined in [31].

In Chapter four we discussed the results of implementing the fundamentals from the previous chapters to our model. Notably, we corroborated the SN-scaling law and through the approximation of the two lower saddle-nodes in our model, we found the preservation of the scaling law with extended transient periods necessary for the trajectory to unfold completely. We also investigated the transcritical scaling law, examining the divergence phenomenon and potential asymmetry within our model by studying the coefficients that influence the asymptotic behavior. Moreover, during our noise-induced study, we observed an asymmetry phenomenon when considering the Markovian stochastic system, on the heat map 4.6. In Figure 4.11, we visually demonstrated the impact of approximating the lower saddle nodes, revealing a distinct pattern in the time lags. Instead of observing a gradual spectrum of time, we observed the combined effect of the two saddle nodes, emphasizing their collective influence. These findings contribute to a deeper understanding of the dynamics within our model and provide valuable insights into the intricate relationships between system components, noise, and temporal behavior.

As an overall personal reflection, while the journey to completing this thesis presented numerous challenges, the sense of achievement is immeasurable. I feel tremendous proud for the entire team, whose hard work and dedication allowed us to successfully meet our research objectives, particularly in investigating the intricacies of the transcritical bifurcation.

Our work has also unveiled potential areas for further investigation, particularly concerning the potential asymmetric behaviour observed in the lower saddle-node

bifurcations. Despite successfully identifying and providing examples of this phenomenon, formalizing it represents an exciting opportunity for future research endeavors.

Ultimately, I hope that this thesis contributes meaningfully to existing knowledge, and plays a role in optimizing biosensors and synthetic biology, thereby aiding the development of improved treatments.

Bibliography

- [1] Azar, A.T., Vaidyanathan S., *Handbook of Research on Advanced Intelligent Control Engineering and Automation*. IGI Global, (2014).
- [2] Wikipedia contributors, *Sylvester's law of inertia*. Wikipedia, (2023, May 8). https://en.wikipedia.org/wiki/Sylvester_law_of_inertia
- [3] Bellman, R., Cooke, L.K., *Differential-Difference Equations*. The RAND Corporation, (1963).
- [4] Birkhoff, G., Mac Lane, S., *A survey of Modern Algebra*. Macmillan Publishing Co., Inc., (1977).
- [5] The Editors of Encyclopaedia Britannica, *Random walk | mathematics and science*. Encyclopedia Britannica, (2023, June 2), <https://www.britannica.com/science/random-walk>
- [6] Calsina, À., Cuadrado, S., Vidiella, B., Sardanyés, J., *About ghost transients in spatial continuous media*. ScienceDirect, 166, 112915, (2023). <https://doi.org/10.1016/j.chaos.2022.112915>
- [7] Canela, J., Alsedà, L., Fagella, N., Sardanyés, J. *Dynamical mechanism behind ghosts unveiled in a map complexification*. ScienceDirect, 156, 111780, (2022). <https://doi.org/10.1016/j.chaos.2021.111780>
- [8] Cooper, GM., *The Cell: A Molecular Approach..* Sinauer Associates, 2nd Edition, (2000).
- [9] Dai, L., Vorselen, D., Korolev, K. S., Gore, J., *Generic Indicators for Loss of Resilience Before a Tipping Point Leading to Population Collapse*. Science, 336(6085), 1175–1177, (2012). <https://doi.org/10.1126/science.1219805>
- [10] Ferrell J.E., *Bistability, bifurcations, and Waddington's epigenetic landscape*. Current Biology, 22(11), R458–R466, (2012). <https://doi.org/10.1016/j.cub.2012.03.045>
- [11] Fontich, E., Sardanyés, J., *General scaling law in the saddle–node bifurcation: a complex phase space study*. Journal of Physics A, 41(1), 015102 (2007). <https://doi.org/10.1088/1751-8113/41/1/015102>

- [12] FrontlineSolvers, *Optimization problem types - mixed-integer and constraint programming*, Solver, (2012, April 26). <https://www.solver.com/integer-constraint-programming>
- [13] García, R., *Apuntes de Topología y Geometría Diferencial de Superficies*. Universitat de Barcelona, 2019
- [14] Gillespie, D. T., *A general method for numerically simulating the stochastic time evolution of coupled chemical reactions*. *Journal of Computational Physics*, 22(4), 403–434, (1976). [https://doi.org/10.1016/0021-9991\(76\)90041-3](https://doi.org/10.1016/0021-9991(76)90041-3)
- [15] Gillespie, D. T., *Exact stochastic simulation of coupled chemical reactions*. *The Journal of Physical Chemistry*, 81(25), 2340–2361, (1977). <https://doi.org/10.1021/j100540a008>
- [16] Gillespie, D. T., *The chemical Langevin equation*. *Journal of Chemical Physics*, 113(1), 297–306, (2000). <https://doi.org/10.1063/1.481811>
- [17] Gillespie, D. T., *Stochastic Simulation of Chemical Kinetics*. *Annual Review of Physical Chemistry*, 58(1), 35–55, (2007). <https://doi.org/10.1146/annurev.physchem.58.032806.104637>
- [18] Gimeno, J., Jorba, À., Sardanyés, J., *On the effect of time lags on a saddle-node remnant in hyperbolic replicators*. *IOP Science*, 51(38), 385601, (2018). <https://doi.org/10.1088/1751-8121/aad02f2018>.
- [19] Halder, S., Ghosh, S., Chattopadhyay, J., Chatterjee, S., *Bistability in cell signalling and its significance in identifying potential drug-targets*. *Bioinformatics*, 37(22), 4156–4163, (2021). <https://doi.org/10.1093/bioinformatics/btab395>
- [20] Hale, J.K. and Koçak, H., 1991. *Dynamics and bifurcations: with 314 illustrations*. Springer, (1991).
- [21] Haro, A., *Apuntes de Ecuaciones Diferenciales Ordinarias*. Universitat de Barcelona, (2022).
- [22] Haro, A., *Apunts de Models Matemàtics i Sistemes Dinàmics*. Universitat de Barcelona, (2020).
- [23] Haro, A., *Apunts de Sistemes Dinàmics*. Universitat de Barcelona, (2023).
- [24] Ibe, O.C., *Fundamentals of Applied Probability and Random Processes*. In Elsevier eBooks, (2014). <https://doi.org/10.1016/c2013-0-19171-4>
- [25] Joshi CJ, Ke W, Drangowska-Way A, O'Rourke EJ, Lewis N.E., *What are house-keeping genes?*. *PLOS Computational Biology*, 18(7), e1010295, (2022). <https://doi.org/10.1371/journal.pcbi.1010295>

- [26] Karigar, C. S., Rao, S. S., *Role of Microbial Enzymes in the Bioremediation of Pollutants: A Review*. *Enzyme research*, 2011, 1–11, (2011). <https://doi.org/10.4061/2011/805187>
- [27] Kramers, H. A., *Brownian motion in a field of force and the diffusion model of chemical reactions*. *Physica*, 7(4), 284–304, (1940). [https://doi.org/10.1016/s0031-8914\(40\)90098-2](https://doi.org/10.1016/s0031-8914(40)90098-2)
- [28] Kuehn, C., *Scaling of saddle-node bifurcations: degeneracies and rapid quantitative changes*. *Iop Science*, 42(4), 045101, (2008). <https://doi.org/10.1088/1751-8113/42/4/045101>
- [29] Kumar J., Narnoliya L.K., Alok A., *A CRISPR Technology and Biomolecule Production by Synthetic Biology Approach*. In Elsevier eBooks, (2019). <https://doi.org/10.1016/b978-0-444-64085-7.00006-x>
- [30] Kuznetsov, Y.A., *Elements of Applied Bifurcation Theory*. Springer, 2nd edition, (1998).
- [31] Lázaro J.T., Alarcón T., Garay C.P., Sardanyés J., *Semiclassical theory predicts stochastic ghosts scaling*. *Proceedings of the Royal Society A: Mathematical, Physical and Engineering Sciences*, 479(2273), (2023). <https://doi.org/10.1098/rspa.2022.0621>
- [32] Laidler, K. J., *Law of mass action | Definition Facts*. *Encyclopedia Britannica*, (2023, May 17). <https://www.britannica.com/science/law-of-mass-action>
- [33] Lebl J., *Tasty bits of several complex variables*. Oklahoma State university, (2023).
- [34] Libretexts, *16.1: Introduction to Markov Processes*. *Statistics LibreTexts*, (2022). <https://stats.libretexts.org/@go/page/10288>
- [35] Libretexts. 2: *Reaction Rates*. *Chemistry LibreTexts*, (2023). <https://chem.libretexts.org/@go/page/1424>
- [36] Libretexts, *2.10: Stochastic Processes*. *Statistics LibreTexts*, (2022). <https://stats.libretexts.org/@go/page/10138>
- [37] Linares, J., *Procesos estocásticos*. Universidad de Granada, (2022).
- [38] Liu, B., Pappas, C. G., Ottel , J., Schaeffer, G., Jurissek, C., Pieters, P. F., Altay, M., Mari , I., Stuart, M. C. A., Otto, S., *Spontaneous Emergence of Self-Replicating Molecules Containing Nucleobases and Amino Acids*. *Journal of the American Chemical Society*, 142(9), 4184–4192, (2020). <https://doi.org/10.1021/jacs.9b10796>
- [39] Liu, P., Shi, J., Wang, Y., *Imperfect transcritical and pitchfork bifurcations*. *Journal of Functional Analysis*, 251(2), 573–600, (2007). <https://doi.org/10.1016/j.jfa.2007.06.015>

- [40] Lopes, F., Vieira, F. M. C., Holloway, D., Bisch, P. M., Spirov, A. V., *Spatial Bistability Generates hunchback Expression Sharpness in the Drosophila Embryo*. PLOS Computational Biology, 4(9), e1000184, (2008). <https://doi.org/10.1371/journal.pcbi.1000184>
- [41] Milnor, J., 1963, *Morse Theory*, Princeton University Press. (1963), p. 4-8.
- [42] McQuarrie, D. A., *Stochastic approach to chemical kinetics*. Journal of Applied Probability, 4(3), 413–478, (1967). <https://doi.org/10.2307/3212214>
- [43] Otero-Muras, I., Perez-Carrasco, R., Banga, J. R., Barnes, C. P., *Automated design of gene circuits with optimal mushroom-bifurcation behavior*. PubMed, 26(6), 106836, (2023). <https://doi.org/10.1016/j.isci.2023.106836>
- [44] Perko, L., *Differential Equations and Dynamical Systems*. In Springer eBooks, (2001). <https://doi.org/10.1007/978-1-4613-0003-8>
- [45] Perez-Carrasco, R., Guerrero, P., Briscoe, J., Page, K., *Intrinsic Noise Profoundly Alters the Dynamics and Steady State of Morphogen-Controlled Bistable Genetic Switches*. PLOS Computational Biology, 12(10), e1005154, (2016). <https://doi.org/10.1371/journal.pcbi.1005154>
- [46] Rombouts, J., Gelens, L., *Dynamic bistable switches enhance robustness and accuracy of cell cycle transitions*. PLOS Computational Biology, 17(1), e1008231, (2021). <https://doi.org/10.1371/journal.pcbi.1008231>
- [47] Rosales, R.R., *Bifurcations: Baby normal forms*. Massachusetts Inst. of Technology, (2004).
- [48] Sardanyés, J., Alarcón, T., *Noise-induced bistability in the fate of cancer phenotypic quasispecies: a bit-strings approach*. Scientific reports, 8(1), (2018). <https://doi.org/10.1038/s41598-018-19552-2>
- [49] Sardanyés, J., Raich, C., Alarcón, T., *Noise-induced stabilization of saddle-node ghosts*. New Journal of Physics, 22(9), 093064, (2020). <https://doi.org/10.1088/1367-2630/abb549>
- [50] Sardanyés J., Arderiu A., Elena F.S., Alarcón T., *Noise-induced bistability in the quasi-neutral coexistence of viral RNAs under different replication modes*. Journal of the Royal Society Interface, 15(142), 20180129, (2018). <https://doi.org/10.1098/rsif.2018.0129>
- [51] Sardanyés, J., Solé, R., *Ghosts in the origins of life?*. International Journal of Bifurcation and Chaos, 16(09), 2761–2765, (2006). <https://doi.org/10.1142/s0218127406016446>
- [52] Sengupta, D., Kar, S., *Deciphering the dynamical origin of mixed population during neural stem cell development*, Biophysical Journal 114(4), 992–1004, (2018). <https://doi.org/10.1016/j.bpj.2017.12.035>

- [53] Song H., Smolen P., Av-Ron E., Baxter D.A., Byrne J.H., *Bifurcation and Singularity Analysis of a Molecular Network for the Induction of Long-Term Memory*. *Biophysical Journal*, 90(7), 2309–2325, (2006). <https://doi.org/10.1529/biophysj.105.074500>
- [54] Sriram, K., Rodriguez-Fernandez, M., Doyle, F. J., *A Detailed Modular Analysis of Heat-Shock Protein Dynamics under Acute and Chronic Stress and Its Implication in Anxiety Disorders*. *PLOS ONE*, 7(8), e42958,(2012). <https://doi.org/10.1371/journal.pone.0042958>
- [55] Strogatz, S. H., *Nonlinear Dynamics and Chaos: With Applications to Physics, Biology, Chemistry, and Engineering*. CRC Press, (2015).
- [56] Strogatz, S., Westervelt, R.M., *Predicted power laws for delayed switching of charge-density waves*. *Physical Review*, 40(15), 10501–10508, (1989). <https://doi.org/10.1103/physrevb.40.10501>
- [57] Szostak, N., Wasik, S., Blazewicz, J., *Hypercycle*. *PLOS Computational Biology*, 12(4), e1004853, (2016). <https://doi.org/10.1371/journal.pcbi.1004853>
- [58] National Human Genome Research Institute. (n.d.), *Synthetic Biology*. <https://www.genome.gov/about-genomics/policy-issues/Synthetic-Biology>
- [59] National Human Genome Research Institute. (n.d.), *Transcription*. <https://www.genome.gov/genetics-glossary/Transcription>
- [60] Novak, K., *Numerical Methods for Scientific Computing* Equal Share Press, (2022), p. 174-175.
- [61] Trickey, S. T., Virgin, L. N., *Bottlenecking phenomenon near a saddle-node remnant in a Duffing oscillator*. *Physics Letters*, 248(2–4), 185–190, (1998). [https://doi.org/10.1016/s0375-9601\(98\)00665-3](https://doi.org/10.1016/s0375-9601(98)00665-3)
- [62] Troutman, J. A., *Piecewise C1 Extremal Functions*. In Springer eBooks (pp. 197–233), (1983). https://doi.org/10.1007/978-1-4612-0737-5_8
- [63] Vidiella, B., Guillamon, A., Sardanyés, J., Maull, V., Pla, J., Conde, N., Solé, R. V., *Engineering self-organized criticality in living cells*. *Nature Communications*, 12(1), (2021). <https://doi.org/10.1038/s41467-021-24695-4>
- [64] Zimmermann, R., Qaim, M., *Potential health benefits of Golden Rice: a Philippine case study*. *Food Policy*, 29(2), 147–168, (2004). <https://doi.org/10.1016/j.foodpol.2004.03.001>

Appendix A

.1 Additional insight

.1.1 Proof of Theorem 1.12 using Hamiltonian arguments

Proof. Consider the Hessian matrix of f :

$$H = \begin{bmatrix} A_{11} & A_{12} \\ A_{21} & A_{22} \end{bmatrix}$$

The determinant of H , denoted as $\text{Det}(H)$, is defined as $\text{Det}(H) = A_{11}A_{22} - A_{12}^2$. By hypothesis it is negative, which implies that H is non-degenerate, as it is not zero.

Next, we proceed to explore the eigenvalues of H by solving the equation $\det(H - \mu I) = 0$, where I is the identity matrix and μ represents the eigenvalues we are seeking. This leads us to a second-degree equation:

$$\mu^2 - (A_{11} + A_{22})\mu + A_{11}A_{22} - A_{12}^2 = 0$$

Using elementary algebra, we know that the constant term of the equation is the product of the roots, which in this context are the eigenvalues. By applying our established relationship $A_{12}^2 > A_{11}A_{22}$, we observe that the eigenvalues have opposite signs, therefore the conditions for a saddle node point are met, indicating that H is indefinite.

We can now apply Lemma 1.20, which guarantees the existence of two curves x_{\pm} of fixed points in a neighborhood of (x_0, λ_0) , where $x_{\pm}(\lambda_0) = x_0$. Hence, proving (1).

(2) Directly follow from the fact that the curves x_{\pm} are defined in a neighbourhood of λ_0 such that they are the solution set of $f(x, \lambda) = 0$.

(3) According to Lemma 1.20, the derivatives $x'_{\pm}(\lambda_0)$ must be the two linear independent solutions of:

$$A_{11}\eta^2 + 2A_{12}(x_0, \lambda_0)\eta\tau + A_{22}(x_0, \lambda_0)\tau^2 = 0$$

By solving this equation, the derivatives can be written in the following form:

$$x'_{\pm}(\lambda_0) = \frac{-2A_{12} \pm \sqrt{4A_{12}^2 - 4A_{11}A_{22}}}{2A_{11}} = \frac{-A_{12} \pm \sqrt{A_{12}^2 - A_{11}A_{22}}}{A_{11}}$$

□

.1.2 Structure of the Gillespie Algorithm (SSA)

Equation 3.5 forms the core principle of the stochastic simulation method, SSA. [17] It suggests that τ follows an exponential random distribution with an average (and standard deviation) of $\frac{1}{a_0(x)}$, where $a_0(x) = \sum_{j=1}^M a_j(x)$. Meanwhile, j is an independent integer random variable with point probabilities of $\frac{a_j(x)}{a_0(x)}$.

There are several accurate Monte Carlo methods to create samples of τ and j based on these distributions. One simple approach is the direct method, which is established by employing the standard inversion generating method of Monte Carlo theory. In this method, we draw two random variables r_1 and r_2 from a uniform distribution within the unit range, and set:

$$\tau = \frac{1}{a_0(x)} \ln \left(\frac{1}{r_1} \right), \quad (2)$$

$$j = \text{the smallest integer satisfying } \sum_{j=1}^n a_j(x) > r_2 a_0(x). \quad (3)$$

This method (or any equivalent one) allows us to follow a stochastic simulation algorithm (SSA) to build an accurate numerical representation of the $X(t)$ process. The steps of the SSA are as follows:

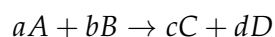
1. Initialize the time $t = t_0$ and the system's state $x = x_0$.
2. With the system in state x at time t , compute all $a_j(x)$ and their sum $a_0(x)$.
3. Generate values for τ and j using equations 10a and 10b (or their equivalent).
4. Implement the next reaction by setting t to $t + \tau$ and x to $x + \nu_j$.
5. Document the pair (x, t) as needed. Repeat from Step 1, or finish the simulation.

Remark .1. It is important to implement conditions for stopping the calculations when the predetermined time or reaction count is reached, or when the sum of the a -values, a , becomes zero.

.1.3 Law of Mass Action and Michaelis-Menten-Hill equation

Law of Mass Action: The law of mass action states that the rate of any chemical reaction is proportional to the product of the masses of the reacting substances, with each mass raised to a power equal to the coefficient that occurs in the chemical equation.

For a general reaction of the form:



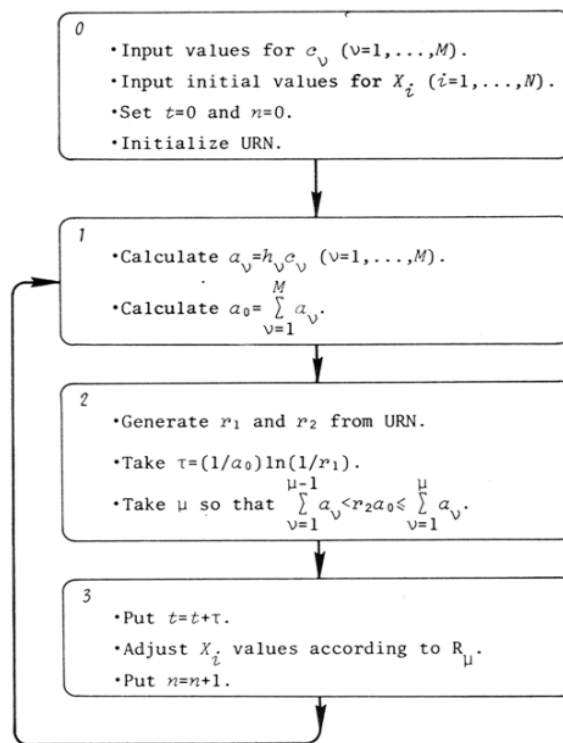


Figure 12: Figure taken from [15], schematic of the stochastic simulation algorithm.

where A and B are reactants, and C and D are products, the rate of the reaction can be expressed as:

$$r = k[A]^a[B]^b$$

where $[A]$ and $[B]$ represent the concentrations of reactants A and B , respectively, k is the rate constant, and a and b are the stoichiometric coefficients for A and B , respectively.

Michaelis-Menten-Hill (MMH) equation: The MMH equation is given by:

$$v = \frac{V_{\max} \cdot [S]}{K_m + [S]}$$

where:

- v is the reaction rate or velocity.
- V_{\max} is the maximum reaction rate, which represents the rate of the reaction when the enzyme is fully saturated with substrate.
- $[S]$ is the substrate concentration.
- K_m is the Michaelis constant, which represents the substrate concentration at which the reaction rate is half of the maximum rate. It is a measure of the affinity of the enzyme for the substrate.

In summary, the law of mass action is a fundamental principle in chemistry that relates the rate of a chemical reaction to the concentrations of the reacting species. It serves as the basis for understanding reaction rates and has applications in various fields, including chemical kinetics and enzyme kinetics.

Corollary .2. *Rates derived from the Law of Mass Action or Michaelis-Menten-Hill kinetics satisfy condition (3.6).*

Proof. In the context of the Law of Mass Action, the rate of a chemical reaction is proportional to the concentrations of the reacting species raised to their respective stoichiometric coefficients. As the system size Ω increases, the concentrations become larger, and the rate $W_i(X)$ scales up proportionally, satisfying the scaling relationship.

Similarly, in the case of Michaelis-Menten-Hill kinetics, the rate of an enzyme-catalyzed reaction is characterized by the Michaelis-Menten equation, which involves the enzyme and substrate concentrations. When the system size Ω is large, the concentrations become significant, and the macroscopic rate $W_i(X)$ can be approximated by scaling up the intrinsic rate $w_i(x)$ with respect to the concentrations, following the scaling relationship.

Therefore, the rates derived from the Law of Mass Action or Michaelis-Menten-Hill kinetics satisfy the scaling relationship because they capture the behavior of the system at a macroscopic scale by scaling up the intrinsic rates or dynamics at the microscopic or molecular level. \square

Appendix B

.1 Numerical Tools

Numerical tools were employed to integrate the delay differential equation (DDE) model using a 7th-8th order Runge-Kutta-Fehlberg method, thanks to Josep Sardanyés, and also a Runge-Kutta-Verner algorithm of orders 8 and 9, thanks to Àngel Jorba. The numerical approximation used automatic step size control and a local relative tolerance of approximately 10^{-15} , even though it was adaptive depending on the problem requirements.

To understand how the numerical solution approximated the DDE model, it is important to note some distinctions compared to standard ordinary differential equation (ODE) solvers. The DDE given by Eq. (4) can be written as

$$\frac{dx}{dt}(t) = f(x(t), x(t - \tau)),$$

where f is a suitable function and τ represents the time delay. The initial condition, denoted by a continuous function u on the interval $[-\tau, 0]$, plays a crucial role. The initial value problem can be treated as a chain of ODEs within each interval $(l\tau, (l + 1)\tau)$, where l is a positive integer. Thus, a natural approach for integrating such DDEs is to employ a standard ODE solver and integrate within each distinct interval.

Consequently, the DDE model is effectively solved by considering a standard ODE solver and performing integration within each individual interval.

For graphic representation, Gnuplot, MATLAB and Python libraries such as Seaborn and Matplotlib has been used.

.1.1 Newton-Raphson and Citardauq formula

Newton-Raphson program to calculate the fixed points and critical values.

In order to avoid or control subtractive cancellation, we have used an implementation of the Citardauq¹ formula, avoiding the numerical instability of solving the second-degree equation.

The Citardauq formula [60] consists of using:

$$x_{\pm} = \frac{2c}{-b \mp \sqrt{b^2 - 4ac}} \quad (4)$$

¹As the reader may see, Citardauq is Quadratic spelled backwards

The combined formula is:

$$x_{-} = \frac{-b - \text{sign}(b)\sqrt{b^2 - 4ac}}{2a}, \quad x_{+} = \frac{c}{a}x_{-} \quad (5)$$

Listing 1: C code

```
#include <stdio.h>
#include <math.h>
#include <stdlib.h>

double** resol(double a, double b, double c, int* num_solutions);

double f(double x, double r) {
    return r + (((1 + x * x) * x) / 2) - x;
}

double df(double x) {
    return -0.5 + 1.5 * x * x;
}

int es_repetit(double x, double** solutions, int num_solutions) {
    for (int i = 0; i < num_solutions; i++) {
        if (fabs(x - *(solutions[i])) < 1e-8) {
            return 1; // x is a repeated answer
        }
    }
    return 0; // x is not a repeated answer
}

void free_solutions(double** solucions, int num_solucions){
    if(num_solucions != 0){
        for(int i=0; i<num_solucions; i++){
            free(solucions[i]); //free memory
        }
    }
    free(solucions);
}

int main() {
    double x0_start = -1, x0_end = 15, x0_step = 0.25; // range
        of initial guess values
    double r = 0.14; // given value of r

    double tolerance = 1e-8; // tolerance for convergence
    int max_iterations = 1000000; // maximum number of iterations

    double roots[1000]; // array to store roots found so far
    int num_roots = 0; // number of roots found so far
    FILE* file = fopen(" NAME OF THE .DAT FILE", "w"); // open
```

file for writing

```

for (double x0 = x0_start; x0 <= x0_end; x0 += x0_step) {
    double x = x0;
    int i = 0;
    for (; i < max_iterations; i++) {
        double fx = f(x, r);
        double dfx = df(x);
        double dx = -fx / dfx;
        x += dx;
        if (fabs(dx) < tolerance) {
            double** solutions;
            int num_solutions;
            double x_nova;

            x_nova = ((1 + x * x) * (1 + x * x)) / (2 * x);

            solutions = resol(-1, 2.78495361941546, -x_nova, &
                num_solutions);
            if (num_solutions == 2) {
                int is_repeated = 0;
                for (int j = 0; j < num_roots; j++) {
                    if (fabs(x - roots[j]) < 1e-8) {
                        is_repeated = 1;
                        break;
                    }
                }
                if (!is_repeated) {
                    // check if the new root is not repeated
                    fprintf(file, "Root found for x0=%.12f:
                        %.15f  %.15f  %.15f\n", x0, x, *(
                            solutions[0]), *(solutions[1]));
                    roots[num_roots] = x; // add the new root
                        to the array
                    num_roots++; // increment the number of
                        roots found so far
                }
            }

            free_solutions(solutions, num_solutions);
            break;
        }
    }
    if (i == max_iterations) {
        fprintf(file, "Root not found for x0=%.12f within max
            iterations.\n", x0);
    }
}

```

```

    return 0;
}

```

Resol uses Pau Soler Valadés' implementation of the Citardauq formula, as shown below.

Listing 2: C code

```

#include <stdio.h>
#include <stdlib.h>
#include <math.h>

#define DELTA 1e-12

double** resol(double a, double b, double c, int *num_soluciones)
{
    double discriminant;
    double **soluciones;

    discriminant = b * b - 4 * a * c;

    if (discriminant < 0) {
        printf("Negative discriminant, no solution\n");
        *num_soluciones = 0;
        soluciones = NULL;
        return soluciones;
    }

    soluciones = (double**)malloc(sizeof(double*) * 2);

    if(soluciones != NULL){

        if (a != 0 || fabs(a) >= DELTA) {
            double x1, x2;
            double sgn_b = (b >= 0) ? 1.0 : -1.0;

            x1 = (-b - sgn_b * sqrt(discriminant)) / (2 * a);
            x2 = c / (a * x1);

            if (fabs(discriminant) < DELTA || discriminant == 0)
            {
                soluciones[0] = (double*)malloc(sizeof(double));
                if(soluciones[0] != NULL){
                    *soluciones[0] = x1;
                    *num_soluciones = 1;
                    printf("Discriminant 0 i a no es 0\n");
                }else{
                    printf("Problems allocating memory\n");
                    *num_soluciones = -1;
                    return NULL;
                }
            }
        }
    }
}

```

```
    }
} else {
    soluciones[0] = (double*)malloc(sizeof(double));
    soluciones[1] = (double*)malloc(sizeof(double));

    if(soluciones[0] != NULL && soluciones[1] != NULL){
        *soluciones[0] = x1;
        *soluciones[1] = x2;
        *num_soluciones = 2;
    }else{
        printf("Problems allocating memory\n");
        *num_soluciones = -1;
        return NULL;
    }
}
} else {
    if (b != 0 || fabs(b) >= DELTA) {
        soluciones[0] = (double*)malloc(sizeof(double));

        if(soluciones[0] != NULL){
            *soluciones[0] = -c / b; // degree 1 equation
            *num_soluciones = 1;
            printf("Equation of degree 1\n");
        }else{
            printf("Problems allocating memory\n");
            *num_soluciones = -1;
            return NULL;
        }
    } else {
        printf("No equation\n");
        *num_soluciones = 0;
        free(soluciones);
        return NULL;
    }
}

return soluciones;
}else{
    printf("Problems allocating memory\n");
    *num_soluciones = -1;
    return NULL;
}
}
```

1.2 Gillespie Algorithm: Heat map Stochastic scenario

Listing 3: C code

```

#include<stdio.h>
#include<stdlib.h>
#include<math.h>
#include<unistd.h>
#include<time.h>

/**
 * Return the probabilities of being in the lower branch or the
 * upper branch after performing n runs of Gillespie.

@param s system parameter, substrate concentration
@param q system parameter, modifies the shape of the bifurcation
@param x initial condition, protein concentration
@param NUM_ITERATION number of Gillespie runs
@param n_iter number of internal runs
@param probability1 result of the probability in the lower
    branch
@param probability2 result of the probability in the upper
    branch
@return void, the results are stored in probability1 and
    probability2.
 */
void gillespie(double s, double q, double x_ini, double CC,
    double interval_startlow, double interval_endlow, double
    interval_starthigh, double interval_endhigh, int
    Max_iterations, int n_iter, double *probability1, double *
    probability2){
    int num_in_interval1=0;
    int num_in_interval2=0;
    for(int iteration = 0; iteration < Max_iterations; iteration
        ++){
        double time = .0, tau = .0; // Time // Waiting time

        // W's
        double W1, W2, W3, W4 = .0;
        double W0 = .0; // Sum of Wi's

        // Uniform z's
        double z1, z2 = 0;

        // Initial population
        double x = x_ini* CC;

        double W[4];

        for (int it = 0; it < n_iter; it++) {

```

```
// Transition rates for each reaction
W1 = CC * 0.14;
W2 = x;
W3 = CC * s * q * x * x / (CC * CC + x * x);
W4 = CC * s * s * x * x / (CC * CC + x * x);

W[0] = W1;
W[1] = W2;
W[2] = W3;
W[3] = W4;

// Compute z1, z2
z1 = drand48();
z2 = drand48();

// Compute W_0 = sum W's
W0 = W1 + W2 + W3 + W4;

// Compute waiting time, tau
tau = (1.0 / W0) * log(1.0 / z1);

// Reaction at time tau
double suma = 0;
int kk = 0;

while (suma < z2 * W0) {
    suma += W[kk];
    kk++;
}

if (kk == 1) {
    x = x + 1.0;
} else if (kk == 2) {
    x = x - 1.0;
} else if (kk == 3) {
    x = x + 1.0;
} else if (kk == 4) {
    x = x - 1.0;
}

time += tau;

if (x > 0) {
    if (it % 100 == 0) {
        // printf("%.7lf %.4lf\n", time, x);
    }
} else {
    // printf("%.7lf Extinction\n", time);
    break;
}
```

```

    }
}

double norm_x_ts = x / CC;
//printf("Iteration %d: norm_x_ts = %.7lf\n", iteration +
    1, norm_x_ts);

// Check if norm_x_ts falls within the interval
if (norm_x_ts >= interval_startlow && norm_x_ts <=
    interval_endlow) {
    num_in_interval1++;
}

if (norm_x_ts >= interval_starthigh && norm_x_ts <=
    interval_endhigh) {
    num_in_interval2++;
}
}
num_in_interval1=(double)num_in_interval1;
num_in_interval2=(double)num_in_interval2;

// Calculate the probability of norm_x_ts falling within the
    interval
*probability1 = (double)num_in_interval1 / Max_iterations;
*probability2 = (double)num_in_interval2 / Max_iterations;
//printf("prob1 %.7le: prob2 = %.7le\n", *probability1, *
    probability2);

return;
}

```

Code to plot the Heat Maps using Seaborn library:

Listing 4: Python code

```

import pandas as pd
import seaborn as sns
import matplotlib.pyplot as plt

# Open the file in read mode
with open("Probabilitat.txt", "r") as file:
    # Read all lines from the file
    lines = file.readlines()

# Create lists to store the values
u_values = []
prob_branca_sota_values = []
s_values = []

```

```
# Extract the values from the file
for line in lines:
    columns = line.split()
    column1_value = float(columns[0])
    s_values.append(column1_value)

    column2_value = float(columns[1])
    u_values.append(column2_value)

    column3_value = float(columns[3])
    prob_branca_sota_values.append(column3_value)

# Create a DataFrame with the data
df = pd.DataFrame({
    'S': s_values,
    'U': u_values,
    'Probabilidad': prob_branca_sota_values
})

# Reorganize the data into a 2D matrix using pivot
heatmap_data = df.pivot('U', 'S', 'Probabilidad')
heatmap_data = heatmap_data.iloc[:, :-1]

# Plot the heatmap using Seaborn
plt.figure(figsize=(7, 7))
sns.heatmap(heatmap_data, cmap='hot')
plt.show()
```

.1.3 Saddle-node Scaling Law

Program used to find the Scaling Law near SN1 for $q = 2.78495381941348$, $r = 0.14$:

Listing 5: C code

```

#include <stdlib.h>
#include <stdio.h>
#include <math.h>
#include "rkv89.h"

double e[2];

void var0(double t, double x[], int m, double xm[])
{
    xm[0] = 0.14 + e[0] * (e[1] - e[0]) * ((x[0] * x[0]) / (1 + x
        [0] * x[0])) - x[0];
}

int main()
{
    double x[1];
    e[1] = 2.78495381941348;
    double time = 0.0;
    double pas = 0.00001;
    double eps = 1e-9;
    double s_crit=1.392475142707961;
    x[0] = 0.28;
    e[0]=1.392477;

    const unsigned long MAX_ITERATIONS = 1e11;

    FILE *file = fopen("SN1_prova.dat", "w"); // open file for
        writing

    do
    {
        unsigned long iterations = 0;
        time = 0.0;
        x[0] = 0.28;
        pas = 0.00001;

        do
        {
            rkv89(&time, x, 1, &pas, 1, eps, NULL, NULL, var0);
            iterations++;

            if (iterations > MAX_ITERATIONS)
            {

```

```
        printf("Exceeded maximum allowed iterations.\n");
        break;
    }
} while (time < 1e13 && x[0] < 0.45);
fprintf(file, "%.13lf %.16lf\n", log10(fabs(time)), log10
        (fabs(s_crit-e[0]))); // print to file instead of
        console
    e[0] -= 1e-12;
} while (e[0] > s_crit);

fclose(file); // close file

return 0;
}
```

.1.4 Transcritical Scaling Law

Listing 6: C code

```

#include <stdlib.h>
#include <stdio.h>
#include <math.h>
#include "rkv89.h"

double e[2];
double ** resol(double a, double b, double c, int *num_solutions)
    ;

void var0(double t, double x[], int m, double xm[])
{
    xm[0] = 0.14 + (e[0] * (e[1] - e[0])) * ((x[0] * x[0]) / (1 + x
        [0] * x[0])) - x[0];
}

int main()
{
    double x[1];
    double crit;
    e[1] = 2.785;
    double time = 0.0;
    double pas = 0.00001;
    double eps = 1e-7;
    e[0] = e[1] / 2;
    x[0] = 0.25;

    const unsigned long MAX_ITERATIONS = 1e11;
    const double MIN_E1 = 1e-10;

    FILE *file = fopen("transcriticaoriginal.dat", "w"); // open
        file for writing

    do
    {
        unsigned long iterations = 0;
        time = 0.0;
        x[0] = 0.25;
        pas = 0.00001;
        double **solutions;
        int num_solutions;
        solutions = resol(-1, e[1], -1.9389916635675362, &
            num_solutions);
        e[0]=e[1]/2;
        printf("%.9le %.9le %.9le\n", e[1], e[0], x[0]);
        do
        {

```

```
    rkv89(&time, x, 1, &pas, 1, eps, NULL, NULL, var0);
    iterations++;

    if (iterations > MAX_ITERATIONS)
    {
        printf("Exceeded maximum allowed iterations.\n");
        break;
    }
} while (time < 1e13 && x[0] < 0.35);
if (num_solutions == 2) {
    fprintf(file, "%.13lf %.16lf\n", log10(fabs(time)),
            log10(fabs(*solutions[1] - 1.3924768097067324)));
    // print to file instead of console
}
e[1] -= 1e-11;
free(solutions);
} while (e[1] > 2.7849536194134648);

fclose(file); // close file

return 0;
}
```

Appendix C

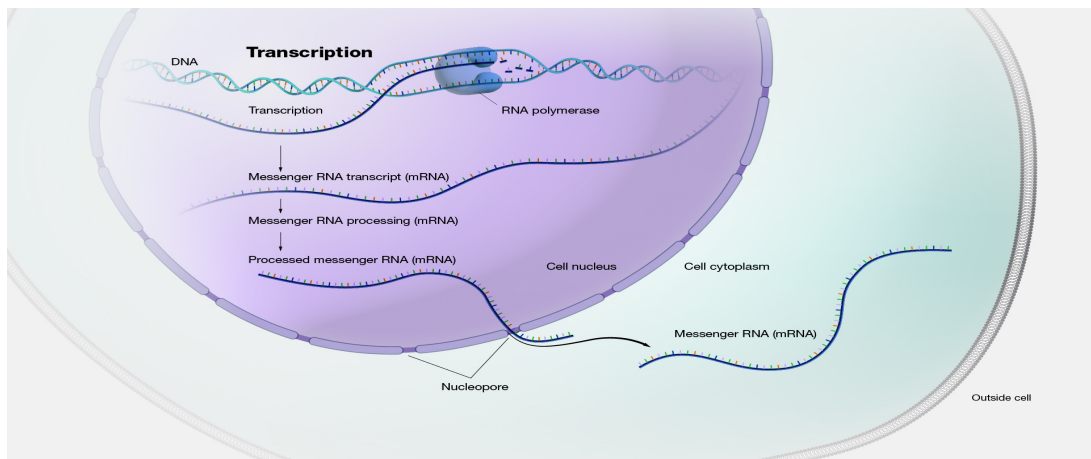


Figure 13: **Transcription Process:** This copy, called messenger RNA (mRNA), carries the gene's protein information encoded in DNA. In humans and other complex organisms, mRNA moves from the cell nucleus to the cell cytoplasm (watery interior), where it is used for synthesizing the encoded protein. Image from [59].

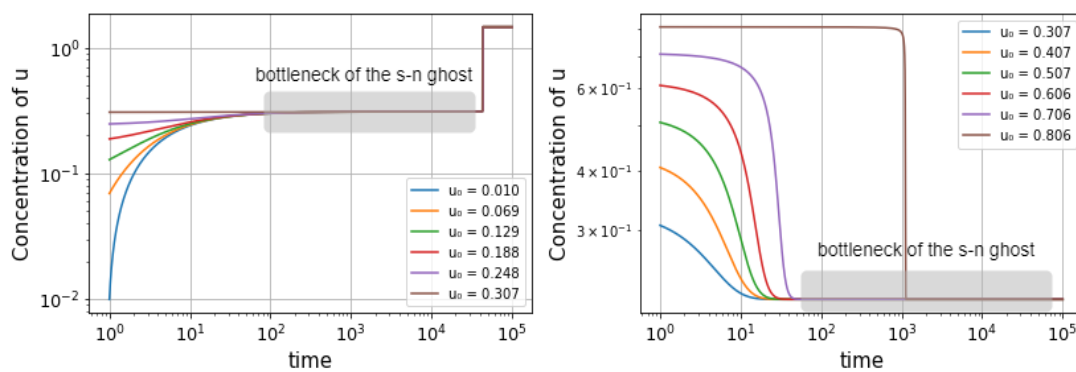


Figure 14: **Ghost effect:** Time series (in log-linear scale) for different initial conditions near bifurcation threshold $s = s + 10^{-8}$ for SN2 and SN3, and $s = s - 10^{-8}$ for SN2 and SN4. In all the analyses, we have used $r = 0.14$ and $q = 5$.